Optimizing the performance of the Freshmaker by studying different operational and hydrogeological variables

A study into a new aquifer storage and recovery (ASR) technique using density dependent flow modelling.

MSc thesis of the research master programme "Earth Surface and Water, track: hydrology"
Faculty of Geosciences
University of Utrecht

The research was performed in collaboration with KWR Watercycle Research Institute

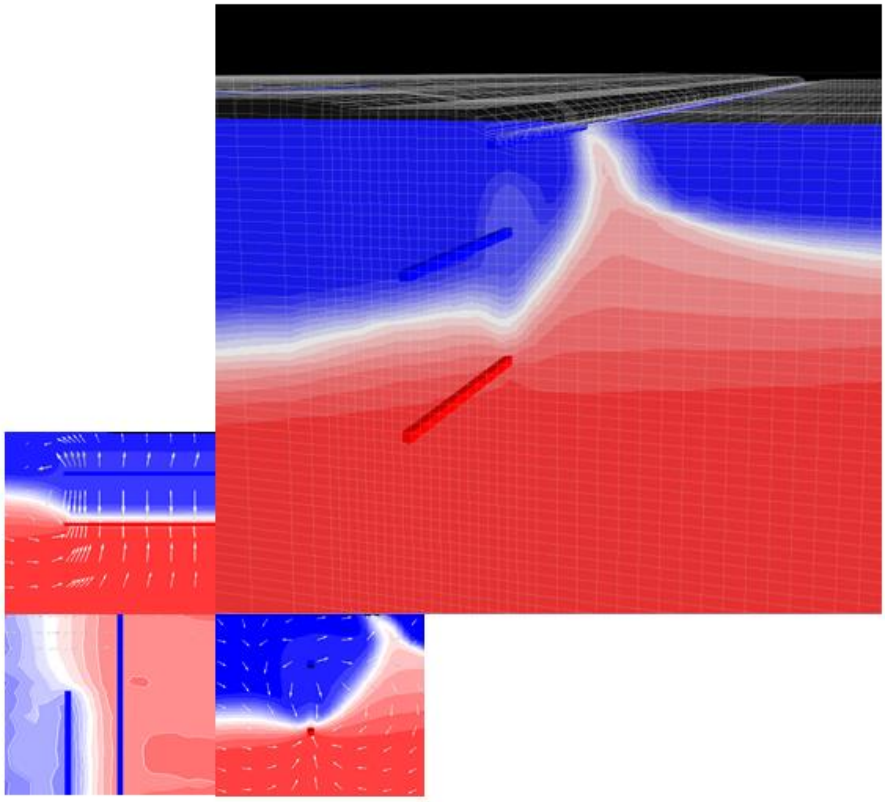

Author:

S. J. van der Linde (3540057)

Supervisors:

K. G. Zuurbier, MSc (KWR)

Prof. dr. R. J. Schotting (UU)

KWR Watercycle Research Institute

Universiteit Utrecht

Preface and acknowledgement

This MSc thesis presents the results of the graduation project carried out to complete the master program Earth Surface and Water: track hydrology at Utrecht University, faculty of Geosciences. During this project, I studied the performance of a new aquifer storage and recovery (ASR) technique called "the Freshmaker".

During the process of writing this MSc thesis I have learned a lot, not just about the field of hydrology but also about myself. Sometimes it was a real struggle and although especially the modelling sometimes brought me to a point of despair, I look back with content. I am very pleased with the final result but I could never have done it on my own. Therefore, I want to take a moment to give thanks to the ones who made this MSc research possible.

First and foremost, I want to thank God for giving me wisdom and guidance throughout my life.

- ..but as for me, I would thank God. He does great things, too marvelous to understand. Marvelous things, without number. He gives rain for the earth and sends water for the fields. (Job 5: 8 – 10). -

I would like to give thanks to my supervisor, Koen Zuurbier. I would have been nowhere without his supervision. Thank you for all your support and feedback during my graduation project. I have definitely become a better and more effective researcher because of you. Thank you for taking me on fieldtrips to the Freshmaker pilot in Ovezande, it really helped me to develop a better feeling with what I was actually studying. I would also like to thank you for sharing your enthusiasm about the Freshmaker and ASR in general. I have to admit, I got infected with the ASR-virus.

Furthermore, I want to thank Ruud Schotting. Although we haven't seen each other often during this project, I want to thank you for being my second reader but also for your great teaching skills during the whole master programme. You always work hard to recruit new hydrology students with your passion for hydrology and mathematics, at least it worked for me. I hope you will enjoy my presentation!

I had the privilege to perform this research as an intern at KWR Watercycle Research Institute and I would like to thank all my colleagues for being so enthusiastic about water. I had a good time in team geohydrology. Jan-Willem Kooiman, thank you for taking the time to talk with me about my career plans. I honestly can't wait to start working in the water sector.

A very special word of thanks goes to my beautiful and amazing girlfriend and fiancé. For the past six months I have possibly been the most boring person to live with ever, but you were always there, supporting my efforts.

Finally, I would like to express my gratitude to my parents for their financial support which made my studies possible and to all my friends who helped me to get out of the groove from time to time.

I hope you will enjoy reading this MSc thesis,

Siebren van der Linde

Utrecht, 19th January 2015

Samenvatting

Een complexe mix van factoren, zoals een groeiende wereldbevolking, klimaatverandering, vervuiling en overconsumptie zet de beschikbaarheid van zoetwater onder druk. Op veel plekken in de wereld is reeds een disbalans tussen het wateraanbod en de watervraag. Deze disbalans kan seizoensafhankelijk van aard zijn (natte winters versus droge zomers) maar kan ook ontstaan tussen jaren met wateroverschot en –tekort.

Eén van de belangrijkste oplossingen om watertekorten te voorkomen is het creëren van voldoende wateropslag. Dit helpt het gat tussen de droge en natte periodes te overbruggen. Hoewel het bovengronds opslaan van water mogelijk is, heeft ondergrondse opslag veel meer potentie gezien de gigantische opslagcapaciteit en de relatief lage kosten. “Aquifer storage and recovery” (ASR) is een reeds beproefde techniek waarmee zoetwateroverschotten in de ondergrond worden geïnjecteerd om weer opgepompt te worden als de watervraag toeneemt. Deze techniek is echter minder geschikt voor de berging van zoetwater in brakke of zoute pakketten. Dichtheidsverschillen tussen het zoete en zoute water zorgen ervoor dat zoetwater opwaarts zal gaan stromen waardoor het niet meer gewonnen kan worden. Dit resulteert in lage zoetwateropbrengsten en tegenvallende resultaten.

De “Freshmaker” is een innovatieve techniek dat de toepasbaarheid van ASR in brakke en zoute pakketten mogelijk vergroot. De Freshmaker bestaat uit twee horizontale putten (HDDWs) boven elkaar. De bovenste put (HDDW1) wordt gebruikt voor de berging en onttrekking van zoetwater, de onderste voor continue interceptie van zoutwater waardoor zoetwaterverliezen worden beperkt. Voor de onderhavige modelstudie is een SEAWAT-model gebouwd met gegevens die beschikbaar zijn gekomen vanuit een proeflocatie in Ovezande (Zeeland), waar de Freshmaker momenteel getest wordt. Het functioneren van de Freshmaker is onderzocht en de Freshmaker is geoptimaliseerd middels verschillende nieuwe ontwerp- en aansturingsadviezen.

Uit het onderzoek is gebleken dat grotere zoetwateropbrengsten mogelijk zijn bij de Ovezande veldproef dan tot nog toe beoogd was. De maximale zoetwaterproductie van de Freshmaker in Ovezande is geschat op ongeveer 6000 m^3. Onder een nabije (drainerende) watergang in Ovezande bevindt zich een zoutwaterkegel. Modelberekeningen hebben aangetoond dat hierdoor de zoetwaterproductie in de eerste drie ASR-cycli wordt gelimiteerd. Door de activiteit van de Freshmaker zal de zoutwaterkegel echter lokaal verdwijnen en na de derde ASR-cyclus zal deze het functioneren van de Freshmaker niet langer negatief beïnvloeden.

Twee 3D-effecten die bij de activiteiten van de Freshmaker optreden zijn geïdentificeerd. Het eerste 3D-effect was opkegeling van zoutwater aan de kopse kanten van de HDDWs, door de beperkte lengte van HDDW2 ten opzichte van HDDW1. Het tweede 3D-effect werd waargenomen in het centrale deel van de HDDWs waar grotere stijghoogtevariaties en kortere stroombanen vanaf het zoet-zoutwatergrensvlak naar de HDDWs resulteerden in opkegeling van zoutwater.

De invloed van operationele parameters (verschillende pompdebieten, variabele duur van zoetwateronttrekking, gevoeligheid voor putstoring, opschaling) op de werking van de Freshmaker is onderzocht. Er bestaat een sterk omgekeerd evenredig verband tussen het succesvol functioneren van de Freshmaker en de onttrekkingsratio tussen HDDW1 en 2. De maximale productie in Ovezande kan worden behaald met een onttrekkingsratio van 1.5. Correct beheer van HDDW2 is van groot belang voor het behalen van de maximale opbrengst. Deze wordt naast het absolute onttrekkingsdebiet ook beïnvloed door de timing van de onttrekking door HDDW2. Uit het onderzoek is gebleken dat het debiet van HDDW2 gedurende de injectiefase zo laag mogelijk moet zijn om verliezen door kortsluitstroming van injectiewater te voorkomen.

Een gedetailleerde beschrijving van het potentiële doelpakket voor een Freshmaker is van cruciaal belang voor het behalen van de maximale zoetwateropbrengst. De Freshmaker kan prima functioneren in de meeste hydrogeologische contexten maar de maximale zoetwateropbrengst varieert sterk. De grootste zoetwateropbrengsten kunnen worden behaald in pakketten met een lage doorlaatbaarheid, anisotrope pakketten en pakketten met een hoge porositeit.

De potentie van de Freshmaker om ASR in brakke en zoute pakketten mogelijk te maken en daardoor de huidige en toekomstige waterstress in kustgebieden wereldwijd te verminderen is met deze studie bevestigd.

Summary

Global population growth, climate change, pollution, and over-exploitation set the stage for a broad range of problems that ultimately affect the future availability and distribution of our most valuable resource: freshwater. Many parts of the world experience seasonal or long-term imbalances between freshwater supply and demand. Increasing freshwater storage helps to bridge the water gap between wet and dry periods and is one of the major adaptations needed to provide sufficient water in times of demand.

Although freshwater can be stored on the surface, storing freshwater below ground has a distinct advantage given the unparalleled storage capacity of aquifers and relatively low costs. A technique that effectively injects freshwater surpluses in the subsurface for use in times of freshwater demand is called "aquifer storage and recovery" (ASR). However, significant freshwater losses may occur when ASR is applied in brackish or saline aquifers as a result of mixing with the native groundwater and buoyancy effects, which displaces the injected freshwater due to density differences between the injected freshwater and native groundwater. The Freshmaker is an innovative technique which improves the application of ASR in brackish and saline aquifers using an advanced setup with two superimposed parallel horizontal directional drilled wells (HDDWs). One shallow HDDW which is used for ASR (HDDW1) and another at a greater depth (HDDW2) to intercept the saltwater that underlays the freshwater lens which limits freshwater losses due to buoyancy driven flow.

In this modelling study, a SEAWAT-model was built with the field data that came available from a pilot site in Ovezande (the Netherlands), where the Freshmaker is currently being tested. The performance of the Freshmaker was studied and the Freshmaker was optimized by proposing some design and operational modifications.

It was found that higher freshwater productions might be feasible at the Ovezande pilot than currently are targeted. The maximum freshwater production of the Freshmaker in Ovezande was derived at about 6000 m^3. A draining ditch is located nearby the Freshmaker at the Ovezande field site, below which a saltwater cone is situated . Modelling simulations have shown that this will reduce the freshwater production in the first three ASR-cycles. Nevertheless, the saltwater cone will be removed by activity of the Freshmaker after the third ASR-cycle and Freshmaker performance will no longer be hampered.

Two 3D-effects that influenced the performance of the Freshmaker were identified. The first 3D-effect was upconing of saline water at the outer ends of the HDDWs due to the limited length of HDDW2 compared to HDDW1. The second 3D-effect was observed in the central part of the HDDWs, where greater hydraulic head fluctuations and shorter flow lines from the fresh-saltwater interface towards the HDDWs resulted in upconing of saline water.

The influence of different operational parameters (e.g. varying pumping rates, varying recovery period lengths, sensitivity to well failure, upscaling) on the performance of the Freshmaker was studied. The performance of the Freshmaker was strongly correlated to the pumping ratio of HDDW1 and 2. The pumping ratio that will produce the maximum recoverable freshwater volume at Ovezande was determined at 1.5. Good management of the pumping rate of HDDW2 is important for successful application of the Freshmaker. The performance is not just sensitive to the absolute pumping rate of HDDW2 but also to the timing of abstraction by HDDW2. It became clear that the pumping rate of HDDW2 during the injection phase should be minimised to prevent short-circuiting of injection water.

A detailed characterization of the target aquifer for a potential Freshmaker was found to be of great importance to achieve the highest freshwater production. Although the Freshmaker may perform well in most hydrogeological settings, the maximum recoverable freshwater volume varies significantly. Larger recoverable volumes of freshwater can be achieved from low hydraulic conductivity aquifers, anisotropic aquifers and highly porous aquifers.

This study verified the great potential of the Freshmaker to alleviate water stress in coastal areas worldwide and showed that the Freshmaker makes successful application of ASR in saline aquifers possible.

Table of Contents

1 Introduction

1.1 The increase of water stress

Global water demand has tripled since the 1950s, while the freshwater resources have declined (Gleick, 2003). Water use is impacted by climate change (e.g., irrigation demand increases with rising temperatures) but more importantly by changes in population, lifestyle, economy, and technology (Kundzewicz et al., 2008). Global population will increase to more than 9 billion by 2050 (UN, 2014) and this will increase the irrigation demand to meet the accompanied larger food production requirements. Food demand is a major factor determining global water demand, since food demand drives irrigated agriculture, which is the largest water consumer with 80% of global water use (Molden et al., 2007). When freshwater is not sufficiently available it thus adversely affects food security. One can therefore predict an increase of water stress since freshwater does not become more abundant but future freshwater demand will increase. Water scarcity refers to a situation where there is excess in water demand over available supply and is already a critical concern in many parts of the world (Fedoroff et al., 2010). By 2025, about 3 billion people will be water stressed (Serageldin, 2001). Proper management of the world's freshwater resources is a crucial factor in alleviating water stress.

1.2 Freshwater resources under projected climate change

Climate and freshwater systems are highly interconnected and therefore global freshwater resources are vulnerable to climate change (Kundzewicz et al., 2007). Especially the projected increased precipitation variability, which is a robust conclusion, consistent across climate model projections, is strongly related to the vulnerability of freshwater resources (Kundzewicz et al., 2007). The greatest vulnerabilities are in semi-arid and arid low-income-countries where precipitation and stream flow are concentrated over a period of a few months and year to year variations are large (Lenton, 2004). Although in some locations of the world the effects might be positive (i.e. increased mean precipitation, stream flow and groundwater recharge), overall, the negative impacts of projected climate change on freshwater resources outweigh its benefits (Kundzewicz et al., 2008). All these changes will enlarge the reliance on groundwater resources since the reliability of surface water decreases (Unsal et al., 2014).

Groundwater systems generally respond more slowly to climate change than surface water systems do. Nevertheless, groundwater resources are significantly affected by climate change. Groundwater recharge is strongly correlated to precipitation/evapotranspiration and stream flow and therefore indirectly to climate change. Decreasing groundwater recharge rates will directly affect the volume of groundwater stored in aquifers. Coastal groundwater systems are susceptible to seawater intrusion (SWI) which is also related to climate change. SWI is caused by decreasing groundwater recharge rates, over-pumping, and sea level rise, which is triggered by thermal expansion of the oceans and melting of ice caps and glaciers (Ranjan et al., 2009). Additionally, groundwater mining and pollution further decrease the size of subsurface freshwater resources.

1.3 Call for a paradigm shift

It is important not to focus just on the physical freshwater resource availability but rather on the interactions between humans and freshwater resources. How humanity adapts to the challenges faced will make all the difference. There are two potential pathways when dealing with water scarcity, i.e. increasing water availability or decreasing water use. As discussed in the sections above, water availability is significantly affected by climate change, while water use is mainly driven by non-climatic factors. The focus of this MSc research is on increasing water availability.

In many locations of the world, the annual net water availability is sufficient to meet the water demand in absolute terms. However, quite often there exists an imbalance (i.e. a phase lag) between periods of freshwater surplus and demand and enhanced climate change will further intensify this imbalance. Increasing freshwater storage is one of the major adaptations which is needed in order to provide sufficient water in times of demand. Enlarging freshwater storage helps to bridge the water gap between wet and dry periods

and therefore alleviate water stress. Unfortunately, surface water storage potential is often limited due to high construction costs, evaporation, lack of space and negative environmental impacts of reservoirs behind dams. Subsurface storage, on the other hand, has unparalleled potential with respect to surface storage. Aquifers have huge storage capacity, water is protected from evaporation and pollutants, and construction costs are relatively low. Despite its potential to increase freshwater availability, subsurface water storage is largely neglected. It is clear that in order to deal with the water problems of the 21st century, a paradigm shift in the water management sector is needed. Instead of focussing adaptation strategies just on surface storage, it is necessary to acknowledge the storage potential of the subsurface. This can only be achieved with the on-going development of existing and new techniques which make sustainable and efficient freshwater storage in the subsurface possible.

1.4 The Freshmaker: a promising technique

A technique that effectively stores freshwater in the subsurface is called "aquifer storage and recovery" (ASR). During the ASR process, freshwater surpluses are injected and stored in the subsurface for use in times of freshwater demand and they are effective for overcoming freshwater shortages. The first ASR-system was installed 1968 and by 2005, 72 known ASR installations were already functioning and more than 100 were in development in the USA only (Pyne, 2005). ASR is also widely practised in the Netherlands, where, for instance, the glass house sector is storing rainwater in the subsurface. Most ASR-systems are storing water in fresh aquifers but about one-third are storing freshwater in brackish or saline aquifers (Pyne, 2005). Although the application of ASR in freshwater aquifers is relatively easy, the application of ASR in saline and brackish aquifers is significantly more complex, as is described in detail in Chapter 2. When ASR is applied in brackish or saline aquifers, success can be hampered by mixing of the injected freshwater with the native groundwater and by buoyancy effects, which displaces the injected freshwater due to density differences between the injected freshwater and native groundwater. These processes may lead to significant freshwater losses. However, especially the locations with brackish or saline aquifers (i.e. coastal regions) will experience increasing water stress in the (near) future. Currently, about 60% of the world's population lives within 60 km of the coast and this proportion will rise to 75% within two decades (Unsal et al., 2014). This, in combination with shrinking coastal groundwater reserves, displays the need to develop new techniques which improves the successful application of ASR in brackish and saline aquifers.

A new innovative technique which improves the application of ASR in brackish and saline aquifers is called "the Freshmaker" (Zuurbier *et al.,* 2013). What distinguishes the Freshmaker from conventional ASR techniques is the use of horizontal directional drilled wells (HDDWs) which came available due to recent developments in hydrologic engineering. Using HDDWs instead of vertical wells increases the potentially recoverable volume of freshwater (Cirkel *et al.,* 2010). The Freshmaker uses an advanced setup with the installation of two superimposed parallel HDDWs (Fig 1.1). One shallow HDDW which is used for the injection and recovery of freshwater and one HDDW at a greater depth which intercepts the saltwater that underlays the freshwater lens. The effect of this interception well is that freshwater is not lost due to buoyancy driven flow, as is the case with conventional ASR-systems.

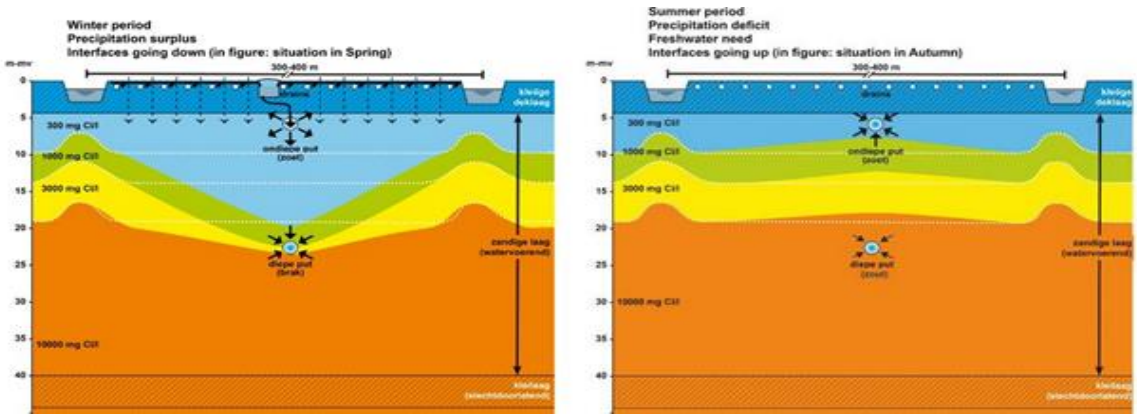

Figure 1.1 - The Freshmaker concept. Left: Injection of surplus precipitation water during the winter period. Right: recovery of injected freshwater for freshwater need during the summer period. Source: www.kwrwater.nl.

1.5 MSc Research

The development of the Freshmaker is important from a water resource management point of view. Thin, brackish aquifers which were previously found unsuitable for ASR may become potential ASR locations due to the HDDW technology and the use of a brackish or saline water interception well. However, the Freshmaker is a new technique and more research is needed in order to exploit its promising potential as an effective solution to alleviate water stress in coastal areas worldwide.

The Freshmaker is currently being field-tested at a pilot location in Zeeland, a province in the South West of the Netherlands. The first results of the pilot indicate that the Freshmaker concept not just works in theory but can indeed be successfully applied in practice. The Freshmaker is a young technique and this is the first pilot study, so there are still unknowns regarding the functioning and optimization of the Freshmaker. A thorough understanding of the design criteria of the technique is important in order to successfully implement the technique at locations which have different hydrogeological boundary or climatic conditions. For the Freshmaker pilot only some basic modelling research has been performed and the understanding of the hydrological dynamics of the fresh/saltwater interface can still be improved. The main goal of this MSc research is to *"study the performance of the Freshmaker at the pilot location and optimize the Freshmaker technique by analysing factors that influence the recovery efficiency and storage capacity"*.

The MSc research project is part of a larger research project in which the Freshmaker has been developed. During the research project sufficient hydrogeological data has been collected which was used to build and calibrate variable-density groundwater models with which the functioning of the Freshmaker was analysed.

The research questions that will be answered to achieve the main goal, are:

- What is the significance of effects on the outer edges of the HDDWs? It is believed that they can be neglected and the processes can be conceptualized in two dimensions.
- What is the maximum freshwater storage capacity of the Freshmaker in the current Ovezande setup and how can this be increased? It is hypothesized that a larger storage capacity can be achieved by different well configurations and freshwater infiltration/saltwater abstraction ratios.
- How well does the Freshmaker perform in a different hydrogeological context? It is expected that larger values of hydraulic conductivity will decrease the recovery efficiency.
- What will happen if the interception well abstraction rates fall for a long period due to well clogging or other errors? It is hypothesized that in a case of significant well clogging or failure the effectiveness of the Freshmaker is only negatively impacted in the recovery phase, not during the injection and storage phases.
- What is the effect of upscaling, i.e. increasing the number of Freshmakers in one aquifer? It is hypothesized that upscaling increases the average recover efficiency of the Freshmaker.
- What is sensitivity of different operational variables on the recovery efficiency of the Freshmaker? It is hypothesized that especially pumping rates have a significant influence.

2 Theoretical framework of aquifer storage and recovery

As explained in Chapter 1, it is important to make more use of the subsurface for freshwater storage given the water related issues of the 21st century. It was also discussed that aquifer storage and recovery (ASR) is a good technique for this but that the applicability of ASR in coastal regions is complex and often limited. ASR is described in detail in this chapter and the current academic literature is discussed. The focus will lay on the application of ASR in brackish and saline aquifers. Different aspects that may limit the success of ASR in these aquifers are discussed individually. Furthermore, some new techniques to overcome these difficulties are discussed.

2.1 ASR

ASR is increasingly being used as a tool to provide additional freshwater storage to balance seasonal freshwater supply and demand. The process of ASR is typically as follows: freshwater (which comes available in periods of surplus) is injected into an aquifer via a well; it is stored in the aquifer and withdrawn (or recovered) when it is needed (Figure 2.1). Pyne (1995) uses a strict definition for ASR in which injection and recovery occurs through the same well. However, in this MSc thesis the definition is less strict: ASR is the subsurface storage of water in aquifers during times of surplus and abstraction in times of demand. Any technique that stores surplus freshwater in an aquifer for later use can called an ASR technique. Managed aquifer recharge (MAR), on the other hand, is an even broader definition, and is the introduction of water into an aquifer (e.g. by wells or infiltration ponds) without necessarily having the direct goal to abstract it again on the same location.

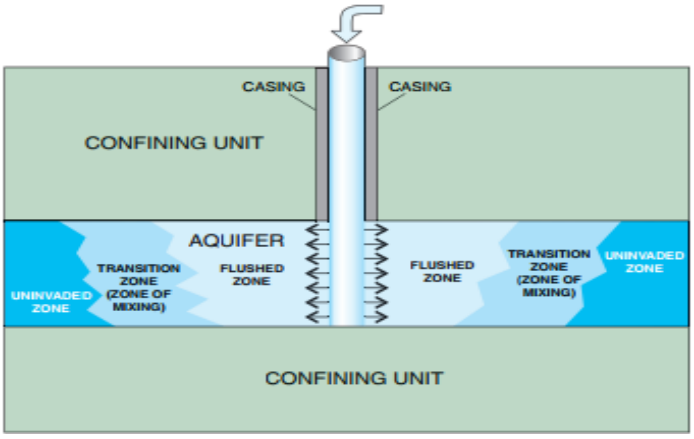

Figure 2.1 - Schematic representation of a typical ASR-system. Source: Reese (2004).

ASR is an alternative to surface water storage such as dams and reservoirs. A distinct advantage of aquifer storage over surface storage is the storage capacity of aquifers. Aquifer systems can accommodate multiyear storage below ground, where it is protected from evaporation and pollutants. Aboveground, water wells can often be located where needed and occupy little space. This makes ASR a cost-effective technique for providing freshwater storage.

It is necessary to successfully store freshwater in the aquifer in order to have a proper functioning ASR-system. The ASR-system has lateral and vertical boundaries, analogous to the walls of a tank (Maliva et al., 2006). When injection takes place in a freshwater aquifer, these "walls" are basically the vertical and lateral boundaries of the aquifer. ASR-systems in freshwater aquifers are usually relatively simple compared to ASR-systems in brackish or saline aquifers. Nevertheless, this does not mean that geochemical processes (fluid-matrix interactions) are not a concern. Injected freshwater will typically not be in chemical equilibrium with the aquifer sediment and native waters. This may result in mineral dissolution and precipitation reactions and various sorption reactions (Maliva et al., 2006). When freshwater is stored in a brackish or saline aquifer it displaces the native, poor quality water and the "walls of the tank" are therefore the boundaries between the stored freshwater and ambient groundwater. ASR-systems in brackish or saline aquifers are hydrogeologically complex and extensive research and modelling is needed before such a system can operate successfully.

2.2 ASR in brackish aquifers

According to Ward *et al*. (2007), the first time the concept of performing ASR in brackish aquifers had been proposed in the literature was by Cederstrom (1947) and became more common in the 1960s and 70s. About one-third of the current ASR-systems is situated in brackish to saline aquifers (Pyne, 2005). This number is expected to increase since more and more freshwater shortages are projected in coastal aquifers (see Chapter 1). ASR-system performance is usually expressed in terms of recovery efficiency. Recovery efficiency (RE) is the ratio of the recovered water to the water injected.

$$RE = \frac{V_r}{V_i} \qquad (2.1)$$

Where:
V_r = volume of freshwater recovered (with a satisfying quality) [L^3]
V_i = volume of freshwater injected [L^3]

In ASR practice, the water that is recovered (V_r) is not limited to water with identical concentration as the injected water but is the volume of water with a concentration up to a concentration limit. This threshold concentration is usually determined by legislation. The ASR-system might not be able to satisfy the water demand when RE is low and therefore fail. Low REs can be caused by various aspects, which include: dispersive mixing between the injected freshwater and native aquifer water, migration of the injected water due to lateral low and density-driven flow and the occurrence of heterogeneities in aquifers (e.g. Missimer et al., 2002; Maliva et al., 2006 Ward et al., 2009). The sections below discuss the processes which are responsible for low REs.

2.3 Lateral flow

The influence of lateral flow on the RE was addressed, for instance, by Bear and Jacobs (1965) and Pavelic et al. (2002). However, since they modelled 2D areal flow, they did not consider density effects (the vertical dimension was neglected). The effect of lateral is different for each phase of the ASR-cycle and can best be understood when looking at Figure 2.2. Lateral flow during the injection phase can result in a plume that is not circular but ovoid: significantly more of the injected water travels downstream than upstream (L_i in Figure 2.2). During recovery, the water that is captured by the well is a mirror image of the injected plume, if pumping at the same rate and for the same duration (L_r in Figure 2.2). It is obvious that if the lateral flow is sufficient to create a significantly non circular injection plume and capture zone, the volume of recovered water will be significantly smaller than the volume of injected water and the RE will be low. It is theoretically possible to obtain near-circular plume and capture zone if the pumping rates during injection and recovery are sufficiently high compared to the lateral flow. However, irrespective of the shape of the injected plume and the well's capture zone, during the storage phase, the injected freshwater can flow down gradient along with the lateral flow. If the injected freshwater drifts during storage it may significantly reduce the recoverable volume of freshwater and hence RE.

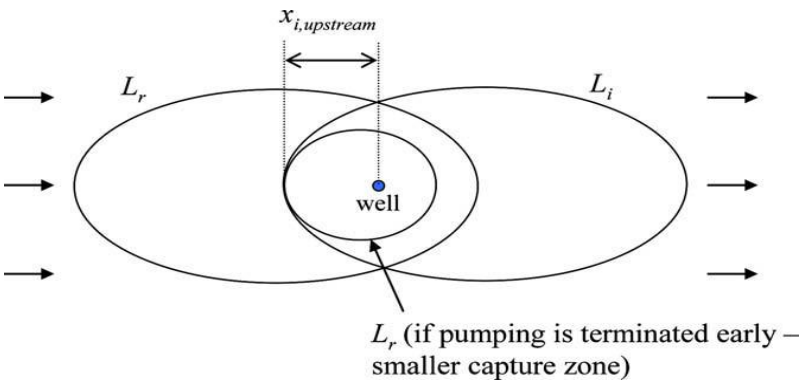

Figure 2.2 - Effect of lateral flow on ASR recovery efficiency. L_i shows the shape of the injected freshwater plume and L_r shows the shape of the capture zone. Source: Ward et al. (2008).

2.4 Density effects

Archimedes Principal (buoyancy) is a major factor determining whether an ASR-system in brackish or saline aquifers will succeed or fail. When there is a difference in density between injected and ambient water, buoyancy processes will always occur. When freshwater is injected into a brackish or saline aquifer, the density contrast between injected and ambient water leads to unstable interfaces at the edge of the injected freshwater bubble. The denser ambient water tends to push towards the bottom of the interface while the lighter injected water tends to flow over the ambient water. As a result, the interface is tilting and the shape of the bubble in transferred from cylindrical to conical (see Figure 2.3). This change in freshwater bubble shape reduces the recoverable volume since the ambient groundwater is now located much closer to the well at the bottom. This saltwater "toe" will reach the well earlier resulting in early termination of freshwater recovery before all of the injected freshwater has been recovered.

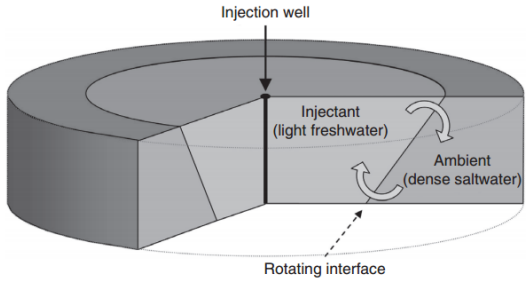

Figure 2.3 - Tilting of the fresh-saltwater interface due to a density difference between injected and ambient water. Source: Ward et al. (2007).

2.4.1 When are density effects significant?

Esmail and Kimbler (1967) were the first to consider reduction of REs due to tilting of the fresh-saltwater interface by to density effects. Despite the fact that the significance of density effects on ASR REs is currently well-known, density effects are still often neglected for practical modelling purposes (Ward *et al.*, 2007). In practice, the assumption that density effects are negligible, may quite often be satisfactory, however they are not verified. There is no straightforward answer to the question whether density effects may be neglected or not. Missimer and Guo (1999) showed that achieving a RE of 80% was possible in a brackish aquifer with a TDS concentration of 4500 mg/L but not when the aquifer had a salinity equal to seawater. They concluded that "*if the aquifer contains water with a TDS of over 20.000 mg/L it is extremely difficult to achieve reasonable recoveries unless the aquifer is thin and has a generally low transmissivity*". However, terms as "relatively", "significant", "thin" and "generally low" have only limit value as a guideline to determine whether density variations can be neglected or not since there is no reference to compare them to. It can be concluded that the answer to the question whether density effects limit the success of a potential ASR project remains in itself quite arbitrary. In fact, while the mechanism behind the loss of RE can be related to interface tilting due to density effects, it is quite often not the absolute density difference between injected and ambient groundwater that determines the success of ASR in a certain location. A complex mix of factors such as freshwater storage time, aquifer dispersivity and aquifer heterogeneities determine whether a given density difference will lead to a reduction of recoverable injected water. Furthermore, the actual significance of density effects may be different for each phase of the ASR cycle. In the next subsections the influence of density effects will be discussed for the different phases separately.

2.4.2 Density effects during injection and recovery

Most authors assumed the most significant tilting of the interface occurred during the storage phase and neglected interface tilting during injection or recovery. Ward et al. (2007) showed that under certain conditions there can indeed be significant density induced tiling during pumping. It may for instance be so that the pumping rate during recovery is not high enough to overcome density induced tilting and the top of the interface may continue to move away from the well. Ward et al. (2007) strictly advise not to disregard the density effects before a fully mixed convection system characterization has been performed. To examine the relative strengths of both free and forced convection the mixed convection ratio (M) is often used. The mixed convection ratio is defined as the ratio of free over forced convection and shown in Equation 2.2 (Ward et al., 2007). The derivation of Equation 2.2 is shown in Appendix A.

$$M = \frac{v_{free}}{v_{forced}} = \frac{2\pi r B \overline{K_z}}{Q} \frac{\rho(C_s) - \rho_0}{\rho_0} \quad (2.2)$$

Where:
v_{free} = free convection [L/T]
v_{forced} = forced convection [L/T]
r = radius of the injected freshwater bubble [L]
B = aquifer thickness [L]
$\overline{K_z}$ = average vertical hydraulic conductivity [L/T]
Q = pumping rate [L^3/T]
$\rho(C_s)$ = ambient water density [M/L^3]
ρ_0 = injection water density [M/L^3]

If M<<1, then forced convection is dominant and interface tilting is relatively insignificant. If M>>1, then free convection is dominant and interface tilting will be significant. As M approaches 1 they are of comparable strength and interface tilting is expected to become significant in this transition zone. Equation 2.2 shows that during storage the system is entirely free convective (Q = 0, so M = ∞). However, it also shows that when aquifers are thick (B is large), or have high vertical conductivities, density driven flow can be significant despite having a relatively low density contrast. It is therefore important to consider all parameters in Equation 2.2 before determining whether density effects during the pumping phase can be safely neglected.

It has been discussed above that the width of the mixing zone between injected freshwater and ambient groundwater had a major influence on the rate at which the interface will rotate. However, Equation 2.2 does not include the effect of dispersion and might therefore overestimate the influence of density driven flow.

2.4.3 Density effects during storage

The volume of water lost during storage because of density effects depends both on the mixing zone width and the amount of interface tilt. According to Esmail and Kimbler (1967) a narrow mixing zone leads to a larger density gradient (defined as the density difference divided by the mixed zone width) and a faster interface tilt. This was also shown though numerical modelling by Ward et al. (2007) who demonstrated that wider mixing zones tend to attenuate interface rotation. Apparently there is a significant interplay between different factors in the ASR-system. The hydraulic conductivity affects the density stratification; dispersivity affects the mixed zone width which affects the density gradient hence the rate of interface tilting. However, despite the presence of a wide mixing zone and a low hydraulic conductivity, significant interface tilting could occur if the water is stored for a significantly long time (Bakker, 2010; Ward et al., 2007). Theoretically, if given sufficient time, even a relatively small density contrast could convert a cylindrical plume into a cone and leads to a reduction in RE.

In order to assess the effect of density driven flow during storage, the mixed convection ratio (Equation 2.2) becomes meaningless. In a free convective system the onset of instability is determined by the value of a dimensionless number called the Rayleigh number (Ra). A form of the Rayleigh number as proposed by Ward et al. (2008) is given in Equation 2.3. The derivation is shown in Appendix B.

$$Ra = \frac{Buoyancy\ and\ gravitation}{dispersion} = \frac{2\overline{K_z}\sqrt{\pi B^3 t}}{\beta_L \sqrt{Q\theta}} \frac{\rho(C_s) - \rho_0}{\rho_0} \quad (2.3)$$

Where:
$\overline{K_z}$ = average vertical hydraulic conductivity [L/T]
B = aquifer thickness [L]
t = injection duration [T]
β_L = longitudinal dispersion [L^2/T]
Q = pumping rate [L^3/T]
θ = porosity [-]
$\rho(C_s)$ = ambient water density [M/L^3]
ρ_0 = injection water density [M/L^3]

When Ra is low, free convection is significantly retarded by the dispersive mixing that occurred during the injection phase. At higher values of Ra, density driven flow is expected to be larger. Equation 2.3 clearly shows the effect of vertical hydraulic conductivity and dispersion, which are proportional and inversely proportional to Ra respectively. At lower values of vertical hydraulic conductivity and at higher values of longitudinal dispersivity the effect of density driven flow is less pronounced.

2.5 Full mixed convection

The full mixed convection system with lateral flow is significantly more complex than the constituent advective or buoyancy driven flow processes alone. Figure 2.4 shows for each phase the hypothetical resulting flow domain that may occur after superposition of radial flow into and out of the well, uniform background flow and density induced buoyancy flow. Furthermore, it can be seen that for each phase the resulting flow fields will be different. The derivation of an analytical solution that describes the full complexity of the mixed convection and temporal changes in the flow field is considered intractable. The analytical solutions that may be found in the literature can account for one or two elements of the problem, but never all of the processes together at once (Ward et al., 2009). This highlights the need for a careful assessment of the full mixed convection system before a planned ASR operation is started, since none of the previously discussed dimensionless numbers is capable of giving complete insight in the system. Bakker (2010) and Ward et al. (2009) developed some ASR-prediction tools which have some predictive power to avoid particularly bad location and reduce the risk of failed projects. Nevertheless, since there exists no analytical solution of the full mixed convection system, numerical modelling will be the only tool left to determine the likeliness of success or failure of a certain ASR "hot spot" found using the ASR prediction tools.

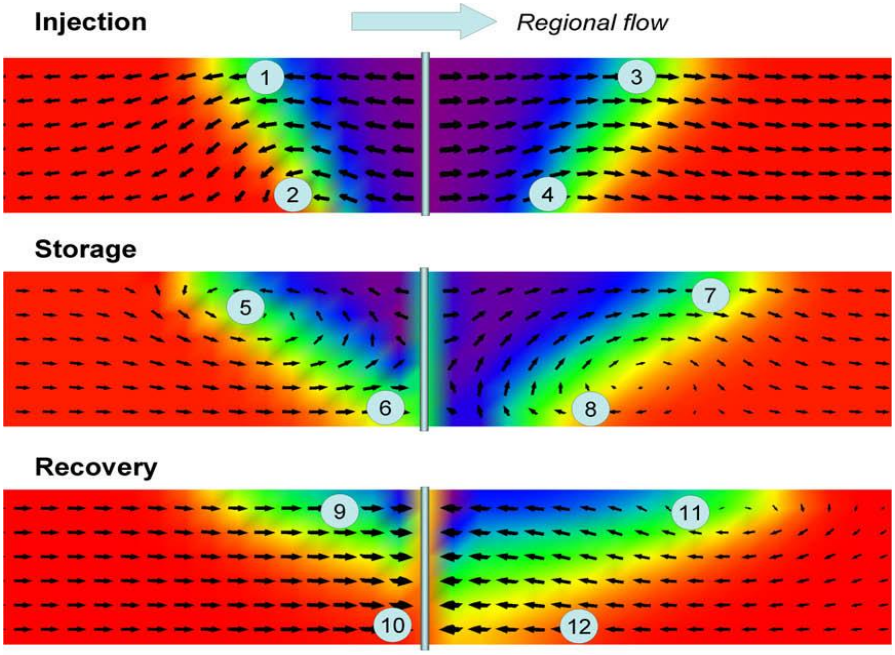

Figure 2.4 - Flow domains that may occur after superposition of radial flow into and out of the well, uniform background flow and density induced buoyancy flow. The domain numbers are explained in Table 2.1 below. Source: Ward et al. (2009).

Table 2.1 Explanation of the different flow fields shown in Figure 2.4.

Number in Fig. 2.4	Mechanism behind resulting flow field
1	Pumping reinforces with density-induced convection but competes with lateral flow
2	Density-induced convection reinforces with lateral flow but competes with pumping
3	Pumping, lateral flow and density-induced convection all reinforce.
4	Pumping reinforces with lateral flow but competes with density-induced convection
5	Density-induced convection competes with lateral flow
6	Density induced convection reinforces with lateral flow
7	Density induced convection reinforces with lateral flow
8	Density-induced convection competes with lateral flow
9	Pumping reinforces with lateral flow but competes with density-induced convection
10	Pumping, lateral flow and density-induced convection all reinforce.
11	Density-induced convection reinforces with lateral flow but competes with pumping
12	Density-induced convection reinforces with pumping but competes with lateral flow

2.6 Influence of aquifer anisotropy and heterogeneity on ASR recovery efficiency in saline aquifers

The shape of the injected freshwater is usually described by using a bubble metaphor. However, when aquifers are heterogeneous and anisotropic (as is often the case in the field) this is actually a wrong representation of reality (Figure 2.5). Ward et al. (2008) showed that when aquifers are anisotropic higher REs may be expected for large density contrasts than in isotropic aquifers. This can be explained by the fact that the density-induced tilting effect is reduced by the lower vertical hydraulic conductivity compared to the horizontal conductivity. As explained above, this coincides with equations 2.2 and 2.3, which predict that lower vertical conductivities give low values for Ra and M and therefore less influence of buoyancy driven flow.

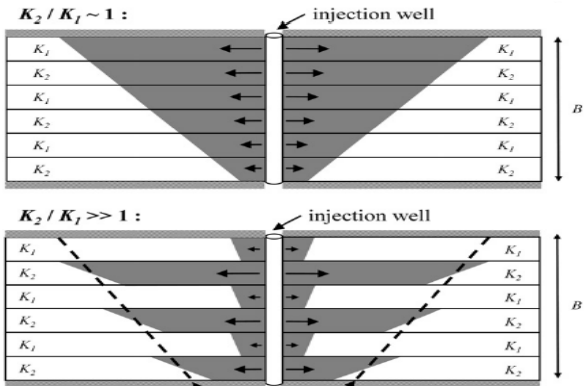

Figure 2.5 - Expected difference in injected plume shape between a homogeneous and heterogeneous aquifer. Source: Ward et al. (2008).

Varcher et al. (2006) proposed that for predicting the RE it is not necessary to take aquifer heterogeneity explicitly into account. No significantly different results were found between simulations with and without aquifer heterogeneity. This can be understood when realizing that during ASR operations, equally more water will be injected but also will be recovered in high conductive layers as in low conductive layers. So the net effect of heterogeneity will be zero. However, ASR-systems in saline heterogeneous aquifers might actually suffer from lower REs due to density effects, which was not considered by Varcher et al. (2006). The process responsible for this is shown in Figure 2.6. Salt water will be flushed out of high permeable layers by the injected freshwater, but salt water will largely remain in layers with low permeability since the freshwater will not be able to penetrate those layers during injection. At the end of injection, water with higher density is located above water with lower density. This is a highly unstable density configuration and leads to a mixing process called fingering. During storage, saltwater can migrate downwards from the low permeability layers and bleed into the high permeable layers containing freshwater. At the same time, buoyant freshwater can flow upwards into the low permeable layers (Missimer, 2002). The result of this fingered mixing is that large volumes of freshwater ultimately become contaminated with saltwater, and that portions of freshwater become "trapped" in the low permeability zones. Consequently this can lead to a serious reduction of RE.

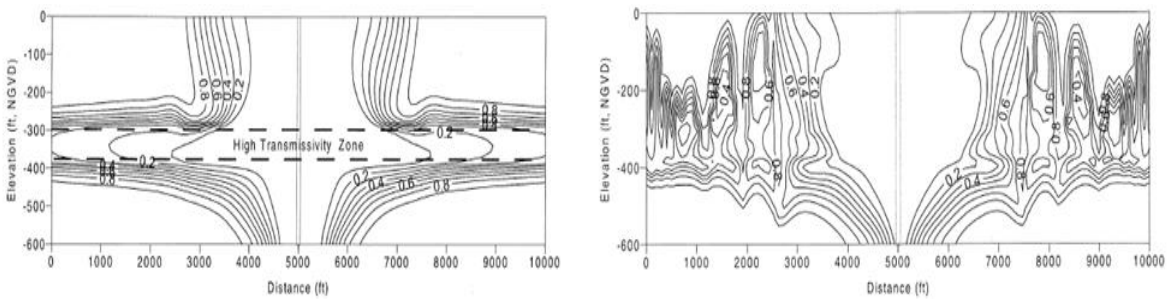

Figure 2.6 - Effect of heterogeneity on ASR performance. Left: during injection, freshwater travels a larger distance in the high permeability zone and becomes overlain by denser saline water. Right: during storage, dense salt fingers will enter the high permeability zone and contaminate the injected freshwater. Source: Missimer (2002).

2.7 Summarizing the constraints of ASR in brackish and saline aquifers

ASR can be a successful technique to provide sufficient water in times of demand. However, the RE may be low when ASR is applied in brackish or saline aquifers. It was shown that there is a wide range of causes which are responsible for decreasing REs. However, these mechanisms may be significant in one phase of the ASR-cycle but insignificant in another phase depending on site-specific hydrogeological conditions. In Table 2.1 the different ASR phases the processes responsible for low ASR REs in brackish and saline aquifers are summarized.

Table 2.2 –Processes responsible for low ASR performance in brackish and saline aquifers.

Mechanism	During the pumping phases	During the storage phase*
Lateral flow	Difference between the shape of injected water plume and well capture zone.	Injected freshwater flows down gradient and becomes unrecoverable.
Density difference	If M>>1, free convection is dominant and interface tilting may be significant.	If Ra is large, buoyancy driven flow may be significant.
Dispersion	Large dispersivity values may result in a wide transition zone and hence a limited effect of density differences.	Large dispersivity values decreases buoyancy driven flow.
Anisotropy and heterogeneity	Higher anisotropy ratios decrease the rate of interface tilt which increases the RE.	Higher anisotropy ratios decrease the rate of interface tilt which increases the RE. However, in layered aquifers the RE may be decreased due to fingered mixing.

** The most important aspect of the storage phase is the length of the storage period. If stored sufficiently long, even small density differences may result in low REs despite other, mitigating factors as a wide mixing zone or a high anisotropy ratio.*

2.8 Strategies to increase RE

In the literature, several strategies to increase the REs in brackish and saline aquifers are proposed. With the use of such techniques it can be possible to obtain reasonable REs at locations that would otherwise be labelled "unsuitable" using the prediction tool developed by Ward et al. (2009). For instance, Pyne (2005) advises to inject a large volume of freshwater (prior to injection of water that is to be recovered) to flush out the native waters and create a buffer zone between the injected freshwater and native aquifer water. This should also reduce the rate of interface tilt due to buoyancy flow since a larger mixing zone is greated. However, such freshwater investments might not be available at the targeted ASR location and buoyancy effects may still lead to early salinization of the bottom of the well for some locations (Zuurbier et al., 2013). Preferential recovery where freshwater is only recovered in the upper part of the aquifer is another technique that might improve RE (Maliva et al., 2006). Zuurbier et al. (2013) showed in a field study that preferential freshwater recovery using multiple partially penetrating wells (MPPWs) successfully increased REs from 15% to 60%.

The Freshmaker (Figure 1.1; Zuurbier et al., 2014) is a new ASR technique by which brackish or saline aquifers become potentially available for freshwater storage. Opposed to conventional ASR-techniques which use vertical wells, the Freshmaker uses horizontal directional drilled well (HDDW) technology. The Freshmaker consists of two superimposed parallel HDDWs. The deeper well functions as an interception well of the brackish/saline water successfully decreassing the loss due to buoyancy driven flow. The shallower well as an ASR-well. Although not only limited to, thin and unconfined brackish/saline aquifers (which were previously thought unsuitable for ASR) become potentially available for freshwater storage.

As explained in Chapter 1, the Freshmaker may have great potential for freshwater management in water stressed coastal regions. The Freshmaker is studied during this MSc Research and will be explained in greater detail in the next chapter.

3 Methods

Application of ASR-techniques in saline and brackish aquifers is often unsuccessful, as is discussed in detail in the previous chapter. However, it was proposed that the new Freshmaker technique may significantly improve the applicability of ASR in coastal aquifers. This chapter explains how the Freshmaker technique was studied during this MSc-research. Section 3.1 describes the Freshmaker currently applied in the pilot study, including a description of the geomorphology and hydrology of the pilot location. Section 3.2 describes the research strategy. The groundwater models that were used are not described in detail in this chapter but the reader is referred to Appendix B where they are described in detail. The data analysis that was performed to calibrate the groundwater models is described in Appendices C and D. The different modelling scenarios that were used in the simulations are explained in Section 3.3.

3.1 Freshmaker Pilot

3.1.1 Geomorphology of the area

The pilot location is situated in the Dutch province of Zeeland, which is located in the south-western delta of the Netherlands. The current landscape, groundwater salinity, and groundwater flow systems of Zeeland are the result of sequential Holocene marine transgressions and regressions, and anthropogenic influence such as peat mining and land reclamation. Zeeland was submerged due to a continuous sea level rise in the Holocene from 7500 BP till 5000 BP (Vos and Zeiler, 2008). During this period, the underlying Pleistocene aquifers salinized by infiltrating seawater which had a higher density and therefore flushed out the freshwater by free convection (Post, 2004). Later, when sedimentation processes began to dominate, the land rose above means sea level since the maximum transgression was reached. This enabled rainwater to infiltrate and peat was formed under the resulting wet, freshwater conditions, covering Zeeland from 3800 BP till 2000BP. Due to the activity of man (who mined the peat and drained the land), and enhanced by marine erosion and land subsidence Zeeland became again totally submerged from 350 AD till 750 AD. The resulting landscape was characterized by tidal creeks and flats. Around 1000 AD, people started to reclaim large pieces of land by the embankment of the supra-tidal flats, creating the so-called polders. These polders were artificially drained and shrinkage of peat and clay resulted in further subsidence of the land surface. The present topography of Zeeland is therefore a result of the age of reclamation: the lower the land surface, the older the land. Since the former tidal creeks consisted of sand, they did not subside like the surrounding clayey and peaty salt marshes and can now be seen as local elevations in the landscape (de Louw, 2011). Such a landscape, in which the present topographical features have reversed their elevation relative to other features, is called an 'inverted landscape' (Figure 3.1).

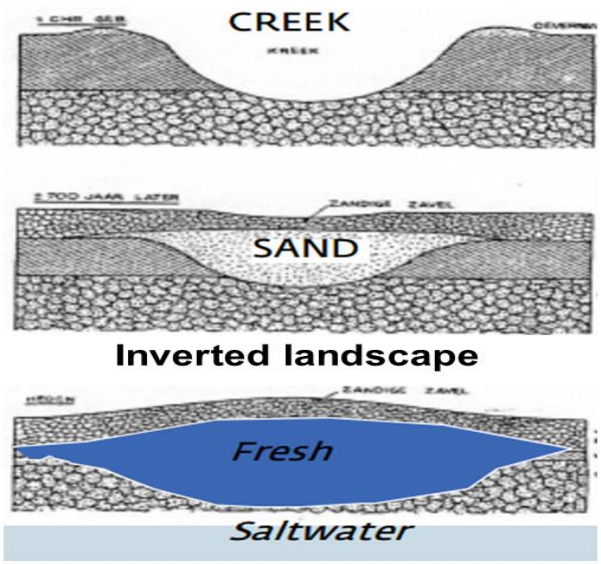

Figure 3.1 - Evolution of a creek ridge (source: Rijkstuinbouwconsulentschap, 1951).

The Freshmaker was installed in a 5 km wide sandy creek ridge near the village of Ovezande (Figure 3.2). The creek ridge has elevations up to 2 m above mean sea level (m-ASL) and is surrounded by peat and clay deposits (0-1.5 m below mean sea level (m-BSL)). The Freshmaker is installed in a phreatic aquifer which is relatively homogeneous, consisting of fine to medium fine sand, with a mean grain size of 150 to 200 um (Figure 3.3). The grain size distribution shows the typical fining-up sequence corresponding to the geological history of a creek ridge. As the tidal creek gradually filled up, the energy of the tidal system decreased. This resulted in smaller particles being transported by tidal processes and hence deposition of finer sediments over time. At a depth of about 30 m-BSL a 2 m thick clay layer is present, separating the upper aquifer from a deeper sandy aquifer. The top of the upper aquifer consists of silty material but the aquifer can still be considered phreatic given the fluctuations of the groundwater table following recharge events.

Figure 3.2 - Location of the Freshmaker pilot.

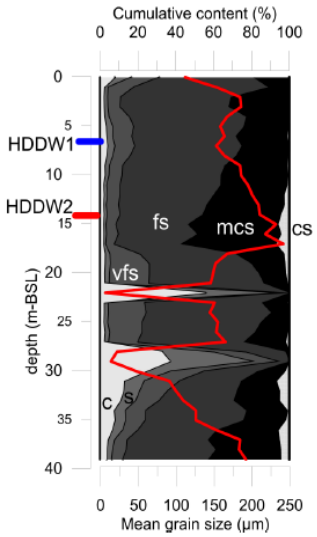

Figure 3.3 - Grain size distribution at MW1. c = clay, s = silt, vfs = very fine sand, fs = fine sand, mcs = medium coarse sand, cs = coarse sand. Mean grain size is indicated in red. Source: Zuurbier et al. (2014).

3.1.2 Hydrology of the area

Freshwater is scarce in the study area since the Freshmaker site is located on a peninsula surrounded by saline water of the Scheldt estuaries and due to seepage of saline groundwater which is a remnant of Holocene transgressions. The hydrology of the pilot location can be divided in two separated regions based on the geomorphology described in Section 3.1.1: 1. Low-lying polders with saline seepage and 2. the sandy creek ridge containing a freshwater lens created by infiltrating freshwater. The Freshmaker was installed at

the creek ridge. Draining water courses on the creek ridge are deep, and have controlled water levels of 0.6 (summer) to 0.7 (winter) m-BSL. During dry periods they salinize to reach electrical conductivities (EC) up to 5000 µS/cm. Water with such an EC can be characterized as brackish.

Continuous vertical electrical soundings (CVES) were conducted to map the lateral extend of the freshwater lens (Zuurbier et al., 2014, Figure 3.4). The CVES results indicate the presence of a freshwater lens with a thickness up to 10 m in the creek ridge and 0-2 m under the low-laying, draining areas. At three monitoring wells near the Freshmaker (locations shown in Figure 3.4) the exact position of the fresh-saltwater interface and the thickness of the mixing zone was found using geophysical borehole logging (EM-39). A freshwater lens thickness of about 9 m and a mixing zone of approximately 6 m at the location of the Freshmaker was found this way.

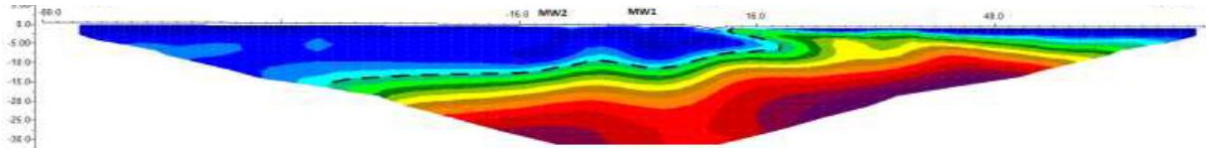

Figure 3.4 - CVES results at the Freshmaker pilot site. CVES trajectory shown in Figure 3.5. Source: Zuurbier et al. (2014).

3.1.3 The Freshmaker at the pilot location

As discussed in Section 2.8, the Freshmaker is an advanced ASR-system. The first major difference between the conventional ASR wells (Chapter 2) is that the Freshmaker uses horizontal directional drilled wells (HDDWs) instead of vertical wells. Using HDDWs instead of vertical wells already increases the potential recoverable volume of freshwater from a shallow freshwater lens (Cirkel *et al.,* 2010). The second major difference is that in the Freshmaker-setup a pair of parallel superimposed HDDWs was installed with the upper HDDW functioning as the ASR-well and the lower HDDW functioning as an interception well. The fresh-saltwater interface can be actively managed with this advanced setup, limiting freshwater loss due to mixing with native groundwater or due to buoyancy driven flow, as is the case with conventional ASR-systems.

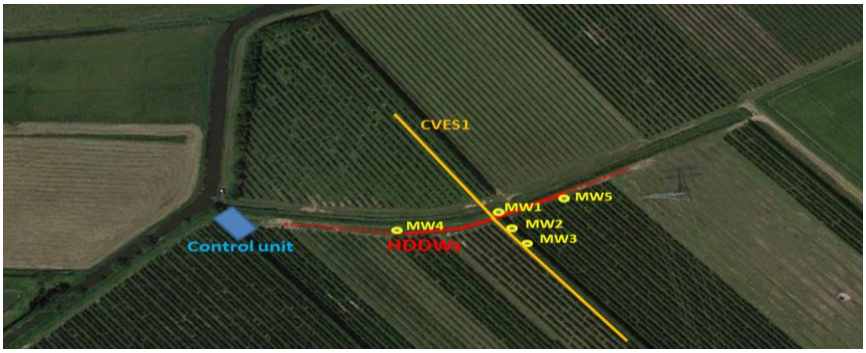

Figure 3.5 - Location of the HDDWs (red line). The solid part of the red line indicates the filter position. Monitoring wells (MW) are shown in yellow.

At the pilot location, the surface level varies from 0.1 to 0.5 m-ASL. The ASR-well (HDDW1) was installed in a borehole transect with a depth of 6.68 to 6.93 m-BSL and the interception well (HDDW2) was installed directly below HDDW1 at a depth of 13.35 to 14.38 m-BSL. Both HDDWs had a filter length of 70 m; the locations of the HDDWs are shown in Figure 3.5. During the field pilot, freshwater surpluses of the winter period were pumped from a nearby water coarse and stored in a 4000 m^3 basin already present at the orchard. After settlement of fine particles at the bottom of the basin, freshwater was pumped from the top of the basin and injected in the subsurface by HDDW1, using a 3 m high standpipe to provide the pressure for injection and making sure the pressure never exceeded 0.3 bar. Freshwater was abstracted by HDDW1 and used for irrigation in times of freshwater demand. During the pilot, saline water was abstracted by HDDW2 daily and discharged in a local water course. Figure 3.6 shows a cross Section of the Freshmaker at the Ovezande pilot location.

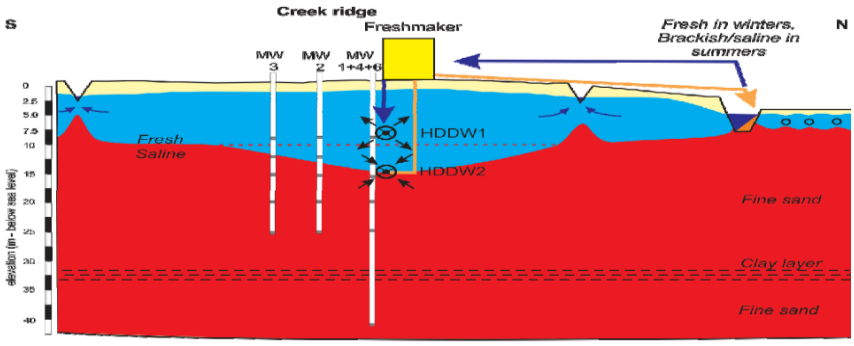

Figure 3.6 - Cross Section of the Freshmaker set-up at the Ovezande pilot. Source: Zuurbier et al. (2014).

3.2 Research strategy

The Freshmaker is currently being tested at the field-scale at a pilot location in Ovezande, the Netherlands. The first step of the research was to increase the understanding of the performance Freshmaker in Ovezande. This was done by means of numerical modelling by which the pilot study operations were mimicked and described. The groundwater model that was constructed for this was called the "**FAP**-model", which is an abbreviation of "the **F**reshmaker **A**pplied in **P**ractice". The FAP-model is described in detail in Appendix B. Data collected at the pilot location were used to build and calibrate the FAP-model. The model calibration is described in Appendix C. There are two versions of the FAP-model, a 2D and a 3D-version. The 3D-model was used to study a significant unknown in the performance of the Freshmaker: the importance of effects on the outer ends of the HDDWs. Zuurbier et al. (2014) neglected edge effects on the outer ends of the HDDWs in a 2D model, however this assumption was not validated.

With a sound understanding of how the Freshmaker works in practice, the next step was to optimize the technique in order to improve its applicability as a solution to freshwater scarcity. The technique was optimized by focusing on two of the major factors which determine the success of ASR in brackish or saline aquifers: 1) the recovery efficiency and 2) the maximum storage capacity. The following subsections describe how both factors were studied during this research.

3.2.1 Recovery efficiency

The recovery efficiency (RE) of the Freshmaker is controlled by many factors, as thoroughly explained in the previous chapter. It is therefore important to understand these controlling factors in order to optimize the technique. Understanding the factors that control the RE gives insight in the potential of the Freshmaker as a solution to the limited applicability of ASR in coastal aquifers. Factors that were believed to limit the RE of the Freshmaker can be divided in two groups: 1) operational variables and 2) hydrogeological variables. The variables of the two groups are shown in Table 3.1. The research strategy followed in this thesis was to study if and how these variables affect the RE of the Freshmaker.

Hydrogeological variables

The effect of most of the hydrogeological variables on the RE of conventional ASR-systems were already discussed in detail in Chapter 2. However, the influence on the Freshmaker RE will most likely be different. During the calibration process of the FAP-model it was already found that the results of the model are highly sensitive to changes in hydrogeological and climatological variables. This was caused by the fact that the Freshmaker was placed in a freshwater lens which shape is dependent on the hydrogeological and climatological variables. It was therefore concluded that the FAP-model was not able to analyse the influence of hydrogeological variables on the RE of the Freshmaker. If, for instance, the hydraulic conductivity was changed, this resulted in a different shape of the initial fresh-saltwater interface. The resulting REs would then no longer be comparable to the RE of the reference-model as the position of the Freshmaker remained fixed. For this reason, another model was constructed which was used to study the influence of hydrogeological variables on the RE. This model was called the "**FAT**-model" which is an abbreviation of "the **F**reshmaker **A**pplied in **T**heory". The FAT-model does not simulate a freshwater lens but has a fixed initial salinity stratification, irrespective of the simulated scenario. Appendix B describes the FAT-model in detail. The different hydrogeological variables studied are listed in Table 3.1.

Operational variables

The FAP-model was used to analyse the influence of the different operational variables listed in Table 3.1 except the "upscaling" variable. As the FAP-model is highly specific for the Freshmaker pilot study, it was found that it was not suited for simulation of multiple Freshmakers in the same aquifer. Instead, the FAT-model was used to analyse the potential benefit of upscaling.

Table 3-1 – Analysed factors that may influence the recovery efficiency of the Freshmaker

Operational parameters	Hydrogeological parameters
1. Variable target volumes	I. Aquifer conductivity
2. Variable recovery phase lengths	II. Vertical anisotropy
3. Potential HDDW2 failure	III. Porosity
4. Decreasing HDDW2 pumping rates	IV. Dispersivity
5. Varying HDDW1 placements	V. Ambient concentration
6. Upscaling	VI. Aquifer heterogeneity
	VII. Background flow

3.2.2 Maximum storage volume

Next to RE, cost-efficiency is an important determinant of the success of an ASR technique. There are many factors playing a role in the cost-effectiveness of the Freshmaker, e.g. construction costs, water price at other sources, energy demand during operation, and maintenance costs. However, cost-efficiency is directly related to the freshwater storage capacity. Even if one would obtain a RE of 100%, the cost efficiency may be low if the freshwater storage volume is small related to the costs. A higher storage volume decreases the investment cost per recovered unit volume of freshwater and makes investment more cost-effective. The FAP-model was used to study the maximum freshwater storage volume of the Freshmaker in the current setup at the pilot site and how it can be increased.

3.3 Modelling scenarios and output analysis

In Section 3.2 is described which research strategy was followed. It follows from this strategy that there are three research tracks (Figure 3.7):

I. Analysis of the simulation of the current pilot study and model calibration (2D and 3D FAP-model);
II. Sensitivity analysis of (a) the operational and (b) hydrogeological variables on the RE of the Freshmaker (both FAP- and FAT-model);
III. Analysis of the maximum freshwater storage and recovery capacity of the Freshmaker in Ovezande (FAP model).

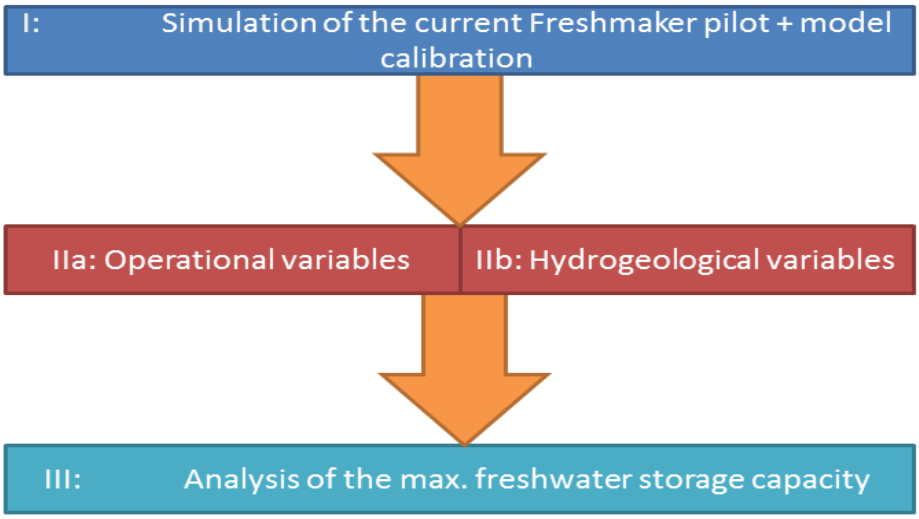

Figure 3.7 – The three research tracks.

Modelling scenarios are described for each research track separately in the next sections. Each model scenario of Track II and III was run for 5 complete ASR-cycles and analysed for RE. This made it possible to study the effect of multiple cycle operations of each variable as ASR performance can improve year-after-year. Values for RE were obtained using the following equation:

$$RE = \frac{V_{out}}{V_{in}} * 100\%$$

Where:
RE = Recovery efficiency [%];
V_{out} = Total recoverable volume [m^3].
V_{in} = Total injected volume [m^3].

V_{out} is dependent on the maximum allowed chloride concentration in the recovered water:

$$V_{out} = V_{recovered} - V_{[Cl]>[Cl,max]}$$

Where:
$V_{recovered}$ = Total recovered volume [m^3];
$V_{[Cl]>[Cl,max]}$ = Volume of recovered water in which the chloride concentration is larger than Cl_{max} [m^3]. The maximum chlorinity for irrigation water is 250 mg/l.

3.3.1 Analysis of the simulation of the current pilot study + model calibration

To analyse the functioning of the current pilot study, the FAP-models (2D and 3D) were run with pumping rates as recorded during the pilot study. The 2D model was calibrated such that modelling results produced the same fresh-salt water interface dynamics as observed in field measurements (borehole loggings with EM-39). For the calibration, meteorological data, water quality data, geophysical borehole loggings (EM-39), and hydraulic head measurements were used. The model calibration is described in Appendix B and data analysis is described in Appendix C and D. Simulations were performed with time steps of one week. The results were analysed on chloride concentrations in the recovered water, RE, and freshwater lens dynamics. The edge effects were analysed by comparing the 2D and 3D results.

3.3.2 Analysis of the effect of the operational variables on the RE of the Freshmaker

The influence of the operational variables was analysed with the FAP-model. The result of each scenario was compared with the reference scenario. The simulated scenarios are described in Table 3.2 below. The influence of upscaling was studied with the FAT-model. The different upscaling configurations are shown in Figure 3.8 below.

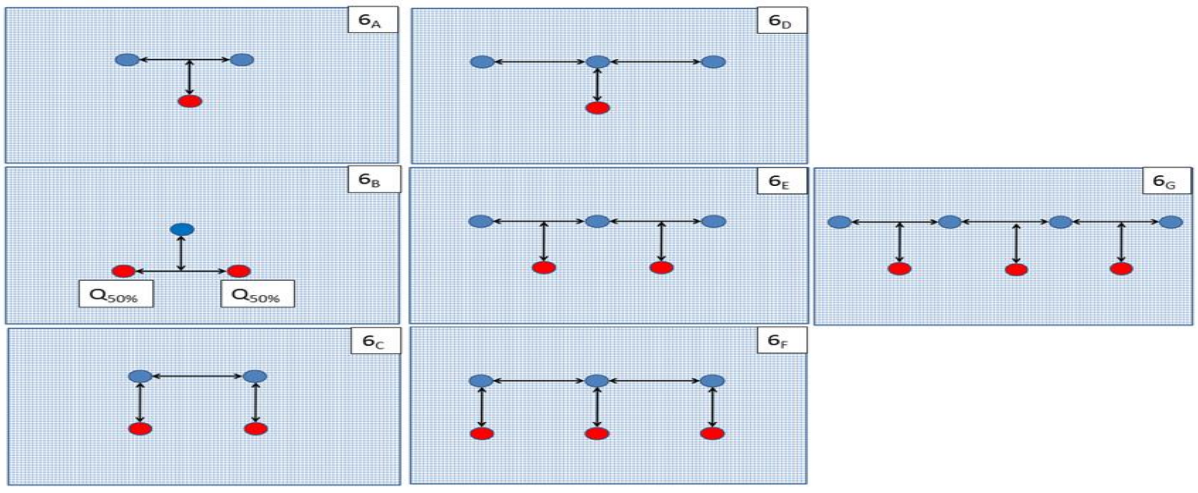

Figure 3.8 - Well configurations for scenario 6A-6G. In blue: HDDW1, in red: HDDW2. Horizontal and vertical distances between the wells were always 20 m and 7m respectively. Note that the fresh-saltwater interface is not shown here but in the description of the FAT-model in Appendix B. The pumping rate of each individual well was equal to the rate described in the reference scenario, except HDDW2 pumping rates of scenario 6_B.

Table 3-2 - Description of the simulation scenarios of the operational variables

Description of the simulation scenarios of the operational variables								
Pumping rate of HDDW1 and HDDW2 for each ASR-phase (m^3/d)								
	Injection (day 1-120)		Storage (day 121 – 180)		Recovery (day 181 - 270)		Idle (day 271-365)	
	Q_{HDDW1}	Q_{HDDW2}	Q_{HDDW1}	Q_{HDDW2}	Q_{HDDW1}	Q_{HDDW2}	Q_{HDDW1}	Q_{HDDW2}
Reference scenario (storage volume of 4000 m^3)								
	33.3	44.4	0	44.4	44.4	44.4	0	44.4
Scenario 1: Variable target volumes								
A (2000 m^3)	16.7	22.2 & 44.4	0	22.2 & 44.4	22.2	22.2 & 44.4	0	22.2 & 44.4
B (6000 m^3)	50	66.7 & 44.4	0	66.7 & 44.4	66.7	66.7 & 44.4	0	66.7 & 44.4
C (8000 m^3)	66.7	88.9 & 44.4	0	88.9 & 44.4	88.9	88.9 & 44.4	0	88.9 & 44.4
D (10000 m^3)	83.3	111 & 44.4	0	111 & 44.4	111.1	111 & 44.4	0	111 & 44.4
Scenario 2: Varying recovery period lengths								
A (45 d)	33.3	44.4	0	44.4	88.9	44.4	0	44.4
B (60 d)	33.3	44.4	0	44.4	66.7	44.4	0	44.4
C (75 d)	33.3	44.4	0	44.4	53.3	44.4	0	44.4
D (2 x 30 d)	33.3	44.4	0	44.4	66.7	44.4	0	44.4
E (3 x 20 d)	33.3	44.4	0	44.4	66.7	44.4	0	44.4
F (4 x 15 d)	33.3	44.4	0	44.4	66.7	44.4	0	44.4

Scenario 3: Potential HDDW2 failure					
Scenario		Duration of HDDW2 deactivation (d)			
		Injection phase	Storage phase	Recovery phase	Idle phase
A	1	1	X	X	X
	2	7	X	X	X
	3	30	X	X	X
B	1	X	1	X	X
	2	X	7	X	X
	3	X	30	X	X
C	1	X	X	1	X
	2	X	X	7	X
	3	X	X	30	X

Scenario 4: Decreasing HDDW2 pumping rates								
A (-25%)	33.3	33.3	0	33.3	44.4	33.3	0	33.3
B (-50%)	33.3	22.2	0	22.2	44.4	22.2	0	22.2
C (-75%)	33.3	11.1	0	11.1	44.4	11.1	0	11.1
D (-87.5%)	33.3	5.6	0	5.6	44.4	5.6	0	5.6

Scenario 5: Varying HDDW1 placements	
Scenario	Scenario description
A	HDDW1 4 m above HDDW2
B	HDDW1 6 m above HDDW2
C	HDDW1 10 m above HDDW2
D	HDDW1 1 m to the left (further away from the ditch)
E	HDDW1 2 m to the left (further away from the ditch)
F	HDDW1 1 m to the right (closer to the ditch)
G	HDDW1 2 m to the right (closer to the ditch)
Scenario 6: Upscaling	
The different upscaling configurations are shown in Figure 3.8.	

3.3.3 Sensitivity analysis of the hydrogeological variables on the RE of the Freshmaker

The sensitivity analysis of the hydrogeological variables was performed with the FAT-model. Seven different parameters were analysed. This resulted in 24 scenarios which are described in Table 3.3 below.

Table 3-3 - Description of the simulation scenarios of the operational variables

Description of the simulation scenarios of the hydrogeological variables	
Reference scenario	
K = 10 m/d; n_e = 0.33; VANI = 1; D_L = 0.1; Initial chloride concentration distribution is described in Appendix B. All the pumping rates are identical to the pumping rates of the reference scenario in Table 3.2.	
Scenario I: Hydraulic conductivity	
Scenario	Hydraulic conductivity (m/d)
A	1
B	5
C	25
Scenario II: Vertical anisotropy (VANI)	
Scenario	VANI
A	2
B	4
C	10
Scenario III: Porosity (n_e)	
Scenario	n_e
A	0.2
B	0.5
Scenario IV: Longitudinal dispersivity (D_l)	
Scenario	D_l (m)
A	0.2
B	1
Scenario V: Native aquifer salinity	
Scenario	Chloride concentration (mg/l)
A	5000 (brackish)
B	10000 (brackish saline)
C	20000 (saline)
Scenario VI: heterogeneity	
For the different configurations, see Figure 3.9	
Scenario VII: Background hydraulic gradient (flow perpendicular on the length of the HDDWs)	
Scenario	dh/dx
A	0.001 (flow velocity: ~10 m/yr)
B	0.005 (flow velocity: ~50 m/yr)
C	0.01 (flow velocity: ~100 m/yr)

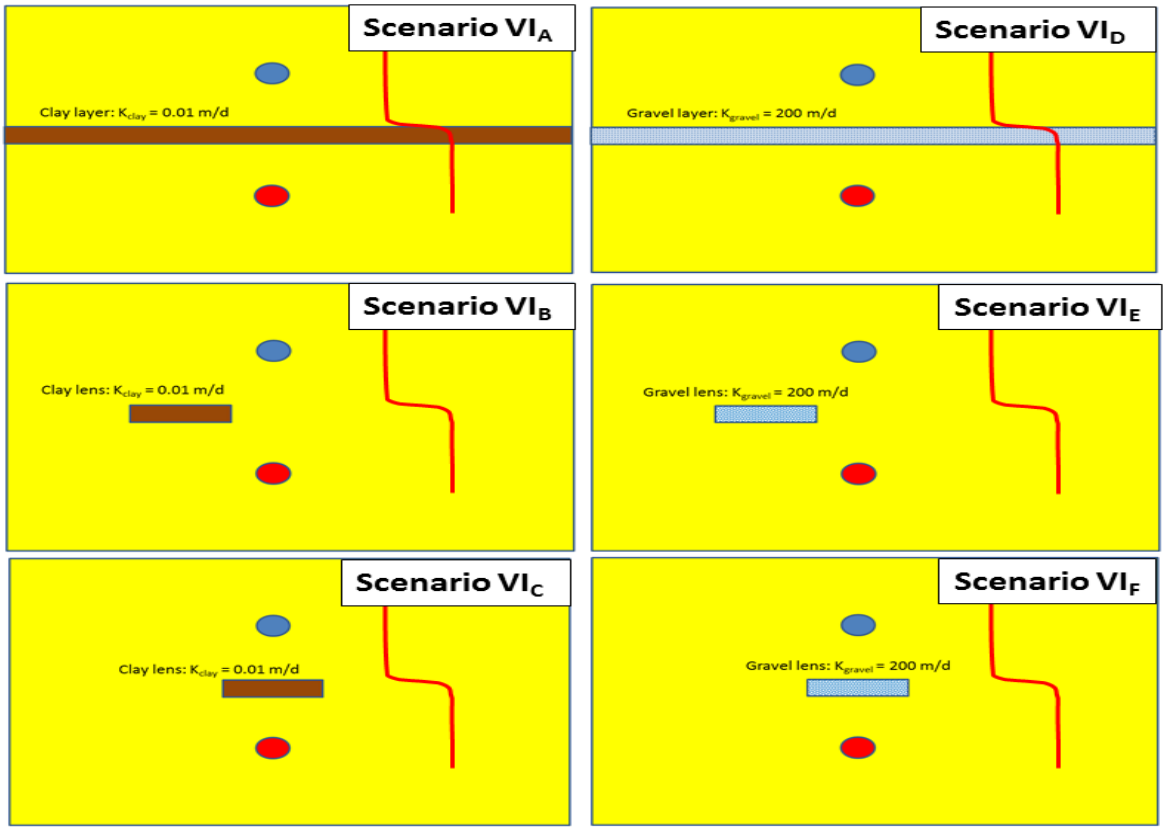

Figure 3.9 - Different configurations to study the influence of heterogeneity. K_{clay} = 0.01 m/d and K_{gravel} = 200 m/d. Layers and lenses have a fixed thickness of 0.5 m. The red line indicates the depth of the fresh-saltwater interface.

3.3.4 Maximum storage capacity of the Freshmaker in Ovezande

The optimal combination of HDDW1 and HDDW2 pumping rates was studied after the simulation results of the scenarios with operational variables were analysed. With knowledge of the individual influence of the pumping rates of HDDW1 and 2 it was possible to determine the maximum storage capacity of the Freshmaker in Ovezande.

4 Results

In this chapter the results of the modelling scenarios are described. In Section 4.1, the outcomes of the Ovezande pilot are shown and the 2D and 3D FAP-model results of the reconstructed pilot in Ovezande are described in Section 4.2. The results of the scenarios which study the influence of different operational variables on the recovery efficiency (RE) are presented and explained in Section 4.3. The outcomes of the scenarios investigating the influence of different hydrogeological settings are described in Section 4.4. Finally, the results of the analysis of the maximum storage capacity of the Ovezande pilot are shown in Section 4.5

4.1 Ovezande pilot: field results

The Freshmaker started its activity in June 2013. In a period of three weeks, a freshwater volume of about 1700 m^3 was injected. This freshwater volume was successfully recovered in the months August and September. After a period of about nine weeks during which saltwater was continuously abstracted by HDDW2 but no freshwater was injected or recovered, Injection phase II started. A volume 4450 m^3 was injected in this phase and later abstracted in Recovery phase II. The complete pumping history is shown in Figure 4.1.

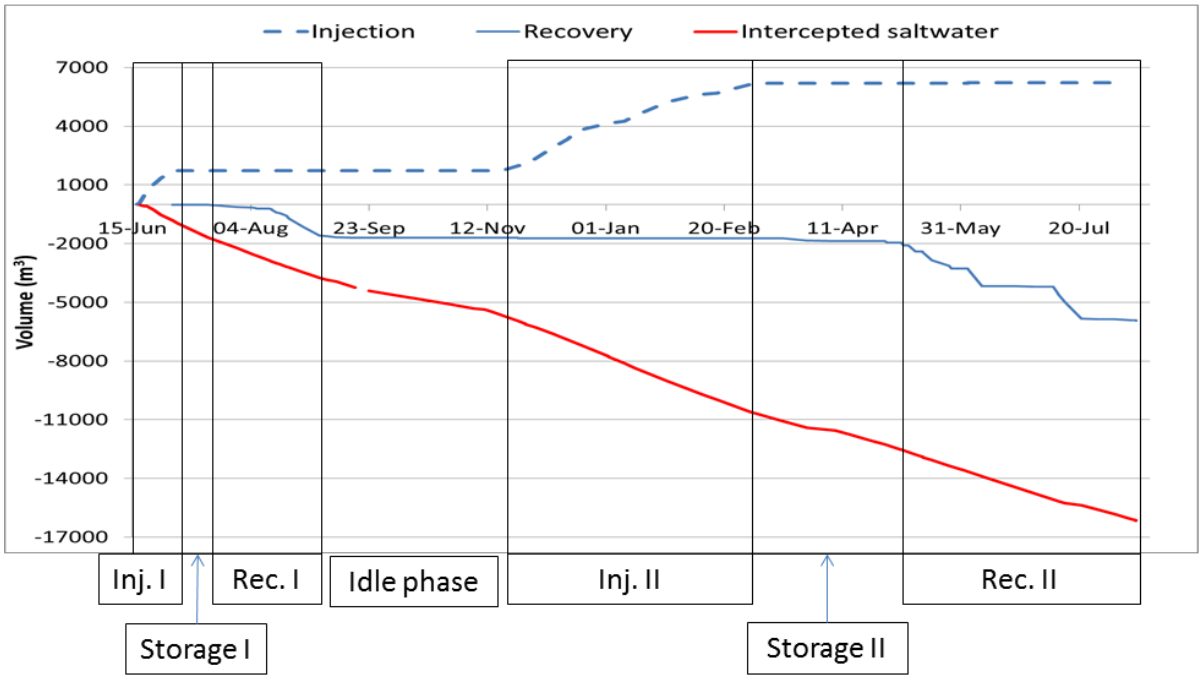

Figure 4.1 – Pumping history of the Freshmaker since the start of operation. The boxes indicate the length of the injection and recovery phases.

Monthly monitoring of the position of the fresh-saltwater interface recorded the effect of the activity of the Freshmaker on the freshwater lens. EM39 measurements done at MW1, which was located in the middle of the Freshmaker (i.e. representative for the FAP-model) are shown in Figure 4.2. The measurements indicate a clear dynamic response of the position of the fresh-saltwater interface on the activity of the Freshmaker. It can be seen that the initial fresh-saltwater interface was effectively lowered in Injection phase I and even further in Injection phase II. The interface moved back up during both recovery phases but was not observed to reach the same position as before the onset of the Freshmaker activity. No movement of the interface was observed during Storage phase II which indicates that abstraction by HDDW2 effectively keeps the interface stable.

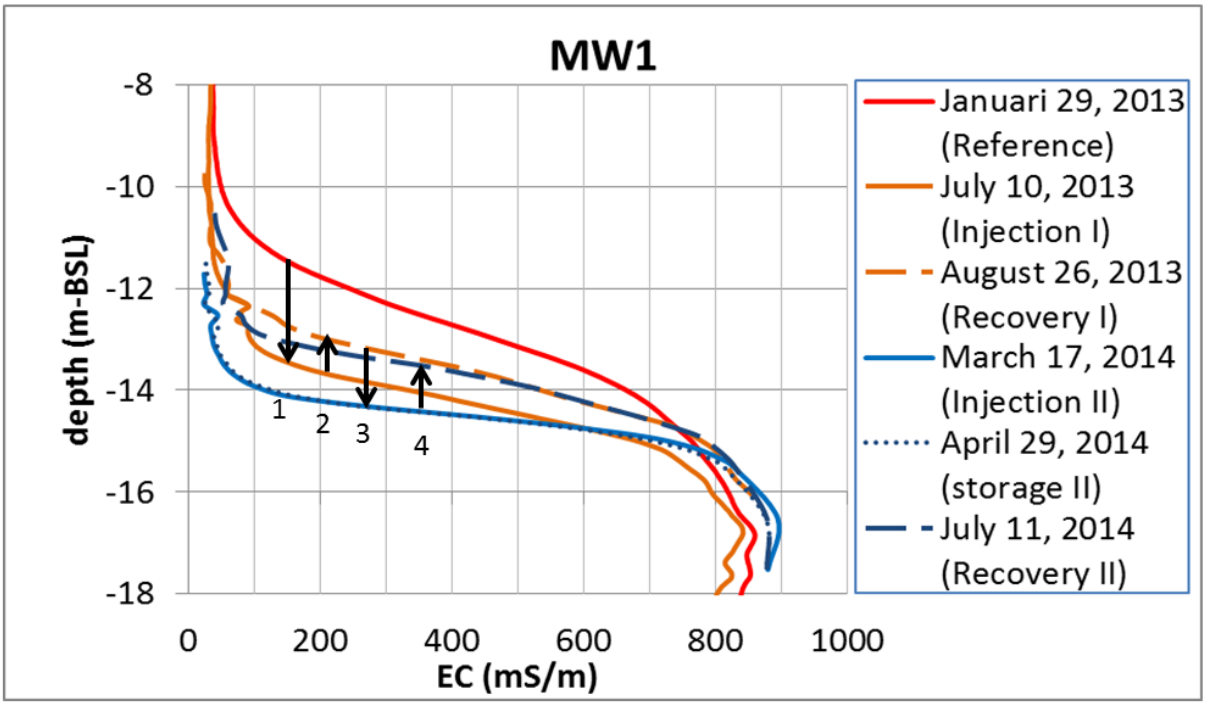

Figure 4.2 – Geophysical measurements at MW1 showing the influence of the activity of the Freshmaker on the position of the fresh-saltwater interface. The electrical conductivity (EC) is a proxy for the salinity. The arrows (1-4) indicate the chronologic displacement of the fresh-saltwater interface.

4.2 Ovezande pilot: model outcomes

It was aimed to reconstruct the dynamics of the fresh-saltwater interface observed during the Ovezande pilot with the FAP-model. The performance of the Freshmaker could be reliably studied with the FAP-model if that model can effectively reproduce the field measurements. The FAP-model was calibrated until it simulated the same dynamics of the fresh-saltwater interface as observed in the field. A summary of the calibration results is given in the next Section (4.2.1). For a detailed description, the reader is directed to Appendix B. The FAP-model outcomes of the Ovezande pilot are described in Section 4.2.2 and 4.2.3.

4.2.1 Summary calibration

The uncalibrated FAP-model was run from 01/02/2013 till 13/08/2014 with stress periods of 7 days and transport steps of 1 day. A total of 81 stress periods were simulated. The Freshmaker started its activity on June 15th 2013 (Stress period 21). The Freshmaker wells were injecting and/or abstracting at the recorded pumping rates as shown in Figure 4.3. Since the FAP-model consists of a 10 m thick slice of the 70 m long HDDW pair, the 2D-model was simulated with 1/7th of the real pumping rate.

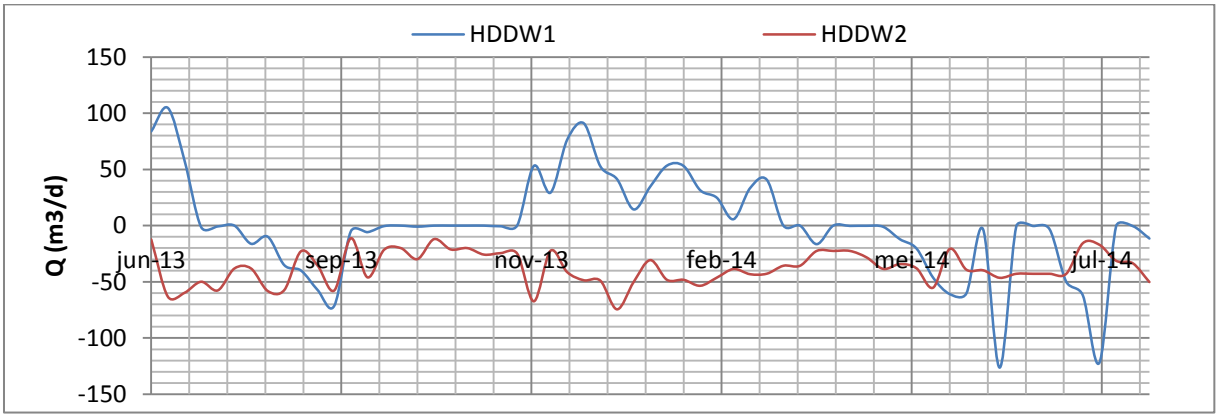

Figure 4.3 - Freshmaker flow rates recorded during the field pilot.

Model simulation outcomes were compared with the TDS measurements which were obtained from geophysical measurements (Appendix C). The initial model results showed a poor fit with TDS measurements (Figure 4.4). The fresh-saltwater interface was modelled at a shallower depth than at which it was in reality and the dynamics of the fresh-saltwater interface were not captured sufficiently. The model was manually calibrated by changing the value of the hydraulic conductivity (K), vertical anisotropy (VANI), river bottom conductance (C), and longitudinal dispersivity (D_L). Furthermore, a more realistic weekly groundwater recharge rate (Q_{rech}) was derived. This recharge rate was based on local meteorological measurements and Penman Monteith (Appendix D). Ultimately, the model simulation results showed a relatively good fit with TDS measurements (Figure 4.5). The initial parameter values and the calibrated parameter values are shown in Table 4.1.

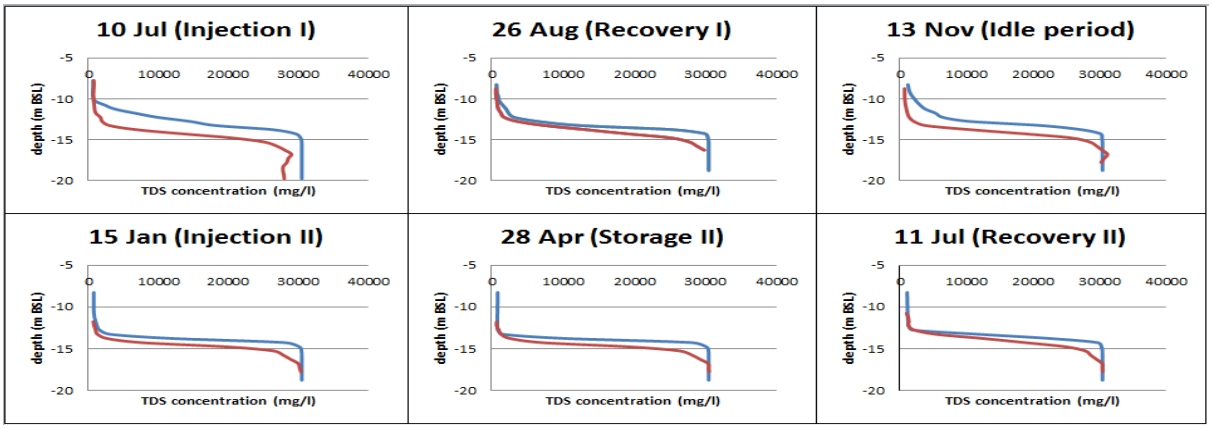

Figure 4.4 – Initial simulation results of the 2D FAP-model for two modelled ASR-cycles. Blue curve = model, red curve = TDS measurement.

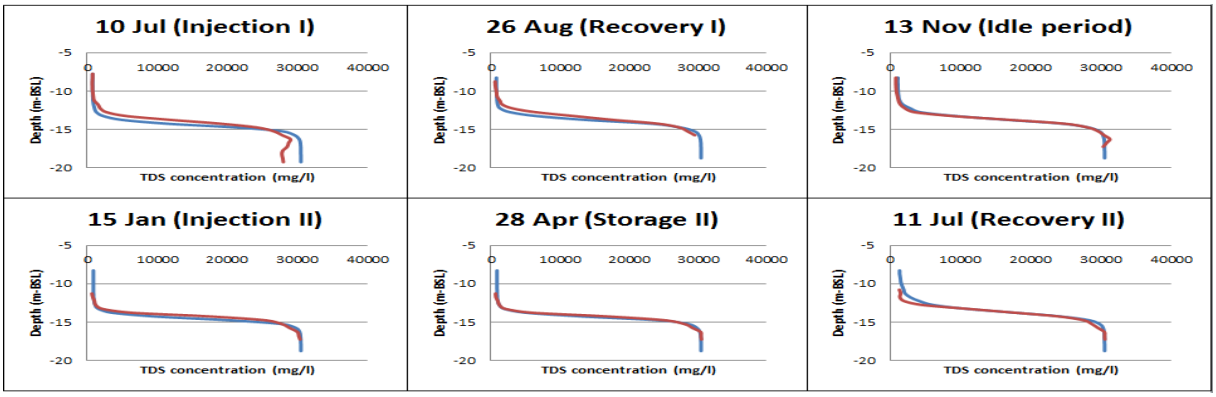

Figure 4.5 - Simulation results after calibration of the 2D FAP-model for two modelled ASR-cycles. Blue curve = model, red curve = TDS measurement.

Table 4-1 FAP-model parameter values before and after model calibration

Parameter	Initial value	Calibrated value
$K_{aquifer}$ (m/d)	10	2.5
$K_{semi\ confining\ layer}$ (m/d)	5	0.45
$VANI_{aquifer}$ (-)	4	1
$VANI_{semi\ confining\ layer}$	6	1
C (m^2/d) (river 1,2,3,4)	1000, 2, 5000, 100000	1000, 2, 10, 33
D_L (m)	0.1	0.33
Q_{rech} (mm/d)	1	0.466

4.2.2 2D- Model results

Reconstruction of the Ovezande pilot confirmed that the Freshmaker successfully achieved a RE of 100% in ASR-cycle I and almost 100% in ASR-cycle II. Figure 4.6 shows the chloride concentrations at HDDW1 and HDDW2. It can be seen that when injections took place, the chloride concentration increased at HDDW1 since the injection concentrations were higher than the ambient chloride concentration. Concentrations in HDDW2 significantly decreased during the injection phases as the increased pressure from HDDW1 resulted in more abstracted water originating from the shallower (less saline) part of the aquifer. It can also be seen that at the end of Recovery phase II (beginning of August 2014) the chloride concentration in HDDW1 quickly increased. The chloride concentration in HDDW1 slightly exceeded the maximum allowed concentration of 250 mg/l in Recovery phase II which shows that the RE of the Freshmaker in Ovezande might be sensitive to recovery rates (which were high from the 30th of June until the 1st of August 2014).

The injected freshwater does not remain fixed at the position of the Freshmaker wells (Figure 4.7). The freshwater bubble drifted towards the ditch because of significant lateral flow. This corresponds with the decrease and increase of chloride concentrations during the storage phases at HDDW1 and HDDW2 respectively (Figure 4.6) as the injected water is replaced by native aquifer water. In Figure 4.7, one can also observe the upconing that occurred at the end of recovery phase II, which led to increased chloride concentrations. The saline water that coned up towards HDDW1 came from the North, i.e. from under the ditch, where the fresh-saltwater interface was shallow, while freshwater inflow from the South was observed.

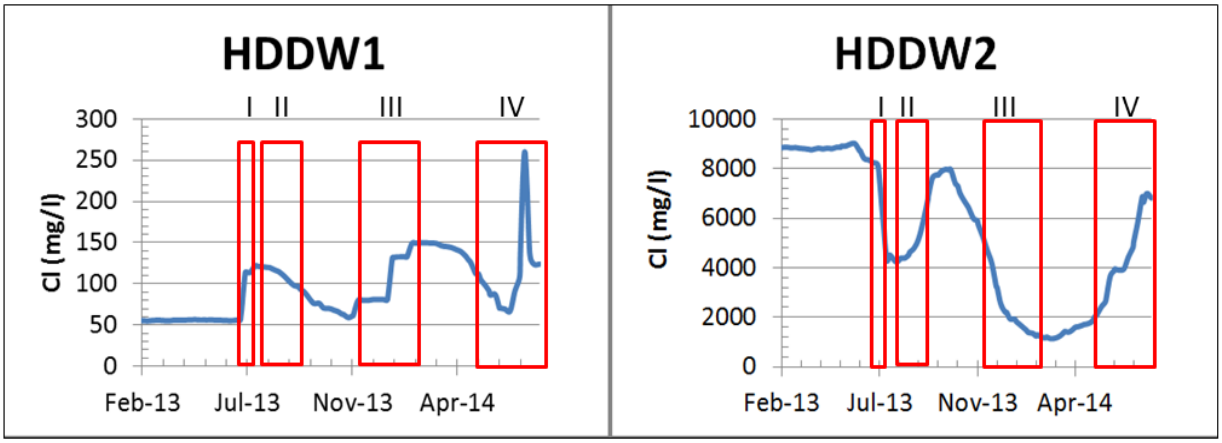

Figure 4.6 - Modelled chloride concentrations at HDDW1 (left) and HDDW2 (right). I: Injection phase I, II: Recovery phase I, III: Injection phase II, and IV: Recovery phase II. The storage phases are in-between I & II and III& IV.

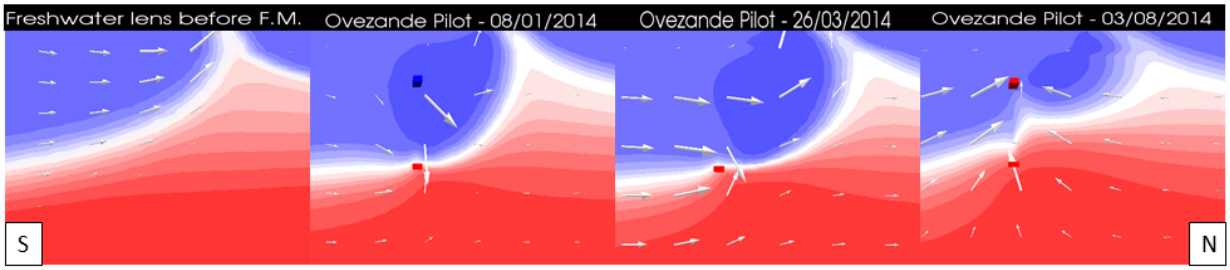

Figure 4.7 - Modelled chloride concentration distributions at injection phase II (left), storage phase II (middle) and recovery phase II (right). Contours are identical for each figure and increase logarithmically from 0 (blue) to 16800 mg/l (red).

4.2.3 3D model results

The results of the 3D model highlighted the effects of the Freshmaker on fresh-saltwater interface dynamics in all three dimensions. A cross-section parallel with the HDDWs is shown in Figure 4.8. The fresh-saltwater interface is effectively lowered and stabilized in a horizontal position during the injection phases. During Recovery phase I, the interface does not move up significantly. However, some upconing could be observed at the outer end of HDDW1. These edge effects are discussed more in detail in Section 4.2.4.

In Recovery phase II, the fresh-saltwater interface moved up along the whole length of the HDDWs (Figure 4.8). The origin of this water was the same as discussed in Section 4.2.2, which can be seen best in Figure 4.10, in which the results along 2 cross-sections perpendicular to the HDDWs are shown. The fresh-saltwater interface was shallower in the direction of the ditch and this shallow interface resulted in significant upconing of saline water.

From a plan view one can see the highest chloride concentrations in the upper part of the aquifer started to disappear in recovery phase II (Figure 4.9, top part). The high concentrations originated from the upconing caused by the draining ditch but as the Freshmaker pilot continued, the upconing under the ditch started to decrease. The decreased upconing under the ditch can also be seen in Figure 4.10 (see the cross-section in the bottom right corner).

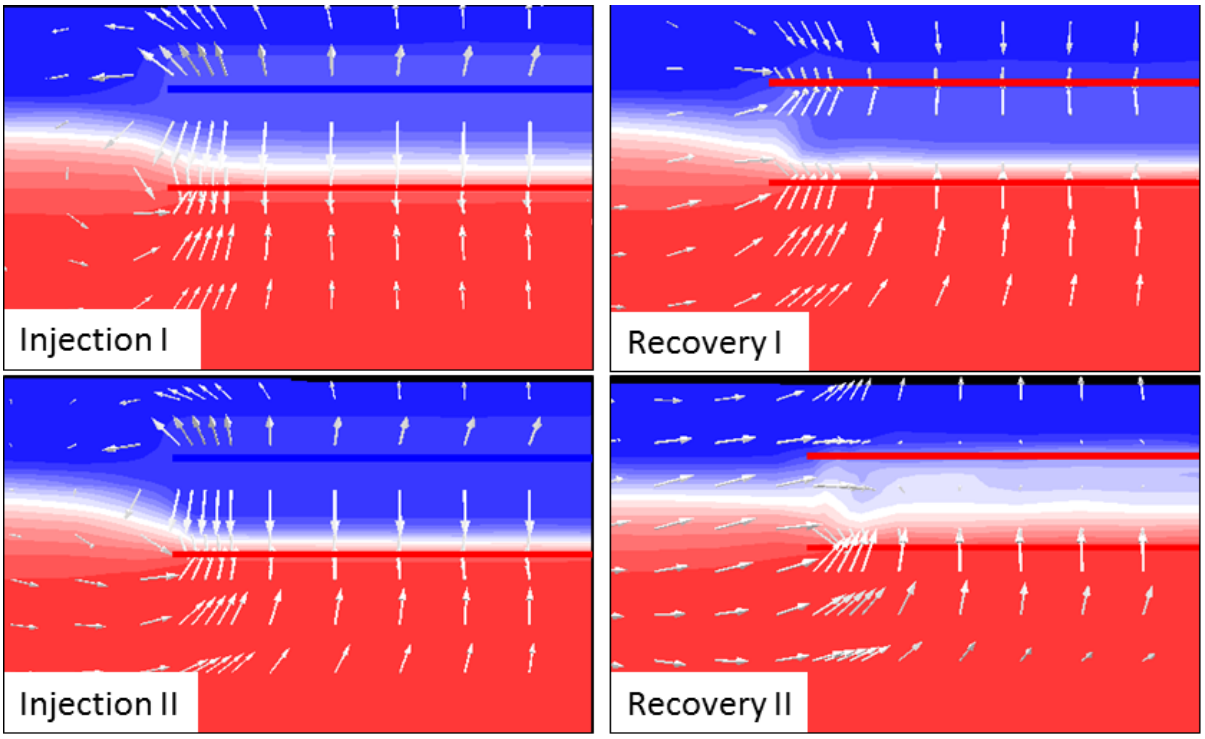

Figure 4.8 - Cross sections parallel on the length of the Freshmaker showing the chloride concentration distrubition in injection and recovery phases I and II. Contours are identical for each figure and increase logarithmically from 0 (blue) to 16800 mg/l (red). The arrows indicate the groundwater flow direction.

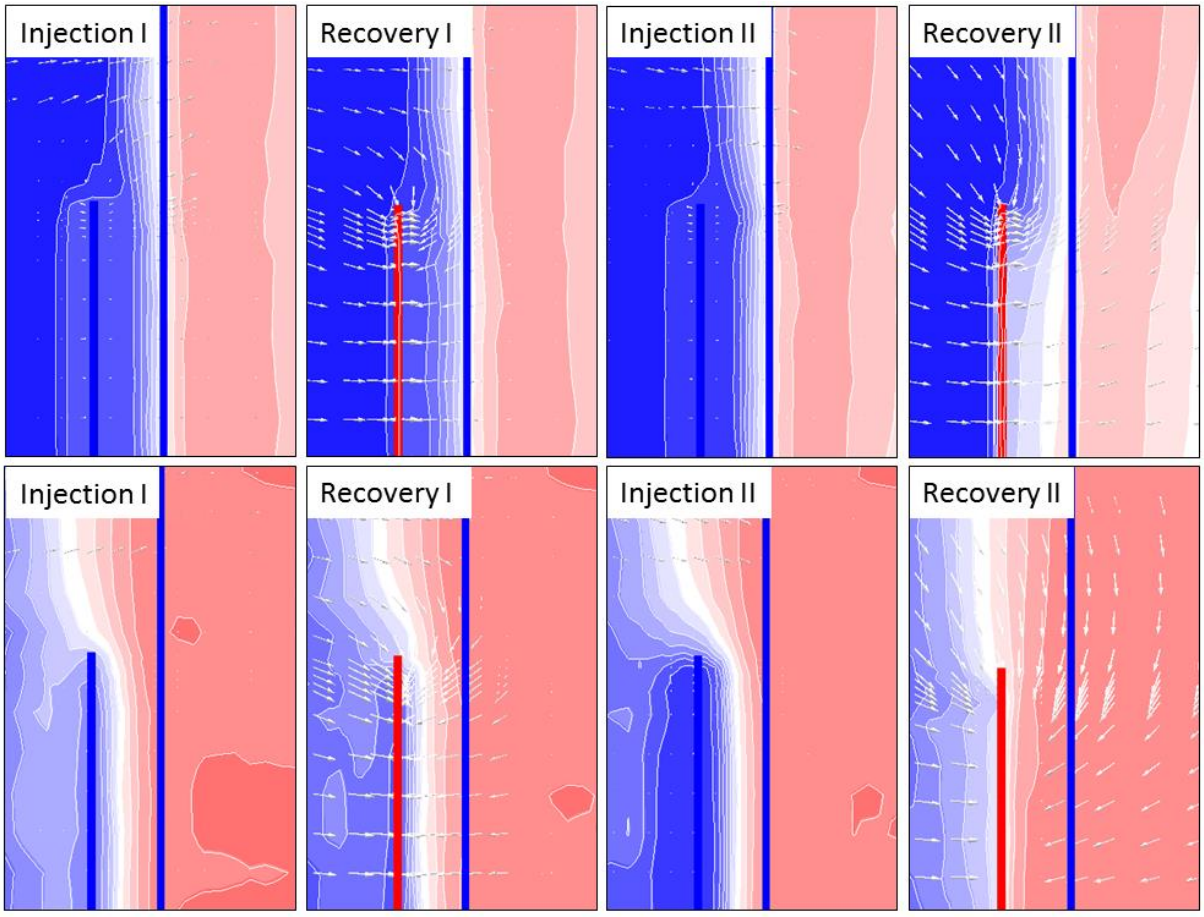

Figure 4.9 – Chloride concentration distribution at the Freshmaker in a top down perspective. The upper 4 figures are at the same depth as HDDW1 (layer 17), the lower 4 figures from in between HDDW1 and 2 (layer 25). The blue line in the middle of each figure represents the draining ditch. Contours are identical for each figure and increase logarithmically from 0 (blue) to 16800 mg/l (red). The arrows indicate the groundwater flow direction.

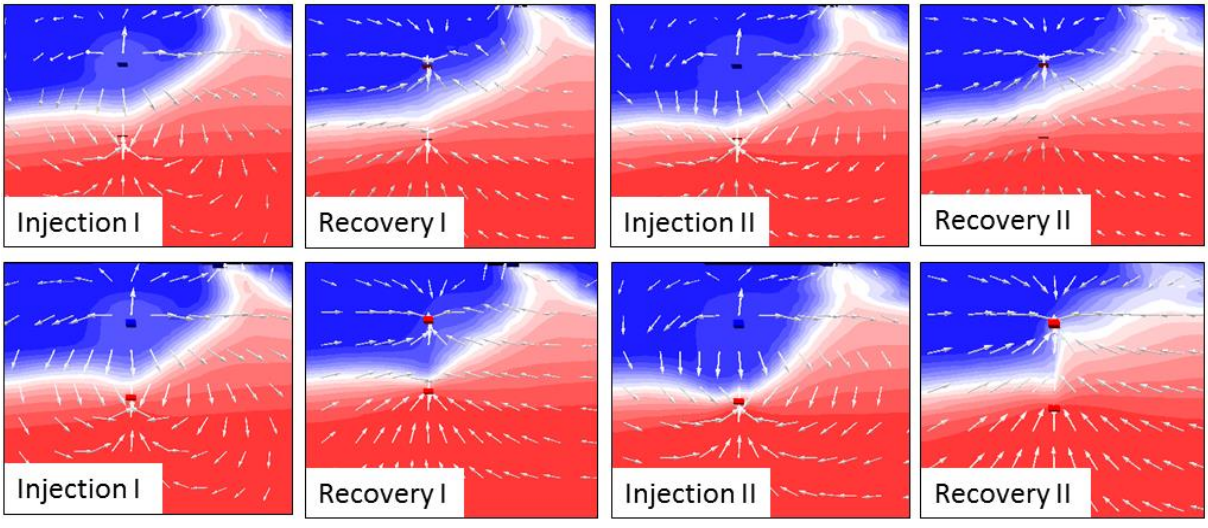

Figure 4.10 – 8 cross sections perpendicular on the length of the Freshmaker showing the chloride concentration distrubition in injection and recovery phases I and II. The upper 4 cross sections are taken from the outer end of the Freshmaker, the lower 4 cross sections from the middle of the Freshkmaker. Contours are identical for each figure and increase logarithmically from 0 (blue) to 16800 mg/l (red). The arrows indicate the groundwater flow direction.

4.2.4 3D-effects

Two different 3D-effects were identified from the 3D-model results. The effect that the 3D-effects of the fresh-saltwater interface had on chloride concentrations abstracted by the Freshmaker is shown in Figure 4.11. The observed effects will be explained and discussed in separate subsections below.

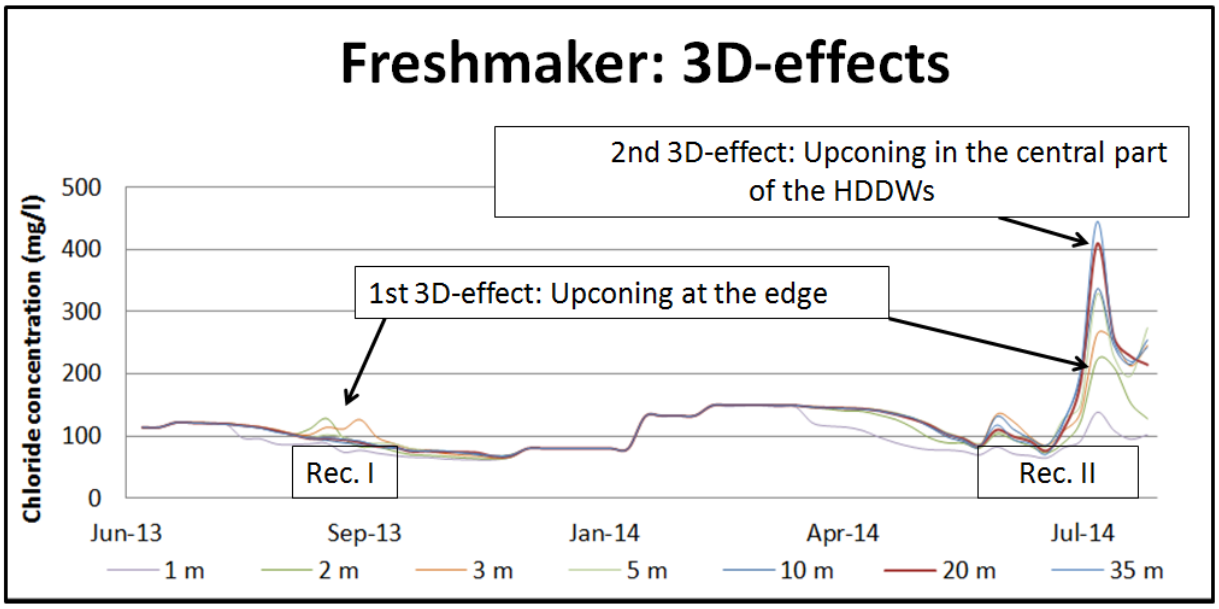

Figure 4.11 – The two 3D-effects identified for the Freshmaker. The different curves are time series of the chloride concentration in the water at HDDW1 at different positions from the outer end (1 m – 35 m). Recovery phase I and II are shown in the boxes above the x-axis.

4.2.4.1 *1st 3D effect: Upconing at the edge*

Upconing of saline water was observed at the edge of HDDW1 during both Recovery phase I and II (Figure 4.8). However, in Recovery phase II, chloride concentration were increasing along the whole length of the HDDWs, which made the relative influence of upconing at the edge less profound. The upconing was caused by the shallower depth of the fresh-saltwater interface at the edge of the HDDWs, where it could not be lowered by HDDW2. It was further enhanced by the flow direction at the edge (note the flow vectors in Figure 4.8). At the edge, a larger share of the water being drawn towards HDDW1 flowed in horizontally, i.e. from the location where the interface was shallower.

The chloride concentrations distribution along HDDW1 during the observed concentration peak in Recovery phase I is shown in Figure 4.12. The upconing (i.e. increased chloride concentrations) was limited to the outer end (the section within 5 m from the edge). The increase in chloride concentrations could also only observed at 2 and 3 m from the edge in Figure 4.11, not at distances further away from the edge. The reason that no increased chloride concentrations can be observed at 1 m from the edge can be explained from the flow vectors in Figure 4.8. At the 1 m from the edge of HDDW1, flow was almost horizontal and the abstracted water originated from the fresh part of the aquifer. At 2 and 3 m from the edge, flow was more vertically oriented and the abstracted water originated from the location where the fresh-saltwater interface could not be lowered by HDDW2 which led to the increase in chloride concentrations. Further than 3 m from the edge, flow was also vertically oriented but the abstraction of HDDW2 kept the interface at depth.

Although overshadowed by the 2nd 3D effect (explained in the next section), it can be observed in Figure 4.11 that the upconing at the edge was even more significant in Recovery phase II than Recovery phase I. The chloride concentrations at 2 m and 3 m from the edge were about two times higher in Recovery phase II than in Recovery phase I.

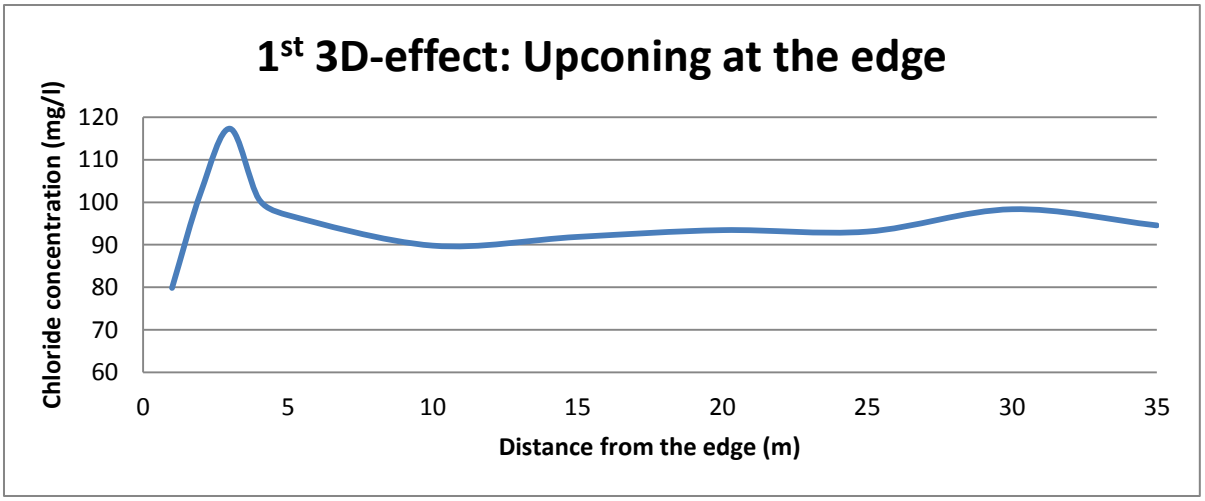

Figure 4.12 - Chloride concentration distribution along HDDW1 averaged over the period 9/9/2013 – 9/14/2013. This covers the concentration peak observed in Recovery phase I.

4.2.4.2 *2nd 3D effect: Upconing in the central part of the HDDWs*

At the end of Recovery phase II, the saline water was closer to the central part than the outer end of the Freshmaker. This was the case at a depth in between HDDW1 and HDDW2 and at the depth of HDDW1 (i.e. layer 17 and 25 shown in Figure 4.10). In Figure 4.10 can also be seen that the fresh-saltwater interface moved up significantly further in the centre, than at the edge of the HDDWs during Recovery phase II. The fact that the fresh-saltwater interface moved closer to the central part, than the edge of HDDW1 is the 2nd 3D-effect.

During Recovery phase II, the concentration differences between the various distances from the edge of HDDW1 became more distinct (Figure 4.11). Chloride concentrations increased over the whole length of the HDDWs but corresponding to the observations that the fresh-saltwater interface was closer to HDDW1, the concentrations at central section of HDDW1 were higher than at the edge of HDDW1 (Figure 4.13).

A difference between the edge and the centre of the HDDWs was also displayed in the hydraulic head variations, which are shown in Figure 4.14. During the injection phases, the hydraulic head in the centre was higher than at the edge of HDDW1. However, during the recovery phases the opposite was the case: the head in the centre was lower than at the edge. The differences between the centre and the edge were greater during the recovery phase than during the injection phase since pumping rates of HDDW1 and 2 opposed each other during the injection phase. The differences were also related to the absolute pumping rates: the greater the pumping rate, the greater the difference between the head at the edge and the head in the centre of HDDW1.

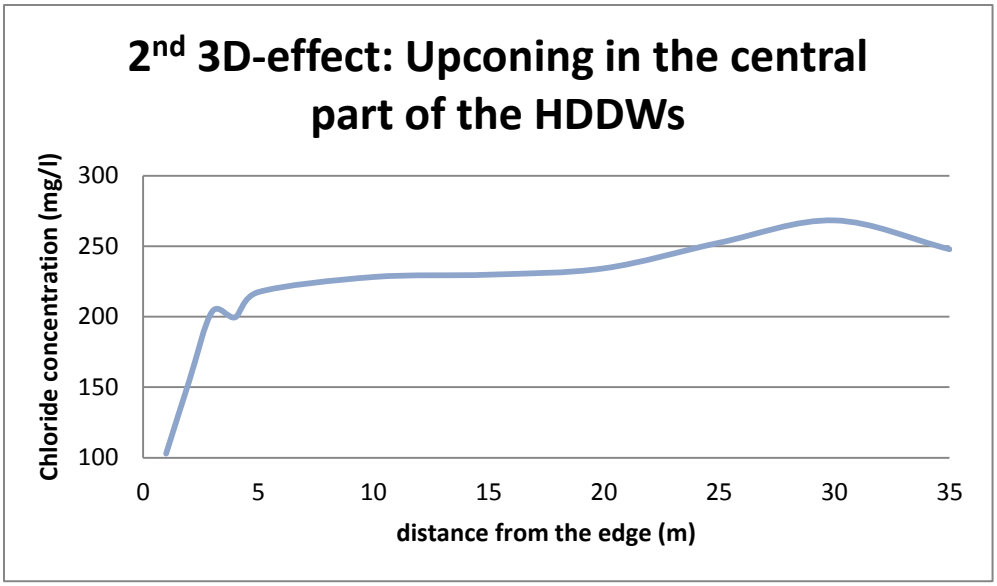

Figure 4.13 – Chloride concentration distribution along HDDW1 averaged over the period 7/14/2014 – 8/14/2014. This covers the concentration peak observed in Recovery phase II.

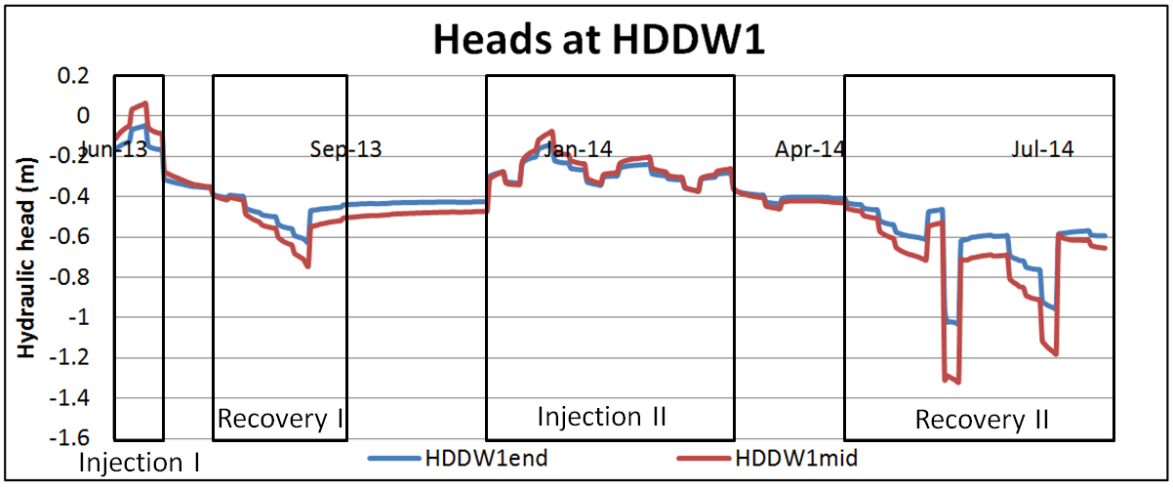

Figure 4.14 – Time series of simulated hydraulic heads at HDDW1. Two curves are shown: the blue curve represents the outer end of HDDW1, the red curve the middle of HDDW1. The four boxes indicate the injection and recovery phases.

4.3 Operational parameters

The modelled scenarios were described in Section 3.3. The results of each scenario will be discussed in a separate subsection.

4.3.1 Reference scenario

The REs of 5 ASR-cycles are shown in Figure 4.15. Initially the RE was 87% but it fell to 78% in the 2nd cycle. From the 2nd cycle onwards the RE steadily increased, reaching 100% in Cycle 4. Though not shown in the figure, it was found that the RE remained at 100% from Cycle 5 onwards. In order to understand the observed RE trend, the salt transport dynamics were analysed in detail.

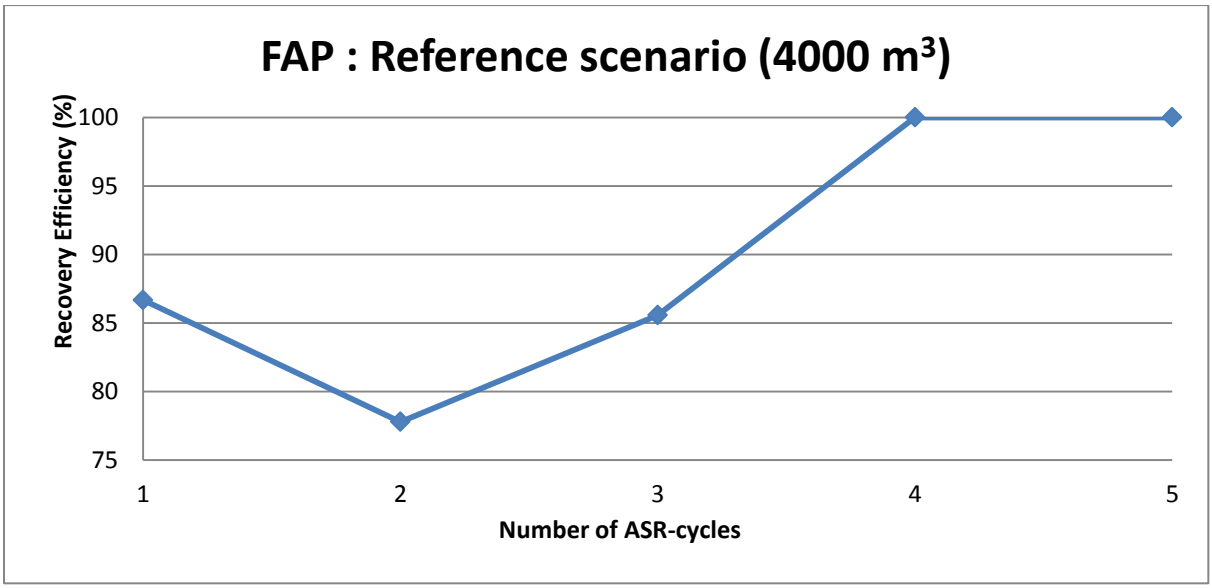

Figure 4.15 - Calculated recovery efficiency per ASR-cycle for the reference scenario, storing 4000 m³. The pumping rates of the reference scenario are shown in Section 3.3.

As already discussed previously (Section 4.2), the main source of salinization was non-symmetric upconing from below, with more upconing occurring at the side of the ditch. The observation that the RE first decreased and then increased were assigned to the upconing initially present under the draining watercourse. When the chloride concentration distributions at the end of each recovery phase were compared for 6 successive cycles, it was observed that the saline water cone became smaller every completed ASR-cycle (Figure 4.16). This was caused by the continuous pumping of HDDW2 during all phases (i.e. also the storage and idle phases) which ultimately thinned the cone. This process of thinning was further enhanced by the combined activity of HDDW1 and 2 in every injection phase. As can be seen in Figure 4.17, the increased pressure at HDDW1 introduced by freshwater injection further "pushed" the upconing down, which also thinned the cone.

The REs of Cycle 2 and 3 were lower than Cycle 1 (Figure 4.15). This can be explained by the fact that the cone with saline water was drawn closer by activity of the Freshmaker in Cycle 1, but was not yet thinned enough by the HDDWs. From Cycle IV onwards, the cone has thinned sufficiently to maintain a RE of 100%.

Long-term chloride concentrations were increasing after the 5th ASR-cycle until they reached a constant concentration (Figure 4.19). This was caused by the fact that the watercourse nearby the Freshmaker started to infiltrate brackish surface water during recovery in summer from Recovery IV onwards. While the ditch was draining again during Injection phase V, the ditch was transferred from a draining ditch into an infiltrating ditch during all ASR-phases from Cycle VI onwards. This can be seen in Figure 4.18: if the aquifer head was lower than the controlled water level in the ditch, the ditch started to infiltrate. From Cycle VI onwards the aquifer head no longer exceeded the controlled surface water level and the ditch was continuously infiltrating. The surface water in the ditch is brackish in summer, but fresh in winter. This can also be seen in Figure 4.16, where the surface water that infiltrated in Injection phase VI had a lower chloride concentration than the surface water infiltrated during Recovery phase V. Nevertheless, the chloride concentration of water

recovered by HDDW1 did not exceed the maximum allowed concentration limit even though the ditch started to infiltrate brackish water since HDDW1 abstracted sufficient freshwater flowing in from other directions.

As the head difference between the aquifer and the surface water level decreased from Cycle 1 – 4, the drainage rate of the ditch decreased and flow patterns started to change. This can be seen from the flow vectors in the yellow parts of the figures shown in Figure 4.16. From Recovery phase I to III less water was flowing towards the ditch until the ditch no longer drained in Recovery phase IV. HDDW1 started to abstract freshwater from the smaller freshwater lens in Recovery phase III and the two freshwater lenses became fully connected from ASR-cycle IV onwards.

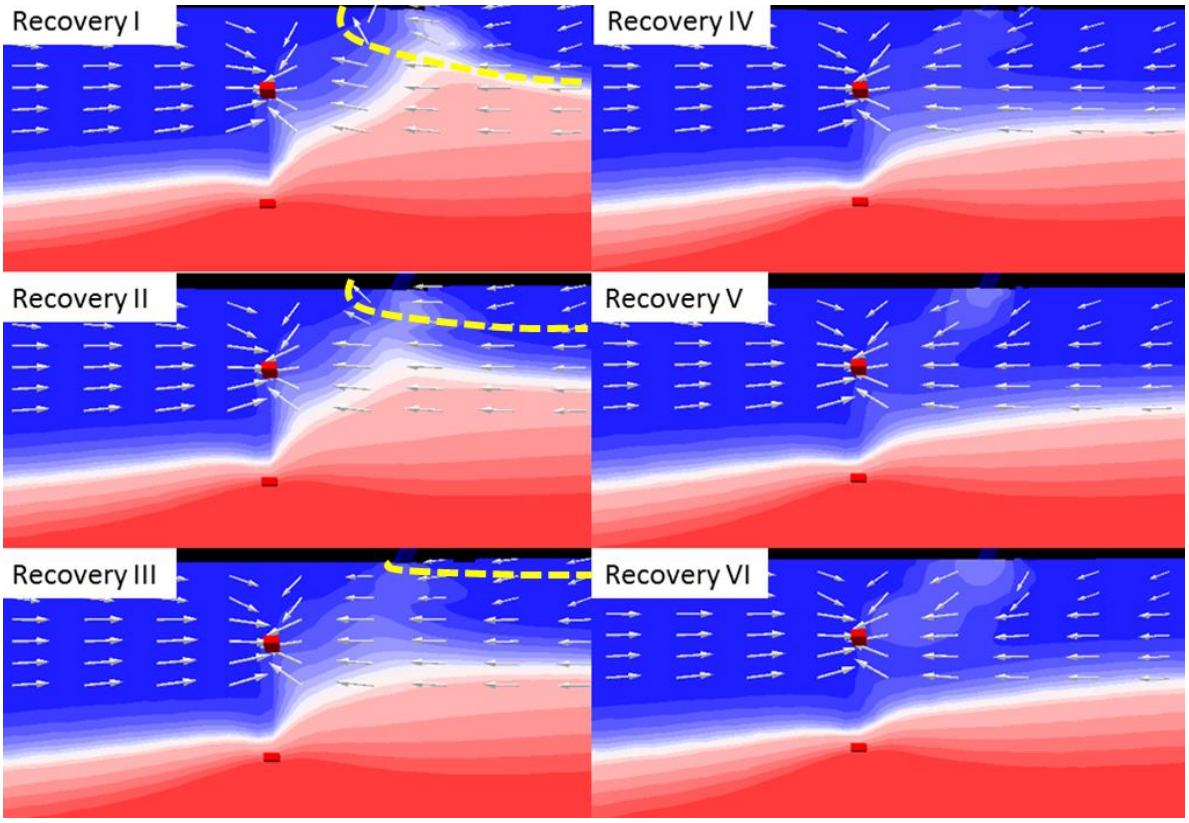

Figure 4.16 - Chloride concentration distribution and flow vectors for 6 recovery phases. Each Figure corresponds to the same day of the ASR-cycle allows comparison. Contours are identical for each figure and increase logarithmically from 0 (blue) to 16800 mg/l (red).

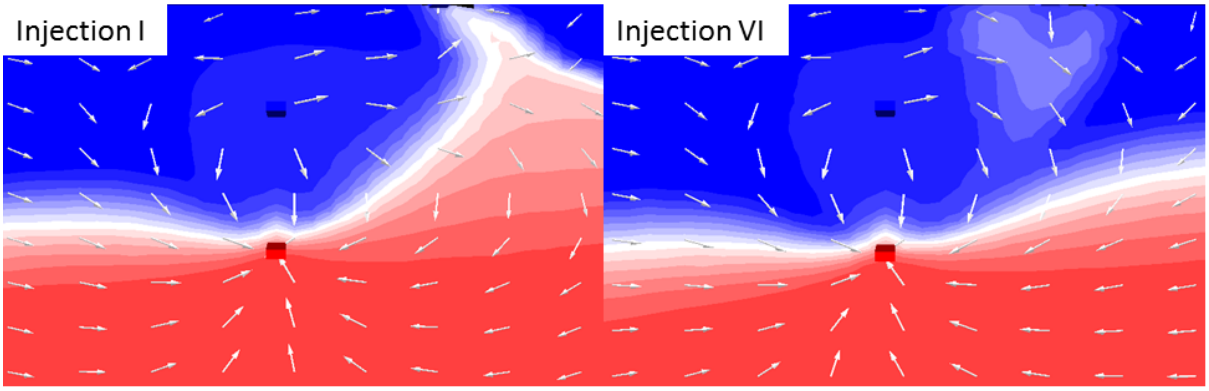

Figure 4.17 - Chloride concentration distribution and flow vectors at injection phase I and VI showing that the upconing is effectively decreased by combined pumping of HDDW1 and HDDW2. Contours are identical for each figure and increase logarithmically from 0 (blue) to 16800 mg/l (red).

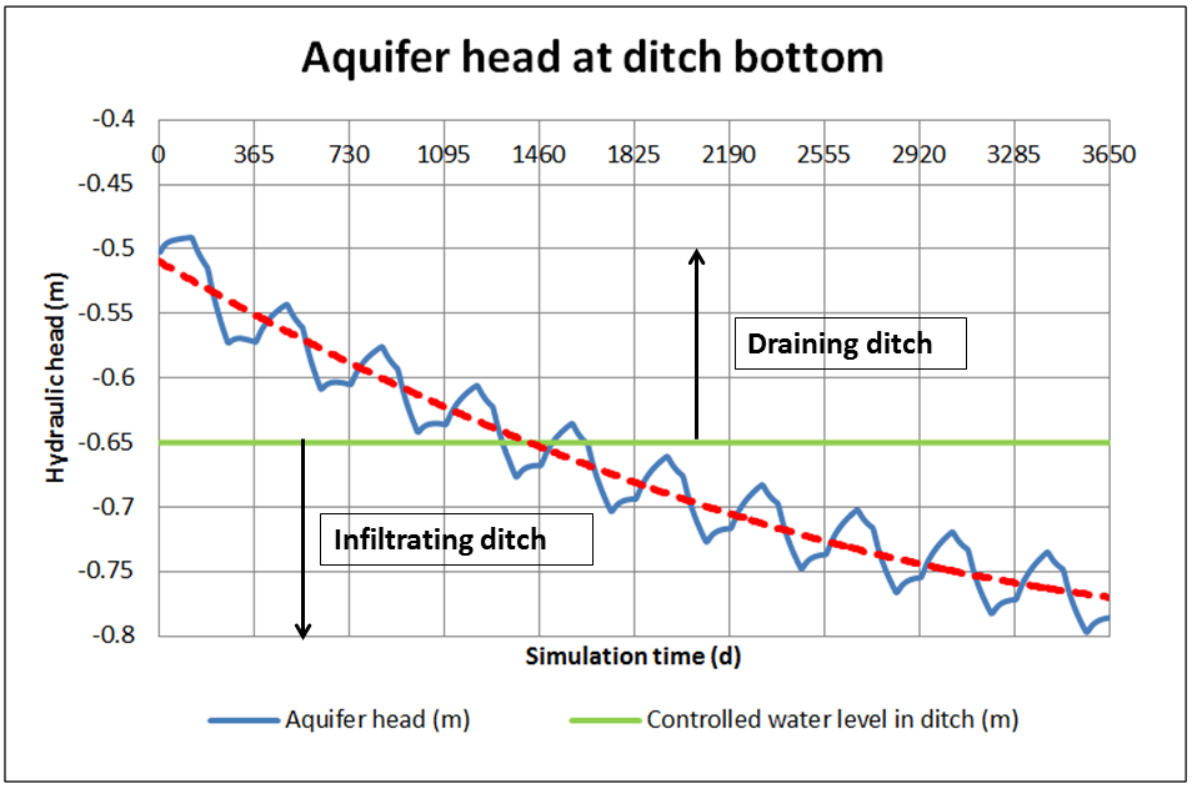

Figure 4.18 – The hydraulic head in the aquifer directly under the ditch (blue curve), the average head per ASR-cycle is given by the dashed red line. The controlled water level in the ditch is given by the green line. If the head in the aquifer is higher than the controlled water level, drainage takes place. If the head in the aquifer is lower than the controlled water level, infiltration takes place.

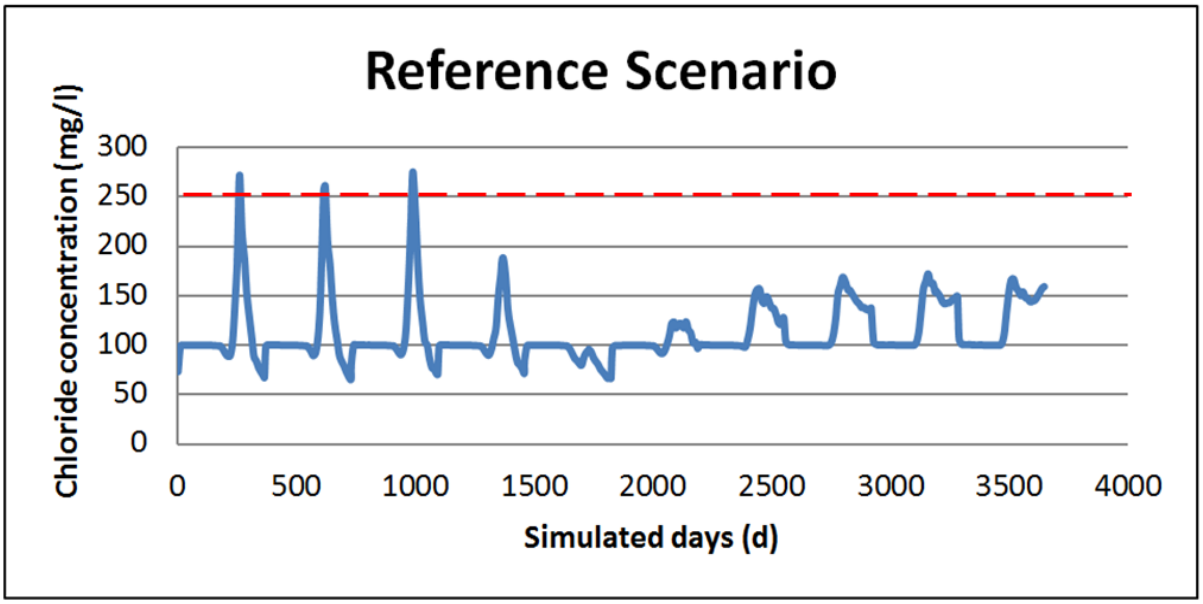

Figure 4.19 - Chloride concentration at HDDW1 for the reference scenario. A total number of 10 ASR-cycles of 365 days are shown. The dashed red line indicates the maximum allowed chloride concentration limit (250 mg/l).

4.3.2 Scenario 1 – Variable target volumes

The results of Scenario 1 are shown in the left plot in Figure 4.20. There appears to be a relation between the target volume and the RE. When the target volume was less than the reference target volume (Scenario A), the RE was always 100%. When larger target volumes were intended, lower REs could be achieved. The RE of Scenario B was initially significantly lower than the reference scenario but still reached 99% in Cycle 4. Scenarios C and D never reached the same RE as the reference scenario but led to maximum values for the RE of 70% and 50% respectively.

Figure 4.21 shows the recovered freshwater volumes which correspond to the REs shown in Figure 4.20. It can be seen that 6.000 m^3 was the maximum recoverable volume. Injecting larger freshwater volumes than 6.000 m^3 (scenarios C and D) did not result in a larger recoverable volume but decreased the maximum recoverable volume instead. Nevertheless, it was always possible to abstract more freshwater than the reference scenario, even if the REs were significantly lower.

Note that the simulated pumping rate of HDDW2 was equal for each scenario. It was analysed whether it was possible to reach higher REs for large target volumes when the pumping rate of HDDW2 was increased too. A higher HDDW2 pumping rate might prevent the upconing responsible for the low REs. All scenarios were ran again while keeping the pumping ratio between Q_{HDDW1}/Q_{HDDW2} constant at 1. The results of the simulations are shown in the right plot in Figure 4.20. The REs did not improve but decreased. The RE of Scenario B did not exceed 50% while the RE reached 100% when the pumping rate of HDDW2 was kept constant.

One mechanism behind this poor performance was that the higher HDDW2 pumping rates increased horizontal flow. The freshwater lens in the North (right lens in Figure 4.22) is significantly thinner than the freshwater lens in which the Freshmaker was installed (left lens in Figure 4.22). This means that the fresh-saltwater interface was shallower in the North and thus high chloride concentrations were present at shallower depth. As HDDW2 started abstracting at higher rates, the significantly more water from the North flowed towards the Freshmaker. The fresh-saltwater interface did not go down, but remained shallow during transport as streamlines were horizontal and the flow system was dominated by pumping, not by density dependent flow. As a result, water with high chloride concentrations were abstracted by HDDW1 leading to low REs.

Another mechanism was that large volumes of freshwater were lost in the injection phases by abstraction of HDDW2 which operated with high pumping rates during scenarios B - D.

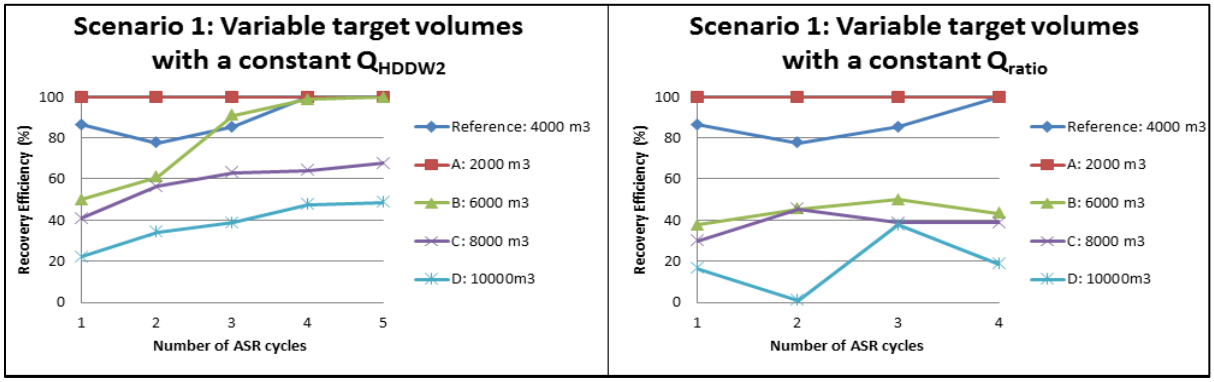

Figure 4.20 - Calculated recovery efficiency of Scenario 1, using two different approaches. Left: the abstraction rate at HDDW2 was kept constant, right: the ratio between HDDW1 and HDDW2 was kept constant.

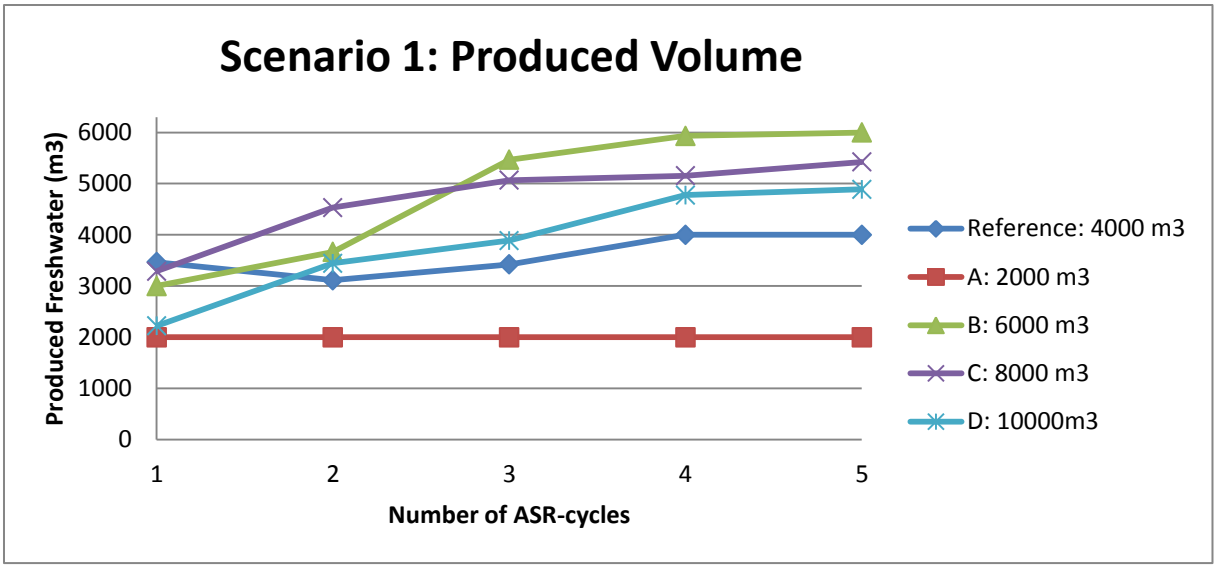

Figure 4.21 – Maximum recovered volume of freshwater in Scenario 1 for different injected volumes of freshwater. The abstraction rate of HDDW2 was kept at a constant rate, equal to the reference scenario.

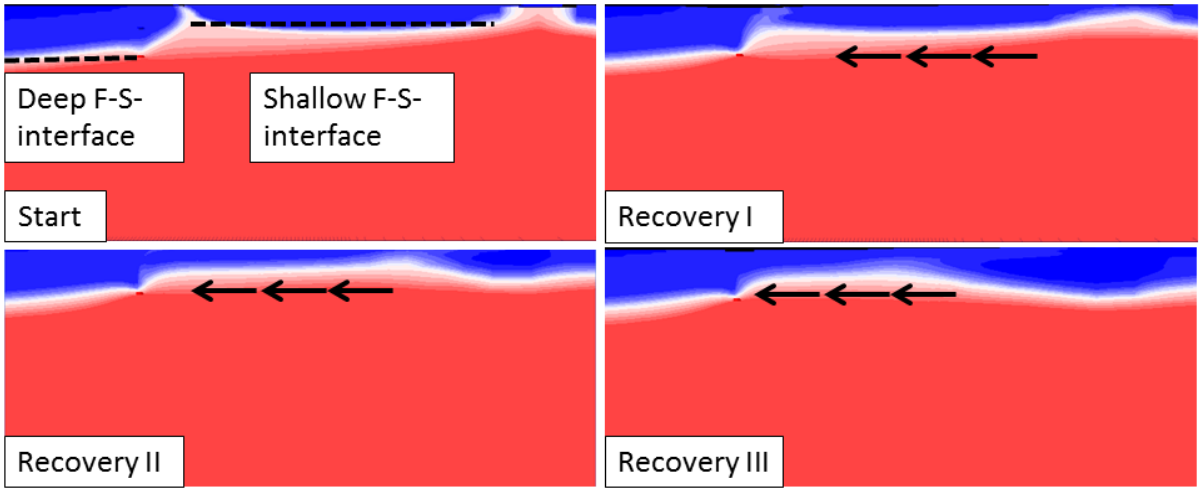

Figure 4.22 - Large-scale chloride concentration distributions from the start until Recovery phase III. Results shown are from Scenario D. The shallow fresh-saltwater interface moved towards the Freshmaker due to significant horizontal flow. Contours are identical for each figure and increase logarithmically from 0 (blue) to 16800 mg/l (red).

4.3.3 Scenario 2 – Variable recovery phase lengths

Figures 4.23 shows the influence of the length of the recovery phase. As the total volume of abstracted water by HDDW1 and HDDW2 remained equal to the reference scenario for all scenarios, the same trend was observed as identified previously in Section 4.3.1. The RE first decreased from Cycle 1 to 2 but increased to 100% after Cycle 4 to stay at that level from Cycle 4 onwards.

Nevertheless, there appears to be a positive correlation between the length of the recovery phase and the RE. When the same amount of water was abstracted in a shorter time span, the resulting RE was smaller.

The influence of splitting up a recovery phase of 60 days in separate recovery series of varying durations is shown in Figure 4.24. For Cycle 1, no significant differences could be observed between the scenarios with separate recovery series (2D-2F) and the corresponding reference scenario with only one recovery series of 60 days. For Cycle 2 and 3, the differences were more distinct but no clear relation between period durations could be observed.

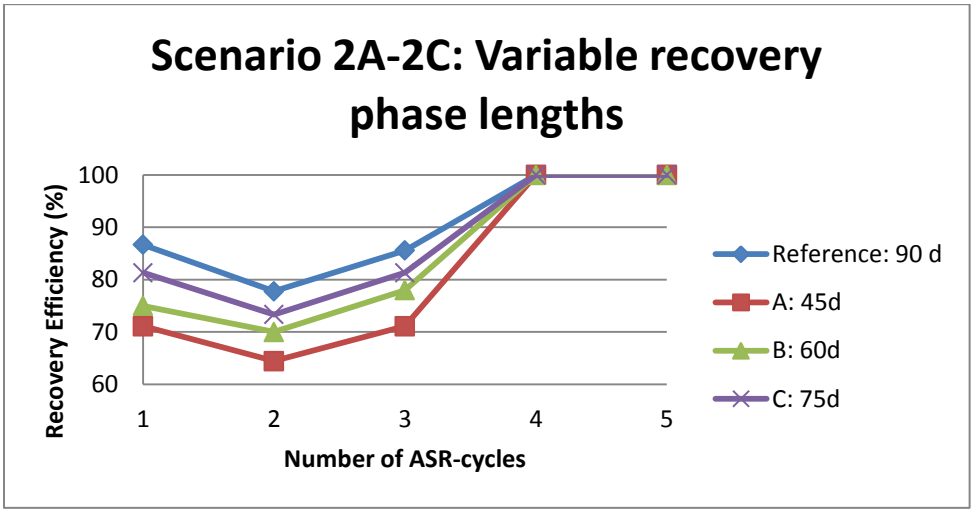

Figure 4.23 - Calculated recovery efficiency for 5 ASR-cycles of Scenario 2_A - 2_C.

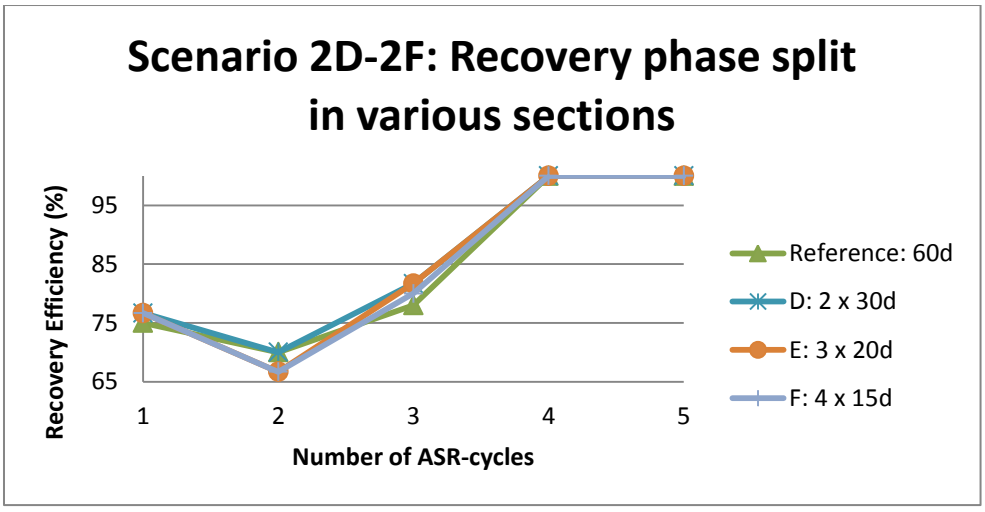

Figure 4.24 - Calculated recovery efficiency for 5 ASR-cycles of Scenario 2_D - 2_F.

4.3.4 Scenario 3 – Potential well failure

Figure 4.25 shows the results from Scenario 3. Higher REs were achieved when HDDW2 was deactivated in the injection phase. RE was decreasing with increasing failure duration in the storage and recovery phases, though slightly faster when failure occurred in the recovery phase. If the failure duration was 7 days, the RE loss was 5% and 6% for failure in the storage and recovery phase respectively. If the failure duration was 30 days, the RE loss was 12% and 14% for failure in the storage and recovery phase respectively. The overall influence of HDDW2 failure on RE was a decrease between 0.5% and 1% per day.

The increase in RE resulting from HDDW2 failure in the injection phase can be accounted to two mechanisms: 1) when HDDW2 fails, the saline water cone under the ditch was drawn less towards the Freshmaker, and 2) when HDDW2 fails, less injection water is abstracted by HDDW2.

However, the RE decreased when HDDW2 failed during the storage phase. Thus, Mechanism 1 cannot be the contribution factor for the RE increase, as the saline water cone is drawn closer by HDDW2 during all phases identically as Q_{HDDW2} was constant. Therefore the RE increase was due to Mechanism 2. If less injection water is abstracted by HDDW2, the volume of freshwater around the Freshmaker will be larger. The size of the injected freshwater bubble at the end of the injection phase for HDDW2 well failure of respectively 1 and 30 days is shown in Figure 4.26. It can be seen that the size (and therefore the total volume) of the freshwater bubble was significantly larger if HDDW2 failure lasted longer.

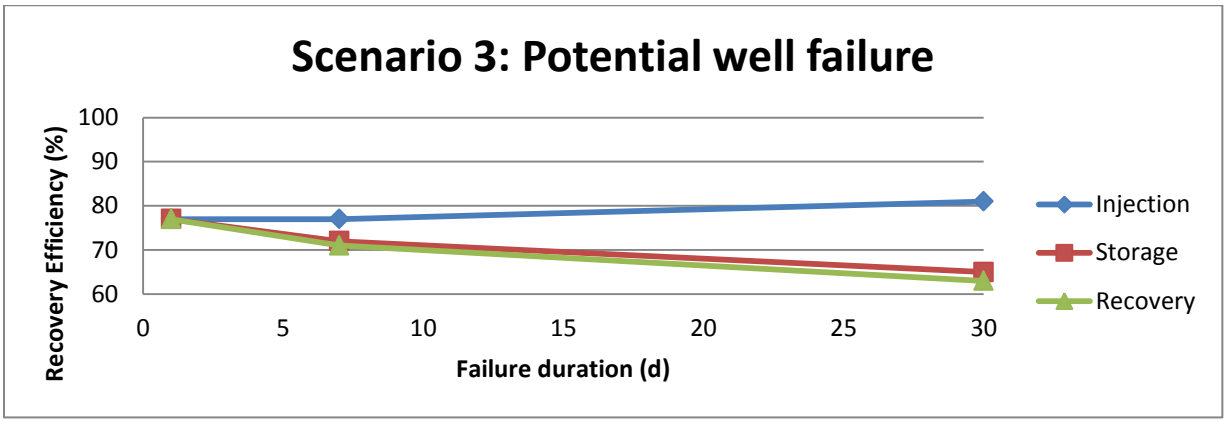

Figure 4.25 - Calculated recovery efficiency for 5 ASR-cycles of Scenario 3.

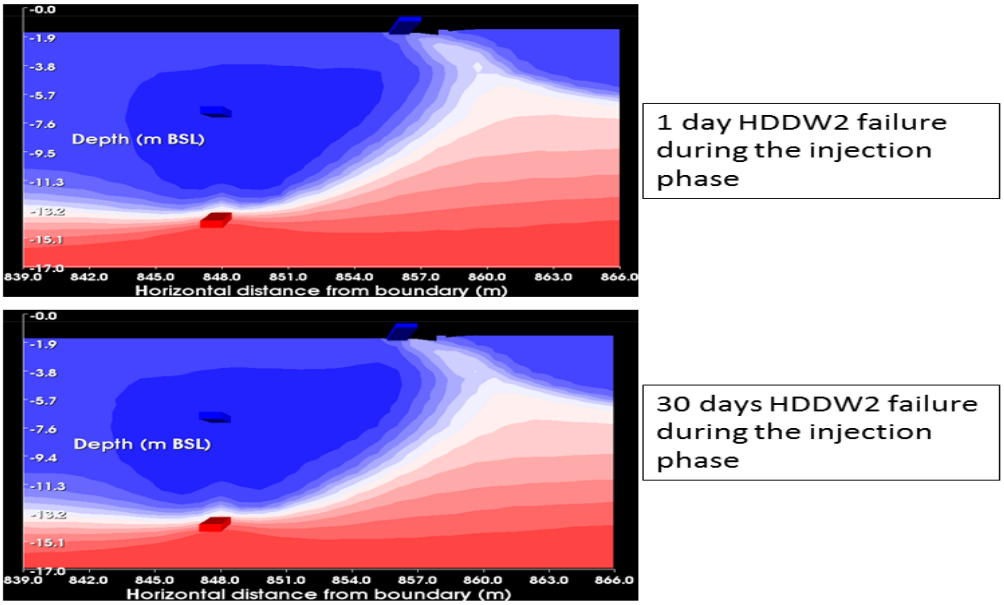

Figure 4.26 - Size of the injected freshwater bubble following a HDDW2 failure of 1 day (upper figure) and 30 days (lower figure).

4.3.5 Scenario 4 – Decreasing HDDW2 pumping rates

The effect of decreasing HDDW2 pumping rates on the RE is shown in Figure 4.27. As HDDW2 pumping rates fell, the RE seemed to increase with respect to the reference scenario. ASR-cycle 2 and 3 showed a RE increase for Scenario A, B, and C. REs in Cycle 4 were lower than the reference. Scenario A reached a RE of 100% in Cycle 5 and although not shown in the figure, Scenario B reached 100% RE in Cycle 6. The REs in Cycle 5 and onwards did not reach 100% when the pumping rates were decreased more than 50% (Scenario C-D).

A pattern was identified in Figure 4.27: decreasing HDDW2 rates seemed to smooth out the effect that was identified for the reference scenario (i.e. salinization due to sinking of the saltwater cone, initially present under the ditch). As HDDW2 pumping rates were decreasing, saline water from the sinking saltwater cone drawn less towards the HDDWs. This resulted in higher RE during ASR-cycles 2 and 3, which otherwise had lower REs due to upconing of saline water originating from under the ditch. However, although now at a lower rate, the salt water cone was still sinking in. This resulted in a prolonged RE decrease as the saline water cone had not settled sufficiently.

The resulting effect of spreading the influence of the sinking saltwater cone on the average RE of 5 cycles is visualized in Figure 4.28, which displays the average RE of the simulated ASR-cycles for all scenarios. The highest RE (with an average of 95%) was obtained with a 50% pumping rate decrease. Average REs decreased with lower HDDW2 pumping rates than Scenario B. Note that this figure is only valid for the first 5 ASR-cycles. From Cycle 6 onwards, the results will be different since all scenarios except Scenario C and D had reached 100%.

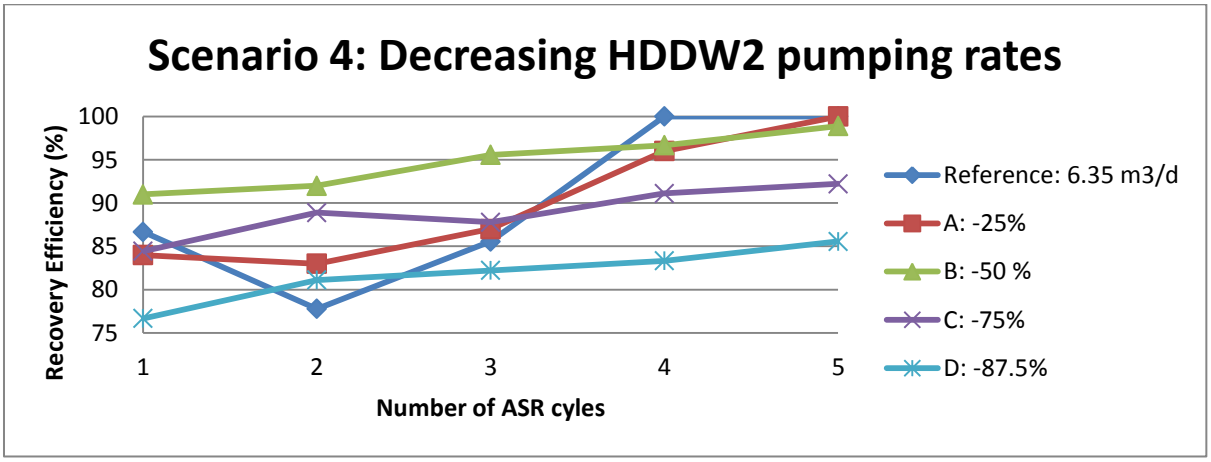

Figure 4.27 - Calculated recovery efficiency for ASR-cycle 1-5 of Scenario 4.

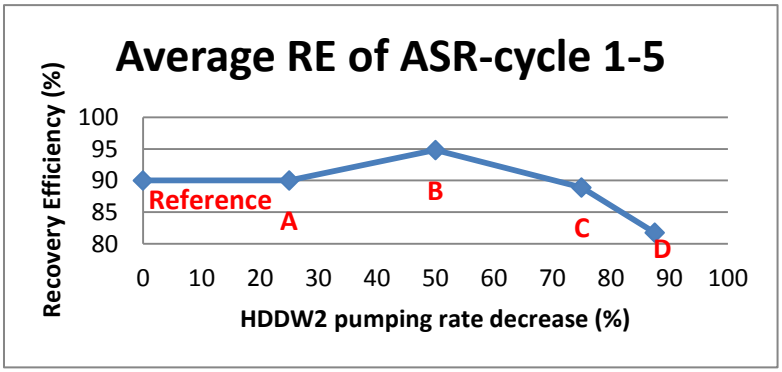

Figure 4.28 - Average recovery efficiency of ASR-cycle 1-5 following the decreases in HDDW2 pumping rates. The corresponding scenarios can be identified with the red letters next to the data points.

4.3.6 Scenario 5 – Varying HDDW1 placements

Figure 4.29 shows the influence of the location where HDDW1 is placed on the RE. The location of HDDW2 and the pumping rates of both HDDW1 and HDDW2 were kept constant in all scenarios. The distance between HDDW1 and HDDW2 was strongly correlated to the RE. The greater the distance between HDDW1 and HDDW2, the higher the RE. If the distance between HDDW1 and HDDW2 was increased to 10 m, the RE never fell below 100% (Scenario C).

Nevertheless, when the distance was smaller than the reference distance (Scenarios A and B), REs significantly increased during multiple ASR-cycles. For instance, Scenario A started with a RE of only 40% but reached 80% in Cycle 5. This significant RE increase after Cycle 1 was caused by the same principle as discussed before: the saltwater cone under the ditch sank after multiple ASR-cycles.

The influence of the salt water cone under the ditch is also reflected in the results of Scenario D – G. REs improved significantly when HDDW1 was placed only 1 m further to the left (i.e. further from the ditch), and they never fell below 100% when HDDW1 was placed 2 m to the left. On the other hand, when HDDW1 was placed 1 or 2 m to the right (i.e. closer to the ditch), REs decreased. However, after 5 ASR-cycles, the upconing under the ditch was sufficiently decreased that it was also possible to achieve 100% RE when HDDW1 was placed 1 or 2 m to the right.

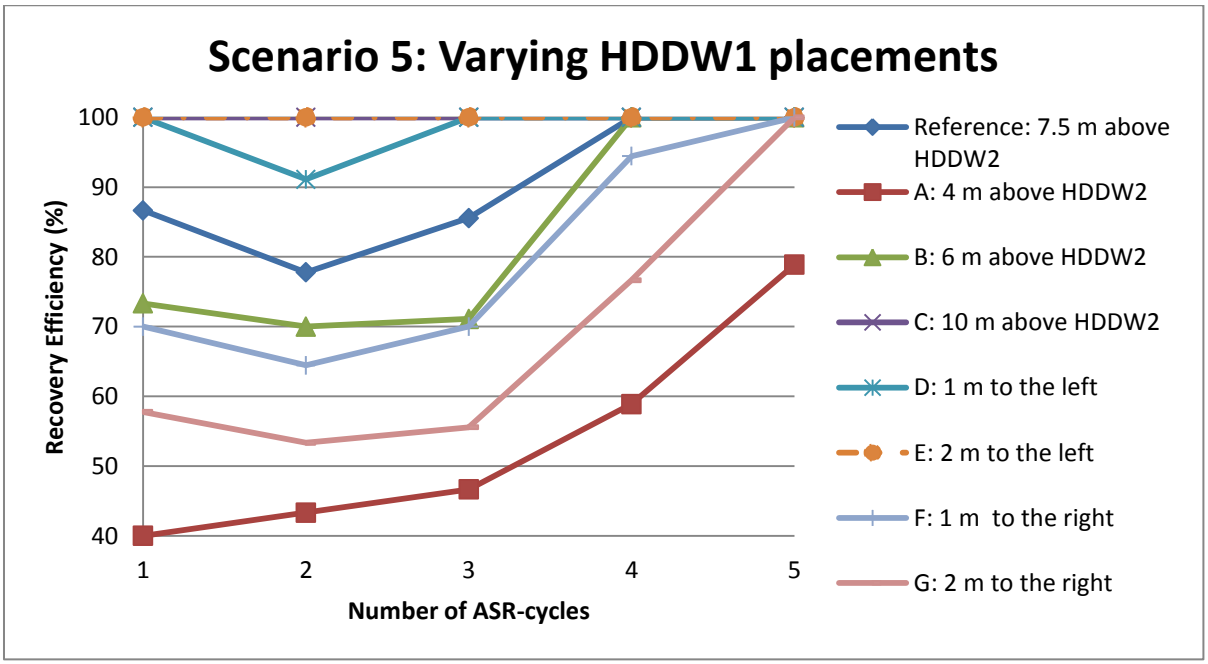

Figure 4.29 - Calculated recovery efficiency for 5 ASR-cycles of Scenario 5 storing 4000 m³ of freshwater. Note by Scenarios D – G : to the left equals to the South (i.e. further from the ditch), to the right equals to the North (i.e. closer to the ditch).

4.3.7 Scenario 6 – upscaling

A description of the different upscaling scenarios can be found in Section 3.3. Two methods were used to determine the resulting RE for the scenarios where more than one ASR-well was simulated:

(1) Pumping from a well which abstracts water with chloride concentrations exceeding the allowed limit is immediately terminated, the other wells will continue until they also abstract water with concentrations exceeding the limit. The resulting RE is the average RE of all wells used in the scenario.
(2) The concentration of the water that is abstracted by all wells is averaged. If the average chloride concentration exceeds the allowed concentration limit, pumping from the well which pumped up water with the highest chloride concentrations is aborted. The other wells continue until the average concentration exceeds the limit again etcetera. The resulting RE is the average RE of all wells used in the scenario.

The results are shown in Table 4.2. The RE decreased with respect to the RE of the reference scenario when two ASR-wells (upper wells) and one interception well (lower well) were used (Scenario A). The same scenario but with a 2nd interception well (Scenario C) resulted in a RE increase from 71% to 87%. The results were identical for RE determination method 1 and 2.

Two interception wells under one ASR-well, while keeping the abstraction rates identical to the reference scenario increased the RE from 71% to 80% (Scenario B). This can be explained by the fact that the area of upconing under the ASR-well was larger than could be captured by one interception well alone. Installing two interception wells increased the area over which upconing was limited, increasing the RE.

Scenario D and E showed identical results. Lower REs than the reference scenario were obtained when the 1st determination method was used and no significant difference was observed when the 2nd determination method was used. Using Method 1, the outer ASR-wells salinized relatively fast with respect to the ASR-well in the middle. Nevertheless, even though the ASR-well in the middle could remain active for a long period, it was only 1/3 of the total number of wells. Therefore the resulting average REs of scenarios D and E were lower than the reference scenario. This also explains why the RE of Scenario G obtained with Method 1 was higher than the REs of Scenario D and E. In Scenario G there were 4 wells in total, so 2 wells in the middle. These wells were also active longer and made up 1/2 of the total number of wells which is a larger weighing factor than 1/3 resulting in a higher average RE. Use of the 2nd determination method resulted in a higher RE for scenarios D-G as all wells could be active for a longer period because of dilution with (fresher) water from wells in the middle.

Upscaling of the Freshmaker, using the exact same number of ASR-wells as interception wells and placing them vertically resulted in a significant increase in RE (scenarios C and F) according to both Method 1 and 2.

Table 4-2 - Calculated recovery efficiency of scenario 6 using two calculation methods. The calculation methods are described in the main text. The ASR-wells represent HDDW1 and the interception wells HDDW2.

Scenario	1st method	2nd method	Configuration (ASR-well : interception well)
Reference	71	71	1 : 1
A	55	55	2 : 1
B	80	80	1 : 2
C	87	87	2 : 2
D	60	72	3 : 1
E	63	73	3 : 2
F	84	97	3 : 3
G	71	83	4 : 3

4.4 Hydrogeological parameters

4.4.1 Scenario I: Hydraulic conductivity

The results of Scenario I are shown in Figure 4.30. The results show that scenarios with lower hydraulic conductivities than the reference scenario (I_A and I_B) were able to achieve 100% RE in Cycle 1 already. This was a significant improvement with respect to the RE of the reference scenario where the RE in Cycle 1 was 70% and increased to 93% in Cycle 3. The RE was lower when a higher hydraulic conductivity was simulated (Scenario I_C). This scenario was run for 5 ASR-cycles since the results were significantly different from Scenarios I_A and I_B. Cycle 1 and 2 had low REs (60%) but increased to 88% in cycle 3 only to decrease again in cycle 4 (74%). Although, the behaviour of Scenario I_C was not well understood there appears to be a strong positive inverse relation between the hydraulic conductivity and the RE.

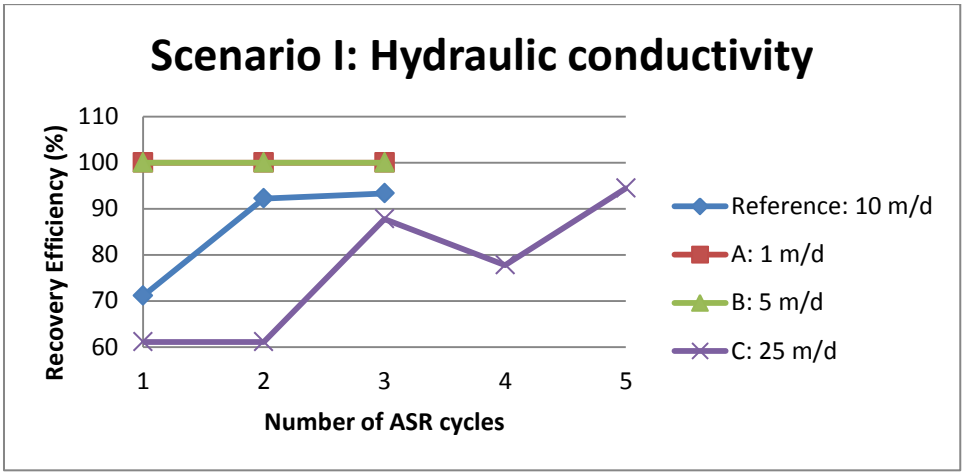

Figure 4.30 – Calculated recovery efficiencies of Scenario I. Note that only scenario I_C was extended for 5 ASR-cycles.

4.4.2 Scenario II: Vertical anisotropy

A similar relation was observed for Scenario II as was observed for Scenario I. The results are shown in Figure 4.31. The RE increased to 100% for all scenarios in which a vertical anisotropy was simulated. Even a vertical anisotropy of 2 resulted in a significant increase in RE. This can be explained by the fact that the increased vertical resistance to flow leads to less vertical flow and more horizontal flow. As a consequence, there will be less upconing of salt water as there is less vertical flow. Furthermore, a vertical anisotropy of 2 means that the vertical hydraulic conductivity was 5 m/d. Simulations with a isotropic hydraulic conductivity of 5 m/d also reached a RE of 100% (Scenario I_B).

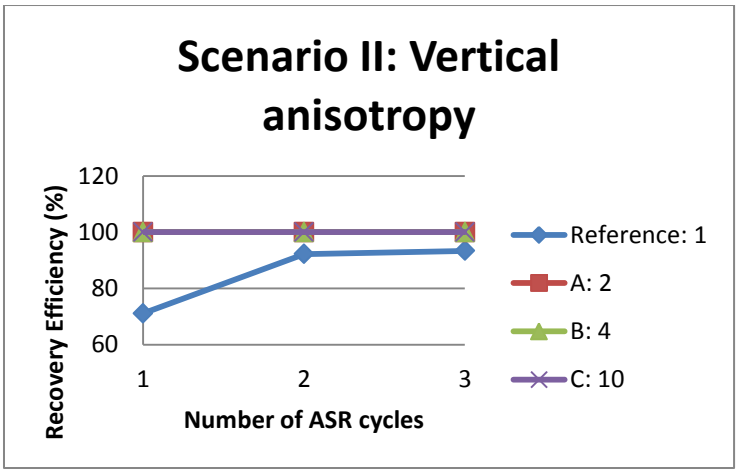

Figure 4.31 - Calculated recovery efficiencies of Scenario II. Note that the hydraulic conductivity of the reference scenario was 10 m/d.

4.4.3 Scenario III: Porosity

Injection of 4000 m^3 freshwater was simulated for a porosity range of 0.2 – 0.5. The results are shown in Figure 4.32. The achieved REs were lower for a porosity of 0.2 (Scenario A) than for a porosity of 0.5 (Scenario B). The difference was 25% in cycle 1, 22% in cycle 2 and 19% in cycle 3. A lower porosity with the same specific discharge (i.e. injected volume) means that the flow velocity in the pores is higher. Saline water will thus reached the ASR well faster when the porosity was lower, which explains the observed decrease in RE.

The Freshmaker increases the size of the freshwater lens by the injection of freshwater which displaces the fresh-saltwater interface. However, the maximum increase of the freshwater lens is determined by the distance between HDDW1 and 2. Further displacement of the fresh-saltwater interface than HDDW2 is not possible due to abstractions at HDDW2. If the porosity is high, an identical distance between the HDDWs means a larger potential freshwater storage volume than if the porosity is low. This explains why the maximum achievable RE was lower with a lower porosity: a larger volume of freshwater was injected than could be stored. As a result, a significant volume of freshwater was lost due to abstraction by HDDW2 each ASR-cycle.

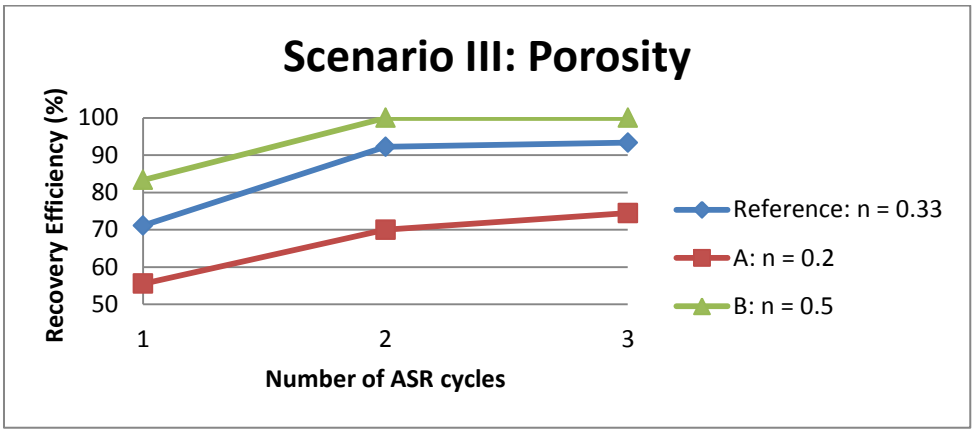

Figure 4.32 - Calculated recovery efficiencies of Scenario III.

4.4.4 Scenario IV: Dispersion

The results of Scenario IV are shown in Figure 4.33. Apparently, dispersion has a distinct effect on the RE. This was caused by the increased amount of mixing that results from larger dispersivities. The sensitivity of the RE to the value of the dispersivity is very large. If the longitudinal dispersivity increased from 0.2 m to 1 m the RE significantly decreased. Where it was possible to achieve a RE of 80% with a dispersivity of 0.2, the RE was only 20% with a dispersivity of 1 m. Increasing the dispersivity even further resulted in a RE of 0%. It can be concluded that the dispersivity is strongly correlated to the RE: the larger the dispersivity, the lower the RE.

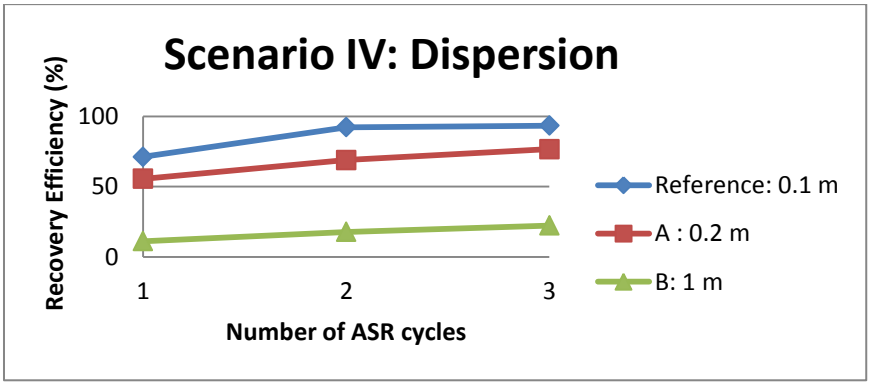

Figure 4.33 - Calculated recovery efficiencies of Scenario IV.

4.4.5 Scenario V: Ambient chloride concentration

The results of Scenario V are shown in Figure 4.34. The effect of the ambient chloride concentration was that REs were significantly higher than the reference scenario when the simulated ambient chloride concentrations were lower (Scenario V_A and V_B: 5000 and 10000 mg/l respectively). Scenario V_A and V_B could both achieve a RE of 100% in ASR-cycle 2. The RE decreased when the ambient concentration was higher than the reference scenario (Scenario V_C: 20000 mg/l). In ASR-cycle 2, the RE of Scenario V_C was about 15% lower than the reference scenario.

There is therefore a relation between the ambient concentration and the RE. A lower ambient concentration results in a higher RE. Density effects were believed to be the main contributors to this observed relation.

The density effects were studied using the chloride concentration distributions as shown in Figure 4.35. The concentration distributions showed that saline water (20000 mg/l) was less easily displaced than brackish water (5000 mg/l) in the injection phase. In the storage and recovery phases, the fresh-saltwater interface tilted due to the fact that convection by gravity and pumping reinforced each other. This tilting was faster for the scenario with saline water as convection by gravity is stronger for denser water. As a result, the fresh-saltwater interface in the scenario with saline water was located closer to HDDW1 at the exact same day of the ASR-cycle than the scenario with brackish water. This led to more upconing and therefore a lower RE. Nevertheless, after 3 cycles, all scenarios were able to achieve a RE higher than 90%.

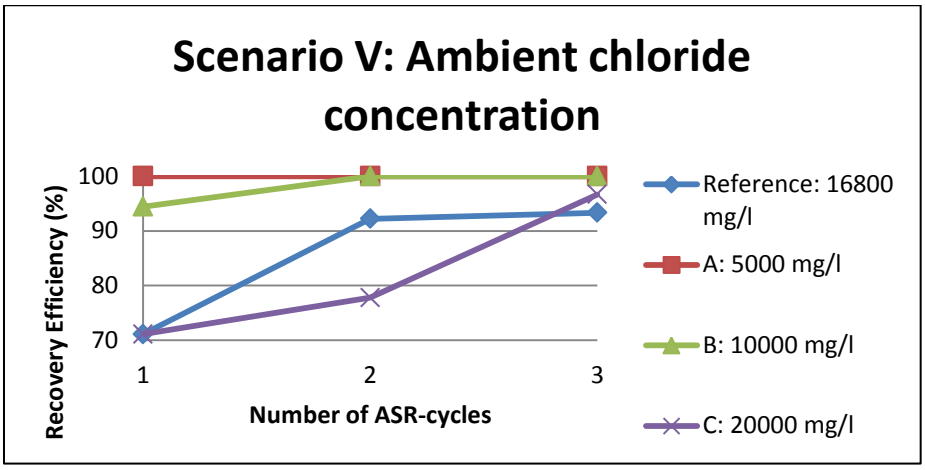

Figure 4.34 - Calculated recovery efficiency of Scenario V.

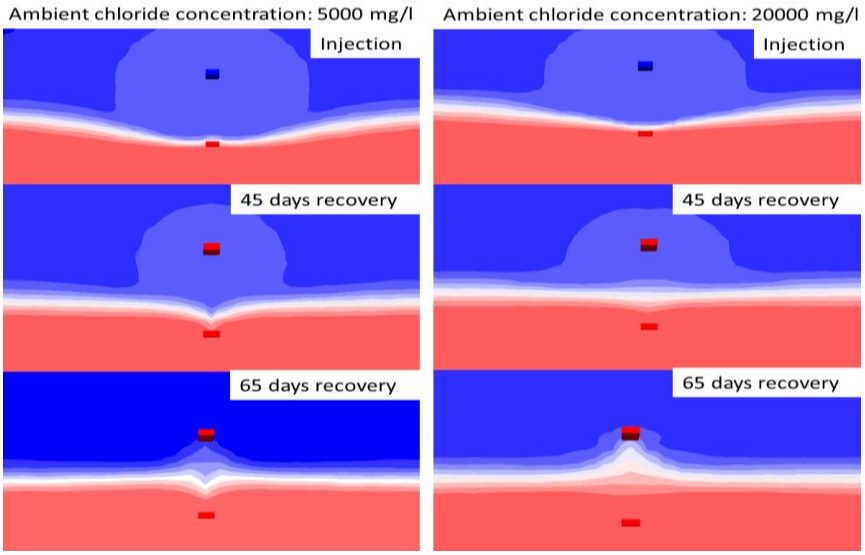

Figure 4.35 - Chloride concentration distributions at the injection phase, 45th, and 65th day of the recovery phase for two scenarios. Left: Scenario A (5000 mg/l), right: Scenario C (20000 mg/l).

4.4.6 Scenario VI: Heterogeneity

The REs for the different heterogeneity scenarios are shown in Figure 4.36. Chloride concentration distributions for several time frames are shown in Figure 4.37. A distinction was made between scenarios with a clay layer or clay lenses (Scenario A-C) and scenarios with a gravel layer and gravel lenses (Scenario D-F). Layers were continuous and lenses were non-continuous features in the aquifer.

In general, Scenarios A-C resulted in a higher RE than the reference scenario. However, when a clay lens was simulated left of the HDDW pair (Scenario A), the RE was lower than the reference scenario. The reason for this decrease was identified from the chloride concentration distributions, as displayed in Figure 4.37. Not all saline water was flushed out of the clay lens during the injection phase and the lens was therefore functioning as a saline water source. The lens which contained saline water was located closer to HDDW1 than the fresh-saltwater interface and was therefore responsible for the earlier arrival of saline water at the well. The saline water in the clay lens was flushed out effectively with an increasing number of ASR-cycles. As a result, the RE in cycle 3 was even higher than the reference scenario. The higher RE in cycle 3 was caused by the fact that the clay lens no longer contained saline water. Furthermore, the presence of the lens increased the resistance to vertical flow and therefore partly protected HDDW1 from upconing.

Saline water also remained in the clay lens when the lens was in between HDDW1 and HDDW2 (Scenario B). However, opposed to Scenario A, the achieved REs of Scenario B were higher than the reference scenario, also in ASR-cycle 1 and 2. Apparently, the positive effect of a resistance to vertical flow between HDDW1 and 2, which limited upconing, was stronger than the negative effect of having an extra nearby saline water source.

100% RE was achieved when a clay layer was present between HDDW1 and HDDW2 (Scenario C). This was caused by the fact the saline water present above the clay layer was displaced to the sides by injection of HDDW1 and, more important, drawn vertically into the clay layer due to abstraction by HDDW2. During the recovery phase, the saline water migrated upwards, out of the clay layer. Despite this vertical flow, the saline water was not able to reach HDDW1 as HDDW2 abstractions were already going on for 180 days (injection + storage phase) before recovery started. The saline water had already moved further through the clay layer than it could flow back in the recovery phase, since the recovery phase lasted only 90 days. Furthermore, the saline water moved faster into the clay layer (injection phase) than out of the clay layer (recovery phase) since the combined activity of HDDW1 and 2 enforced downward flow in the injection phase but limited upward flow in the recovery phase.

The situation was different for scenarios with the gravel layer and gravel lenses, which in general led to a lower RE than the reference scenario. Especially the scenario with the gravel layer (Scenario D) had low REs. During the injection phase, the saline water was flushed out from the gravel layer and the layer was filled with freshwater. Nevertheless, in the recovery phase, saline water flowed into the gravel layer from below and was transported a high velocity towards HDDW1 explaining the low RE. Note the flow vectors in Figure 4.37, which indicate the pore velocity, identifying the relatively fast horizontal flow in the gravel layer. Since HDDW2 was pumping continuously, more and more saline water was drawn into the gravel layer (since this was the route with the least resistance to flow) with every passing ASR-cycle. As a result, the RE decreased from Cycle 1 to Cycle 3.

The RE was also lower when gravel lenses were modelled, as this also increased the upconing of saline water flowing horizontally (Scenario E) or vertically (Scenario F) through the lens. Nevertheless, after 3 ASR-cycles, the saline water was displaced sufficiently far from the gravel lenses that high REs could be obtained.

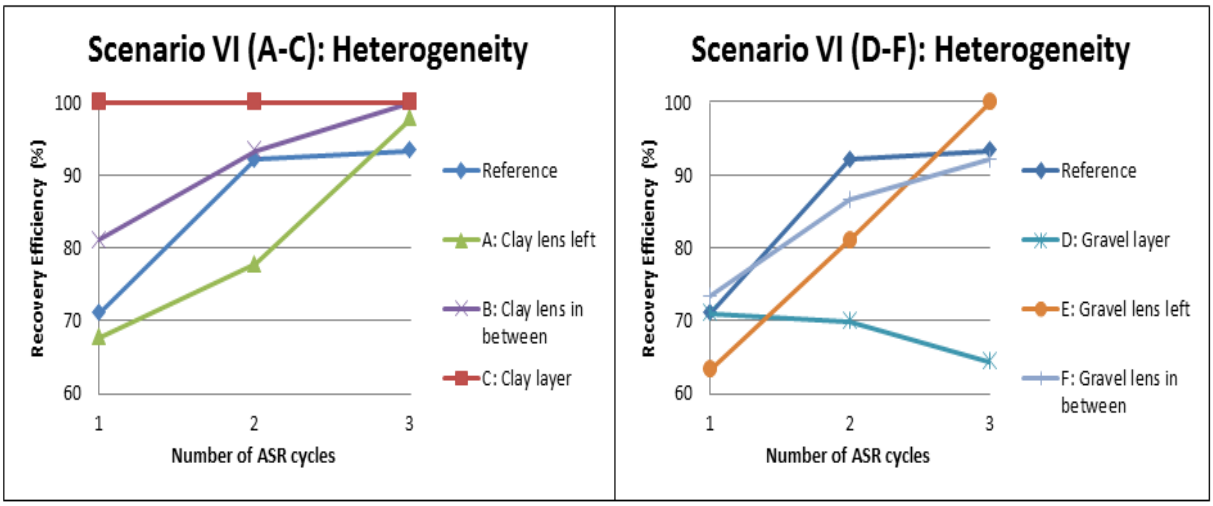

Figure 4.36 - Calculated recovery efficiency of Scenario VI. The left plot shows the results of the scenarios with clay (VI_A - VI_C) and the right plot the results of the scenarios with gravel (VI_D - VI_F).

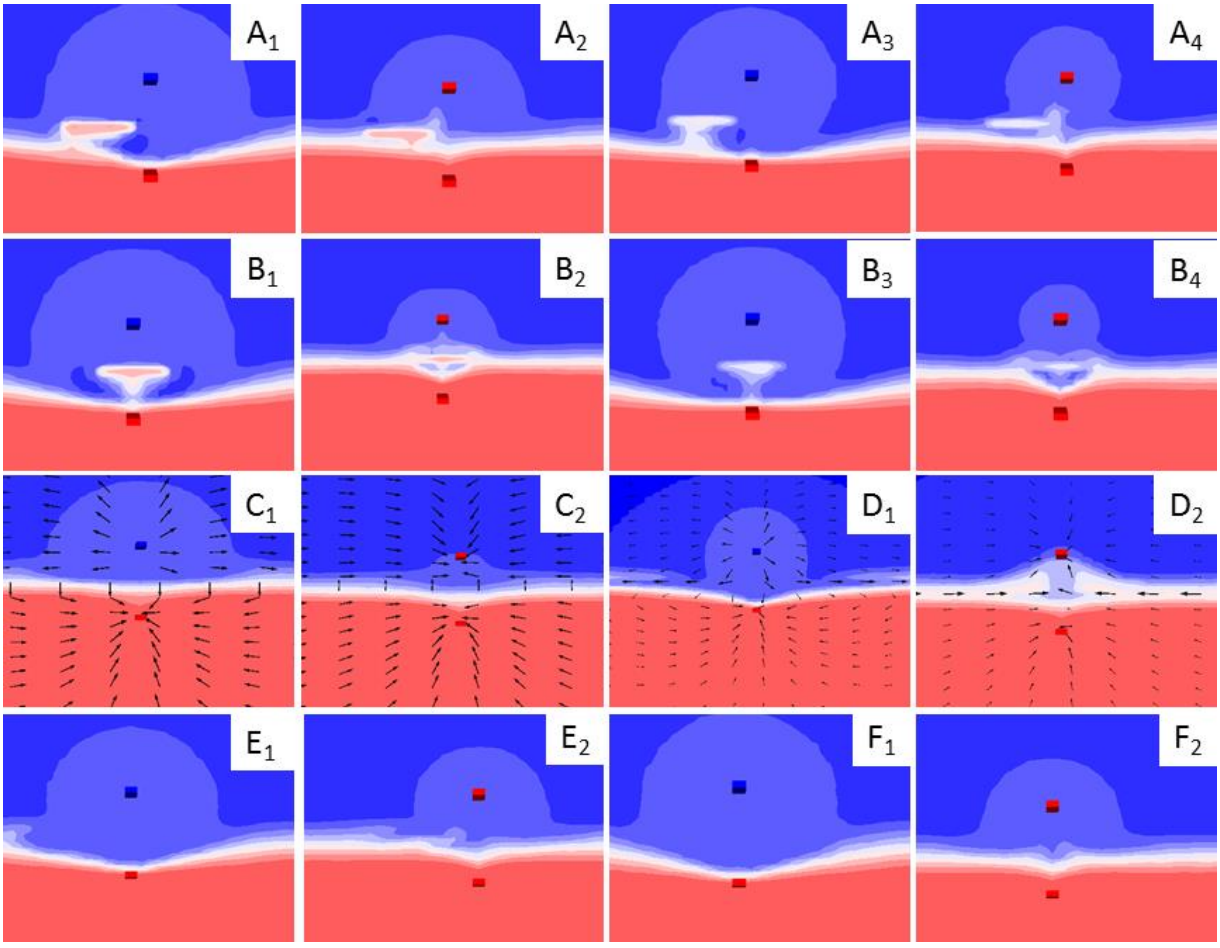

Figure 4.37 - Chloride concentration distributions of Scenario VI_A - VI_F. The indexes indicate: 1) 100% injection phase I, 2) 50% recovery phase I, 3) 100% injection phase III, and 4) 50% recovery phase III. Flow vectors are shown in Figure C1-D2 in order to visualize flow in the clay and gravel layers. Contours are identical for each figure and increase logarithmically from 0 (blue) to 16800 mg/l (red).

4.4.7 Scenario VII: Background flow

The influence of background flow on the RE is displayed in Figure 4.38. The results of Scenario A do not differ significantly from the results of the reference scenario, although the injected freshwater bubble drifted down gradient as can be seen in Figure 4.39. The other scenarios, which had larger head gradients, suffered from significantly decreasing REs.

Due to the significant background flow in Scenario B and C, all of the injected freshwater was lost downstream and hence the Freshmaker was only able to increase the volume of the freshwater lens downstream of the Freshmaker. Downstream of the HDDW-pair the fresh-saltwater interface was lowered but upstream the fresh-saltwater interface remained shallow throughout the injection phase. During the recovery phase, the capture zone of HDDW1 was completely located upstream of the Freshmaker, where the fresh-saltwater interface was still shallow. As a consequence, the REs of Scenarios B and C were significantly lower than the reference scenario. This was different in Scenario A, where the capture zone was also located downstream.

The RE of Scenario B and C got lower with every passing ASR-cycle. This was caused by a slow build up of saline water directly upstream of the HDDW pair, slowly thinning the freshwater lens with every passing ASR-cycle, leading to earlier salinization of HDDW1.

In general, it was observed that a higher background head gradient led to a lower RE.

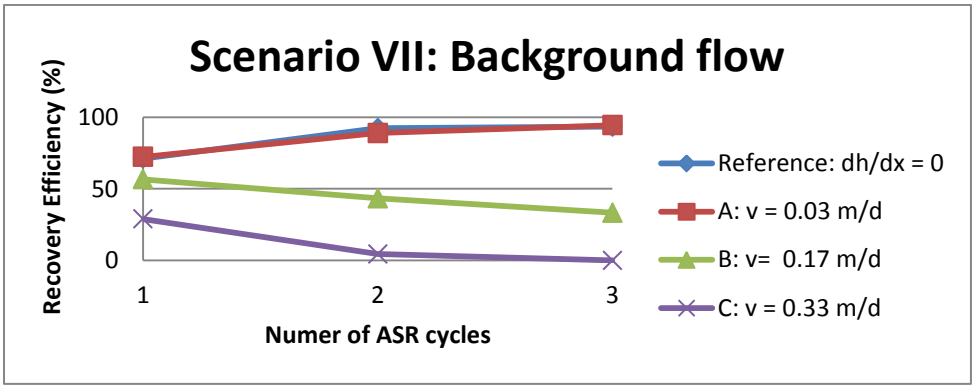

Figure 4.38 - Calculated recovery efficiency of Scenario VI. The flow velocities correspond to the pore velocity (v = q/n).

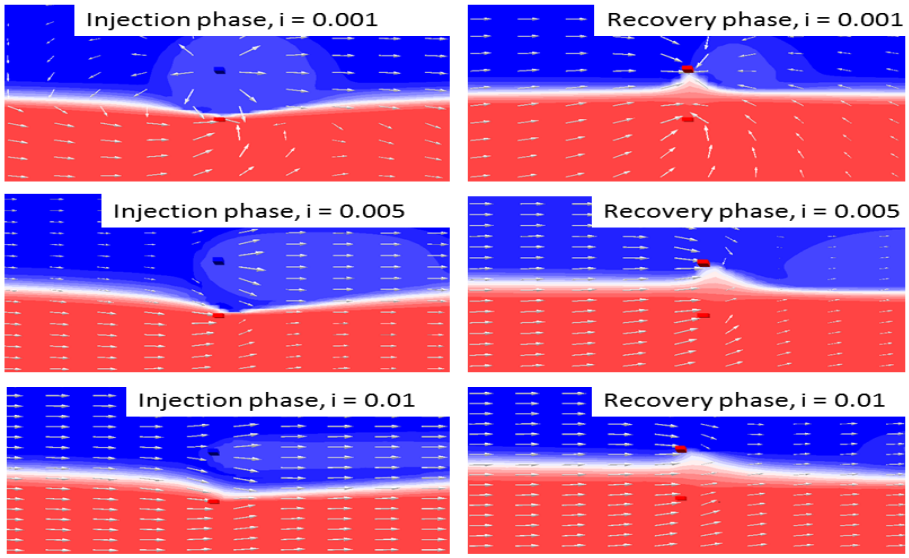

Figure 4.39 - Chloride concentration distributions in Injection phase I and Recovery phase I for three different scenarios. From top to bottom: Scenario VII_A, VII_B, and VII_C. dh/dx = i. Contours are identical for each figure and increase logarithmically from 0 (blue) to 16800 mg/l (red).

4.5 Maximum storage capacity at Ovezande

The results of the scenarios with variable target volumes (Scenario 1) and variable HDDW2 pumping rates (Scenario 4) were used to analyse the maximum storage capacity at Ovezande. Results from Scenario 1 showed that the maximum storage capacity that could achieve a RE of 100% was 6000 m^3. When larger target volumes than 6000 m^3 were simulated (8000 m^3 and 10000 m^3) the RE significantly decreased. In Section 4.3.5 it was concluded that lower HDDW2 pumping rates resulted in higher RE. It was therefore studied whether higher REs and larger produced freshwater volumes could be achieved for larger target volumes when the pumping rate of HDDW2 was decreased too. The modelling results are shown in Figure 4.40.

The first two ASR-cycles showed an increase in the RE with a decrease in HDDW2 pumping rates for both the scenarios injecting 6000 m^3 and 8000 m^3. However, from ASR-cycle 3 onwards, the RE of the scenarios which had a target volume of 6000 m^3 was significantly lower when the pumping rates of HDDW2 were decreased. This trend was not observed for the scenarios with a target volume of 8000 m^3 where the RE after cycle 3 was generally identical for all simulated HDDW2 pumping rates. The differences between the scenarios simulating 75% and 50% HDDW2 pumping rates, tend to become smaller with increasing target volume. They were large for a target volume of 4000 m^3, significantly smaller for a target volume of 6000 m^3 and negligible for a target volume of 8000 m^3.

The maximum recoverable volume gives more insight in the effect of the RE on the freshwater production and is also shown in Figure 4.40. The largest recoverable volume could be obtained for a target volume of 6000 m^3, but only when HDDW2 pumping rates were kept at the same rate as the reference scenario. This pumping rate was 44 m^3/d which coincided with a pumping ratio (Q_{HDDW1} / Q_{HDDW2}) of 1.5 If HDDW2 pumping rates were decreased, the maximum target volumes fell to 4700-4800 m^3.

Even though the lowest REs were obtained for a target volume of 8000 m^3, the maximum recovered volumes were significantly higher for a target volume of 8000 m^3 than for a target volume of 4000 m^3. A target volume of 8000 m^3 resulted in a maximum recoverable volume of 5500 m^3 which was not significantly sensitive to decreasing HDDW2 pumping rates.

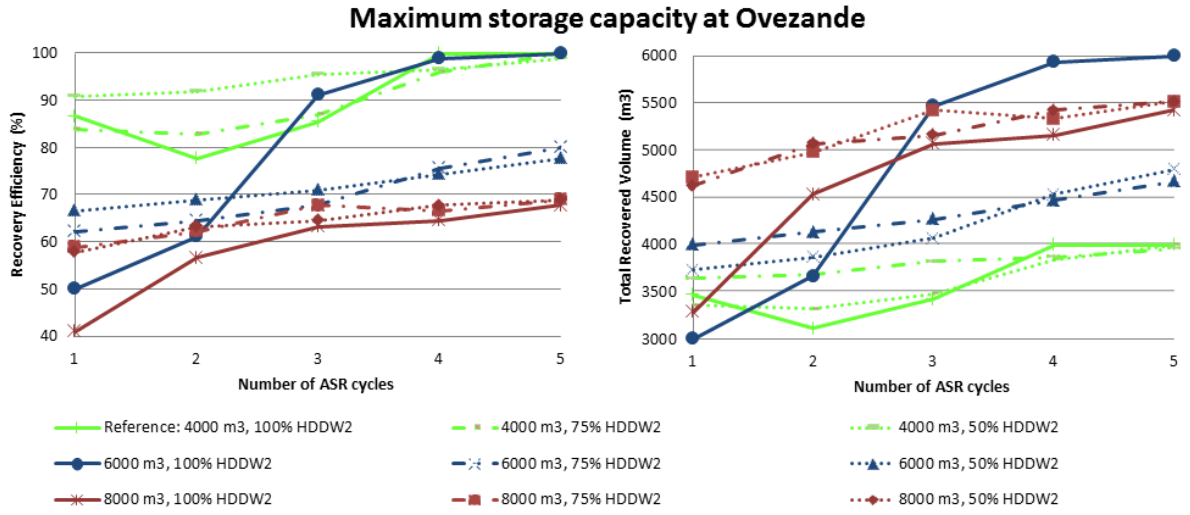

Figure 4.40 - Maximum storage capacity at Ovezande. Left: the effect of different target volumes and HDDW2 pumping rates at the RE, right: the effect on the total recovered volume.

5 Discussion

The sensitivity of the most relevant hydrogeological and operational parameters on the RE of the Freshmaker was analysed via numerical modelling in this study. Furthermore, the performance of the Freshmaker in the pilot was analysed with a numerical groundwater model. Section 5.1 validates the FAP-model, which was used to analyse the Freshmaker at the pilot in Ovezande. Some design modifications which may reduce influence of the observed 3D effects on the chloride concentrations abstracted by HDDW1 are proposed in Section 5.2. The performance of the Freshmaker in Ovezande is discussed in Section 5.3. The influence of different operational and hydrogeological parameters on the performance of the Freshmaker is discussed for each parameter individually in Section 5.4 and 5.5 respectively. The answers to the research questions are given in Section 5.6.

5.1 2D and 3D FAP-Model validation

5.1.1 2D-model performance

The 2D FAP-model was calibrated such that it was able to reproduce the dynamics of the fresh-saltwater interface observed with the EM-39 probe. Pumping data on a weekly basis was used during the process of calibration. Although this was sufficient to reproduce the dynamics of the freshwater lens, some concentration peaks observed with the CTD-diver were not captured by the 2D-FAP-model. This was because some (actual) daily pumping peaks were smeared out over a period of a week in the model simulations. In the field, HDDW1 sometimes abstracted for a period of just a few days which was not captured in the simulation period lengths of 1 week. Nevertheless, the overall dynamics of the fresh-saltwater interface were captured well, from which it was concluded that the 2D-FAP-model was representative for the pilot at Ovezande.

However, the results of the 3D-model showed a significant difference with the results of the 2D-model (Figure 5.1). The calculated chloride concentrations in the water abstracted by the Freshmaker were higher with the 3D-model. It is important to verify whether the assumption to simulate the Freshmaker with a 2D-model is still valid, especially since the results identified there were some 3D-effects that influenced the chloride concentration of the abstracted water (Section 4.2.4) which could not be simulated with the 2D-model.

The next section (5.1.2) discusses the origin of the 3D-effects in detail. The differences between the 2D and 3D model results and the validation of the assumption that the Freshmaker can be modelled with a 2D model is discussed in Section 5.1.3.

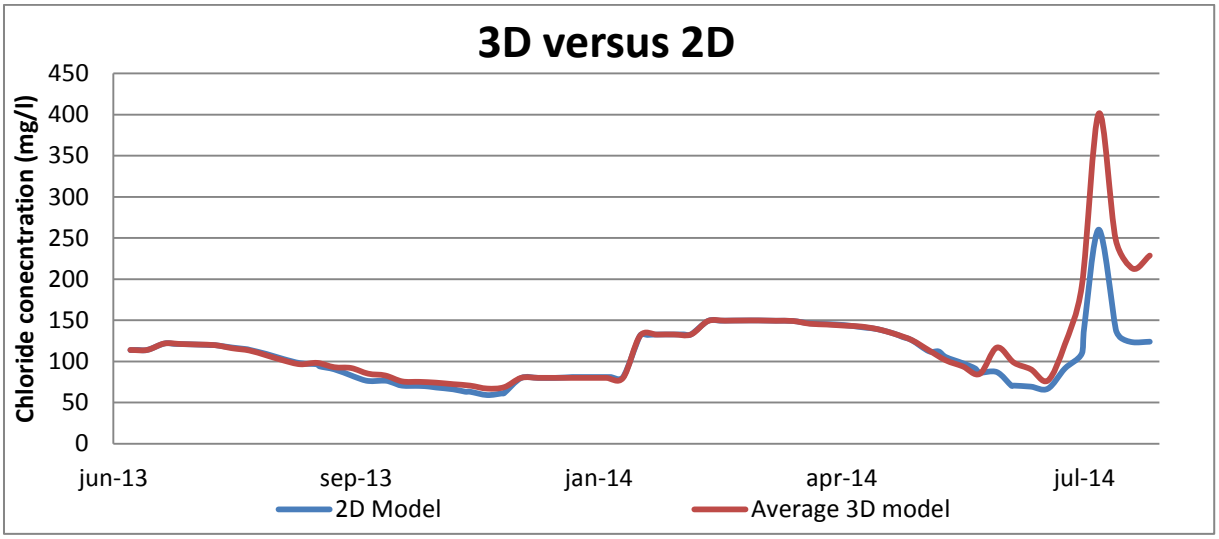

Figure 5.1- Plot showing the difference in chloride concentration at HDDW1 as simulated with the 2D FAP-model (blue curve) and the 3D FAP-model (red curve). The chloride concentrations of the 3D model were the average concentration of all the model cells of HDDW1.

5.1.2 Explanation of the observed 3D-effects

The results of the 3D-FAP model were discussed in Section 4.2. Two 3D-effects were identified:

1. Upconing at the outer ends of the Freshmaker
2. Upconing in the central part of the HDDWs.

The following subsections discuss the different 3D-effects separately.

5.1.2.1 *1st 3D-effect: Upconing at the outer end of the HDDWs*

The outer ends of the HDDWs can be considered as point sources and therefore groundwater flow at the edge is 3D. However, the central section of the HDDWs can be characterized as line sources and therefore groundwater flow can be conceptualized as 2D-flow. So, the groundwater flow regimes of the outer ends and the middle of the HDDWs are different. The effect of the presence of two different flow regimes on the upconing at the edge is conceptualized in Figure 5.2.

The results showed that the upconing at the edge of HDDW1 during the recovery phases was caused by the fact that the fresh-saltwater interface could not be lowered further than the outer end of HDDW2. At the edge, 3D flow resulted in upconing of saline water due to the nearby shallow fresh-saltwater interface. However, in the central part flow was 2D. So the water abstracted by the central part of HDDW1 did not originate from the outer ends (where the fresh-saltwater interface was shallow) but flowed in perpendicular to HDDW1, from the region where the fresh-saltwater interface was effectively brought down by HDDW2.

Although because of this upconing chloride concentrations at the edge increased, the overall effect this had on the average chloride concentration of water produced by the Freshmaker was limited. The concentrations at the outer end were only increased over a length of a few meters (<5 m at both HDDW edges).

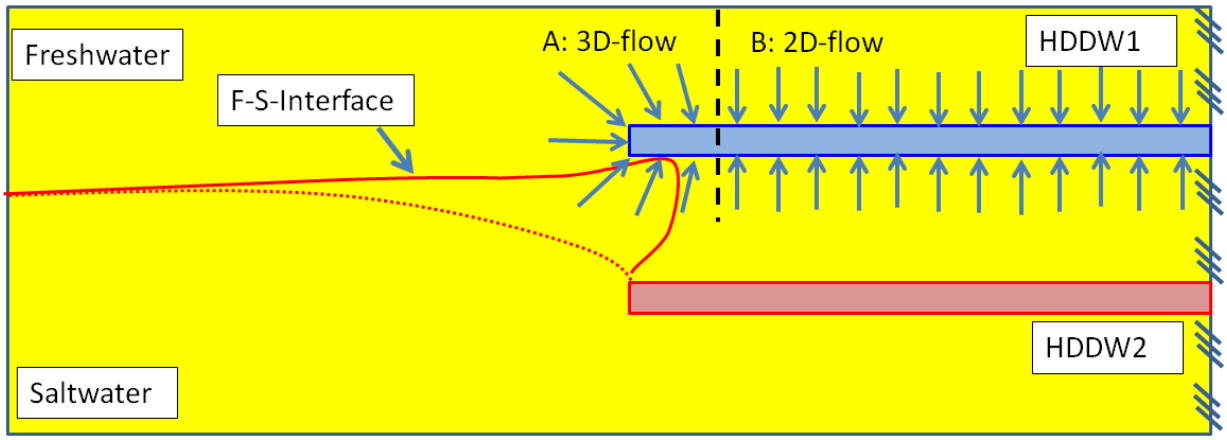

Figure 5.2 – Conceptual representation of the 1st 3D-effect: upconing at the edge of HDDW1.

5.1.2.2 *2nd 3D-effect: Upconing in the central part of the HDDWs.*

The 2nd 3D-effect (upconing in the central part of the HDDWs) was driven by two mechanisms. The first mechanisms was caused by the differences in the hydraulic head variations at the edge and at the middle of HDDW1 (Figure 5.3). Hydraulic heads fluctuated with a larger amplitude at the central part of the HDDWs. This was not only the result of numerical modeling but was also observed in field measurements. Since the differences were influenced by the pumping rates, with a larger pumping rate corresponding to a larger head difference, the upconing of the fresh-saltwater interface in the middle was more significant at a higher pumping rate (i.e. a larger abstracted volume). The result of mechanism one was that groundwater flowed at a higher velocity towards the central part of HDDW1 than towards the outer end.

The second mechanism originate from the different groundwater flow regimes at the HDDWs (Figure 5.4). The horizontal flow lines from the fresh-saltwater interface to HDDW1 were longer in the 3D-flowregime than in the 2D-flow regime. This means that saline water arrived earlier at the central part of HDDW1 than at the edge.

Mechanism one enhanced mechanism two, and the combination of both mechanisms resulted in a closer fresh-saltwater interface and more upconing in the central part than at the outer ends of the Freshmaker.

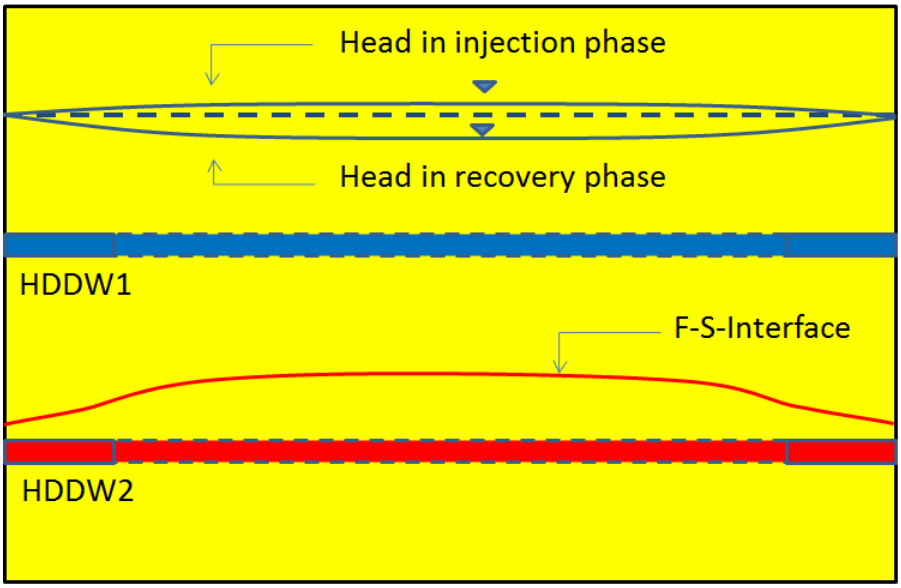

Figure 5.3 – Mechanism 1: Effect of the hydraulic head differences between the edge and the middle part of HDDW1 on the upconing of the fresh-saltwater interface.

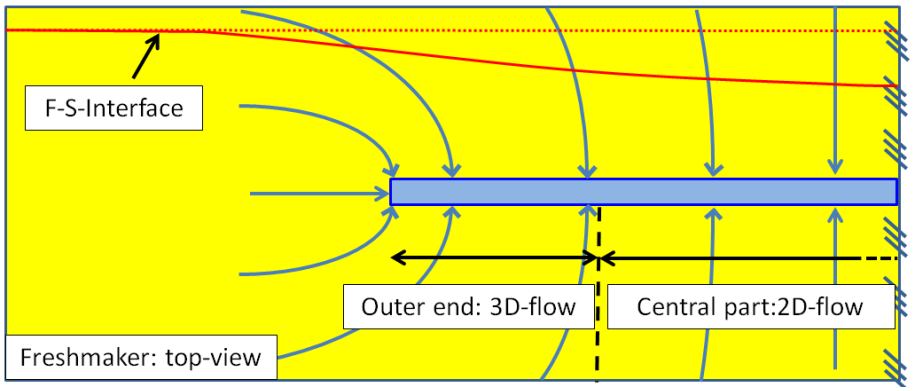

Figure 5.4 – Mechanism 2: Effect of the two different flow regimes on the length of the flow lines from the fresh-saltwater interface towards the HDDWs.

5.1.3 Differences between the 2D and the 3D-model

5.1.3.1 *Validity of the assumption to simulate the Freshmaker in 2D*

Numerical simulations showed that groundwater flow to the HDDWs was 2D-flow for the largest part of the HDDWs, which seems to legitimise the assumption to simulate the Freshmaker with a 2D-model. However, whether the Freshmaker can indeed be simulated with a 2D-model depends on the influence of the 3D-effects on the abstracted chloride concentrations.

The 2D-model was calibrated using data from MW1, after which is was able to reproduce the dynamic movement of the interface in the centre of the HDDWs. Since MW1 is located in the centre of the HDDWs, the recorded movement of the interface was actually the movement with the greatest amplitude, i.e. the movement influenced by the 2nd 3D-effect. Even though the 2nd 3D-effect was indirectly captured in the 2D-model calibration, the 1st 3D effect (upconing at the edge, Figure 5.2) could obviously not be captured with the 2D-model. Whether this condemns the assumption that the Freshmaker can be simulated with a 2D-model depends on the relative influence of the chloride concentrations abstracted by the outer ends versus the average chloride concentrations abstracted by the total HDDW1.

Although the 1st 3D-effect (upconing at the edge) was observed to be significantly stronger in Recovery phase II than I (Figure 4.11), the chloride concentrations in Recovery phase II were significantly lower at the outer end than in the central part of HDDW1 (Figure 4.13). This means that the 2nd 3D-effect (more upconing of the fresh-saltwater interface in the middle of HDDW1) had a relatively larger influence on the chloride concentrations abstracted by HDDW1 than the 1st 3D-effect. As a consequence, the relative influence of the chloride concentrations abstracted by the outer ends was limited compared to the central part.

Since the 2D-model simulated the largest part of the dynamic movement of the fresh-saltwater interface and this was representative for the highest chloride concentrations abstracted by HDDW1, the assumption to simulate the Freshmaker with a 2D-model was therefore valid. However, the HDDWs in the FAP-model simulations represented a length of 70 m. If the length of the HDDWs would be much smaller, the influence of the outer ends becomes relatively more significant and the assumption to neglect the outer ends might be wrong.

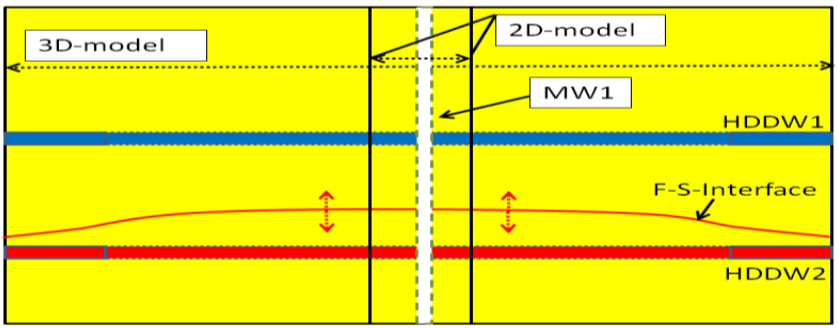

Figure 5.5 - Conceptual representation of the difference between the (cross-sectional) 2D and 3D-model. The 2nd 3D-effect (upconing in the middle part) was captured by the 2D-model as shown by the red line. The length of the HDDWs were 70 m and the width of the 2D model slice was 10 m.

5.1.4 Difference between the 2D and 3D model results

The main reason for the difference between the chloride concentrations simulated with the 2D and the 3D-model originate in the calibration procedure of the 2D model. The model parameters used in the 3D-model were identical to the model parameters derived in the 2D-model calibration. The larger hydraulic head variations that occurred in the middle of the HDDWs (2nd 3D-effect) were already accounted for in the 2D-model calibration. The result was that the use of the model parameters in the 3D-model overestimated the hydraulic head variations in the middle of the HDDWs which in turn exaggerated the dynamic movement of the interface in the 3D-model. This explains why the simulated chloride concentrations during the recovery phases were higher for the 3D-model than the 2D-model (Figure 5.1). No differences were observed in the injection phases since both models were injecting freshwater with identical chloride concentrations.

5.2 Design modifications to limit the observed 3D-effects

The strength of the 1st 3D effect discussed in Section 5.1.2.1 was observed to be sensitive to abstraction rates. Although it was shown that the relative influence could be neglected for the Freshmaker in Ovezande it is not known whether the edge effect can still be neglected if significantly larger volumes of freshwater are to be abstracted at a potential new Freshmaker site. Fortunately, a minor modification of the current Freshmaker design could avoid the potential occurrence of the increase of chloride concentrations at the outer ends of HDDW1. In the current design, the filter lengths of HDDW1 and 2 are identical. If the length of HDDW2 is increased relative to HDDW1, the fresh-saltwater interface can be lowered over a longer length. The capture zone of the outer end of HDDW1 will then abstract less saline water and upconing at the outer end will be limited. More research is needed in order to determine how much longer HDDW2 should become (parameter X in Figure 5.6) and whether this is cost-effective.

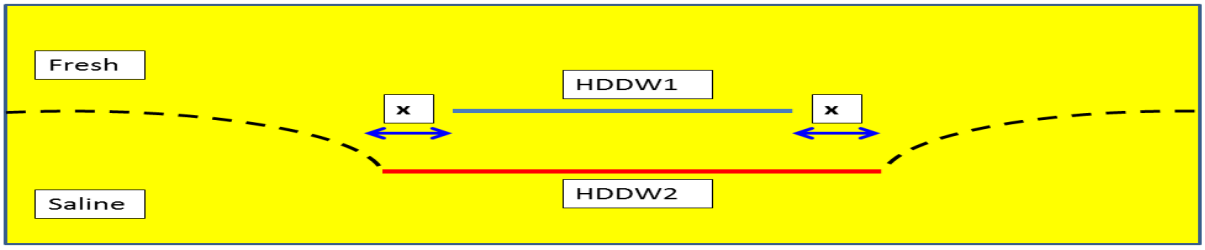

Figure 5.6 – A proposed design modification of the current Freshmaker design: increasing HDDW2 with a length X. This will increase the area over which the fresh-saltwater interface can be lowered.

There are two possible modifications of the current Freshmaker that might decrease influence of the 2nd 3D effect (more upconing in the central part of the HDDWs). If the movement of the interface would occurs more gradual along the whole Freshmaker length this could improve the performance of the Freshmaker.

The first modification is to install HDDW2 with a slight curvature under HDDW1 instead of completely horizontal. The radius of curvature will have to be adapted to the difference in head between the outer ends and the middle of the Freshmaker and therefore to the abstracted volume. Another benefit of using a curved HDDW2 is that it increases the distance between the position of the fresh-saltwater interface and HDDW1 at the onset of the recovery phase. As discussed in Section 5.1.2.2, especially the combination of the relatively small path lengths between the fresh-saltwater interface and HDDW1 and the larger head gradients result in increased upconing in the middle. However, more research is needed to study the effect of the curvature as simply placing HDDW2 at a greater depth might also obtain the desired result.

A second modification that might decrease the head differences between the outer ends and the middle of the Freshmaker is to change the distribution of the holes though which water flows into the wells (Figure 5.7). In the current design the holes are placed at a constant distance from each other. However, if relatively more holes would be placed at the outer ends than at the middle this would force more water to flow towards the outer ends. Since a larger portion of water would now be abstracted at the outer ends, this would decrease the difference between the head fluctuations in the middle and at the outer ends and hence avoid the increased upconing in the middle. However, more research is needed since it is not known whether this modification must also be done in HDDW1. HDDW1 might than abstract more freshwater from its outer ends which could increase the occurrence of the upconing at the edge as discussed in Section 5.1.2.1.

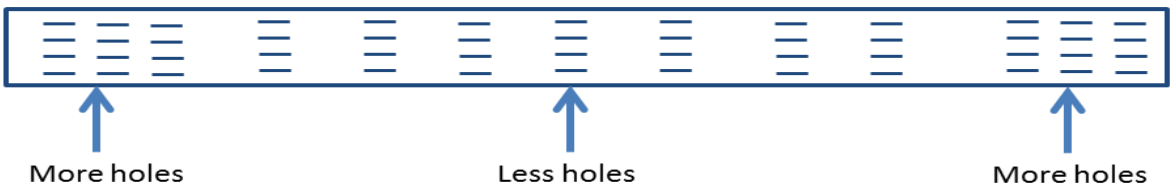

Figure 5.7 - Proposed design modification to decrease the differences in hydraulic head variations between the outer ends and the central part of the HDDWs.

5.3 Performance of the Freshmaker at the Ovezande Pilot

5.3.1 Simulated RE and freshwater production at the Ovezande pilot

The 2D FAP-model successfully reconstructed the movement of fresh-salt water interface during the Ovezande pilot. When the model was run for multiple ASR-cycles injecting 4000 m^3 each injection phase (which is realistic) the most important simulation outcome was that the saltwater cone under the draining ditch had a significant influence on the RE of the Freshmaker. Upconing of saline water from the direction of the saltwater cone resulted in lower REs during the earlier ASR-cycles (1-3).

In the field, 1725 m^3 was injected during Injection phase I and 4450 m^3 in Injection phase II, which differs from the hypothetical ASR-cycles where 4000 m^3 was injected. The simulation of multiple ASR-cycles with the FAP-model indicated that the lowest RE can be expected in Cycle II. However, since the operated ASR-cycles were different from those in the model it might be possible that ASR-cycle III in Ovezande will achieve lower RE then the earlier two cycles. This prediction is confirmed by the observation of some slight upconing of saline water by CTD-diver measurements in the field during recovery phase II. The model simulations pointed out that the origin of this saline water was most likely the upconing initially present under the ditch which means that more saline water will flow towards the Freshmaker in the next ASR-cycles.

Care must be taken in the ASR-cycle of the year 2015 (Cycle III) as it is expected that the RE will be lower than in Cycle II. A RE of 75% is the worst case scenario for Cycle III. The RE will increase to 85% and 100% in ASR-cycles IV and V respectively. However, this is to be confirmed with the FAP-model since the simulated REs might not be comparable, given the differences between the stored freshwater volumes that was simulated with the FAP-model and stored in reality.

5.3.2 Removal of the saltwater cone under the draining ditch

The decrease of the saltwater cone under the draining ditch was not observed by Zuurbier et al. (2014). This was because the model they used was not yet calibrated on field measurements. Although the model gave a good first impression of the performance of the Freshmaker it was not able to simulate the dynamic movement of the fresh-saltwater interface as observed in the field. As discussed in Appendix C, the simulated river bottoms had conductance values that were too high and the hydraulic conductivities were too high. This resulted in horizontal flow rates in the freshwater lens that were too high, limiting the upconing of saline water from below the ditch towards the Freshmaker.

Fortunately, the upconing under the ditch will decrease after a number of completed ASR-cycles. The Freshmaker is thus actively freshening the aquifer. With the disappearance of the saltwater under the ditch, the potential freshwater abstraction capacity of the Freshmaker increases, because less saline water would flow towards HDDW1. This will increase the RE.

There are two freshwater lenses near the Freshmaker. The freshwater lens in which the Freshmaker is installed is thick since it is located on a creek ridge. The one to the North of the Freshmaker is thin since it is located below a drained polder area. As discussed in Section 4.3.1, most of the freshwater flowed in horizontally from the thicker lens in the South. However, as the saltwater cone sank during multiple ASR-cycles, the two freshwater lenses near the Freshmaker became connected. Although this might increase the potential freshwater production of the Freshmaker, more research is needed with the 3D-FAP model since the connection between the two lenses was a very local feature.

As the upconing under the ditch was decreased, the ditch was slowly transferring from a draining to an infiltrating ditch. The water infiltrated in the aquifer was brackish in summer. Although this did not significantly influence the RE of the Freshmaker it is possible to completely avoid the infiltration of brackish water in summer by installing two small sluices in the ditch near the Freshmaker. The sluices can be controlled an EC-sensor. If the EC of the surface water becomes too high, the sluices will close and no water will infiltrate, while the sluices will be opened if the EC is low.

5.4 Operational parameters

5.4.1 Recoverable volume

The simulations with different target volumes identified that the RE of the Freshmaker is sensitive to the injected freshwater volume. It was also shown that scenarios with a relatively low RE could still achieve relatively large volumes of freshwater. Finally, simulations showed that the discharge of HDDW2 was an important factor in determining the maximum recoverable volume of freshwater. If HDDW2 pumping rates were too high the RE and hence the maximum recoverable volume decreased. This was due to increased loss of injection-water by abstraction of HDDW2. There is a threshold pumping rate for HDDW2 at which no freshwater is abstracted during the injection and storage phase. However, this implies the maximum recoverable volume will be limited by the maximum pumping rate of HDDW2. If the abstracted volumes by HDDW1 are too large, HDDW2 can no longer prevent upconing of saltwater.

The maximum recoverable volume of the Freshmaker in Ovezande is believed to be approximately 6000 m^3. Although simulations with a decreased HDDW2 pumping rate could not achieve a higher recoverable volume than 6000 m^3, it is possible that the maximum recoverable volume may be slightly higher if pumping by HDDW2 is completely terminated during the injection phase. When larger volumes of freshwater are injected, more freshwater will be lost by abstractions of HDDW2 during the injection phase. This hypothesis needs to be verified using numerical modelling.

All simulations showed that it must be possible to produce larger volumes of freshwater than is currently targeted in the pilot. The sinking of the saltwater cone under the ditch at the pilot in Ovezande, as observed and explained in Section 4.3, increases the potential storage volume of freshwater. This allows the production of larger volumes of freshwater from ASR-cycle IV or V onwards.

5.4.2 Pumping ratio during the recovery phase

The results discussed in Section 4.3 indicate there is a positive correlation between the recovery phase length and the RE. However, instead of in terms of recovery phase length, this relation can also be explained in terms of the pumping ratio during recovery ($Q_{ratio} = Q_{HDDW1} / Q_{HDDW2}$). Abstracting the same volume in a shorter recovery period means that the abstraction rate of HDDW1 increases and consequently a larger pumping ratio between HDDW1 and HDDW2 since the pumping rate of HDDW2 remained constant. As the RE fell with decreasing recovery phase lengths, i.e. decreasing Q_{ratio}, there is apparently also a relation between the Q_{ratio} and the RE.

Q_{ratio} was not only modified by increasing Q_{HDDW1} but also by decreasing Q_{HDDW2}. Although results of the first 5 cycles were dominated by removal of the saltwater cone, the same relation can be identified. The lower Q_{HDDW2}, the lower the RE.

A correlation between the pumping ratio and RE can also be found in Section 4.3.2 for the scenario with the varying target volumes. Q_{HDDW2} remained constant while the targeted volumes increased. As larger target volumes had to be recovered in the same recovery period length, this implied that Q_{HDDW1} increased. Since it was shown that higher target volumes resulted in lower RE, this confirmed the relation between the pumping ratio and RE.

Although the correlation between the low pumping ratio and the high RE is underpinned by the results described above, there were also some observations that seemed to contradict the proposed relation. First, the fact that the REs (Section 4.3.2) were significantly lower with increasing target volumes while the pumping ratio remained constant does not directly correspond with the hypothesis that the RE decreases with increasing pumping ratio. Furthermore, despite the decreasing recovery period lengths (i.e. increasing pumping ratio), after ASR-cycle 4, the RE was always 100% (Section 4.3.3).

However, these findings do not falsify the proposed relation. The reasons behind the first contradicting observation were that Q_{HDDW2} became so high that HDDW2 abstracted a large portion of the injected freshwater and resulted in thinning of the freshwater lens at the Freshmaker by laterally drawing closer saline water from the thinner section of the freshwater lens. The reason behind the second contradicting

observation was that the salt water cone was sufficiently removed after in ASR-cycle 4 to allow 100% RE for higher pumping ratios also. If higher pumping ratios would be simulated from ASR-cycle 4 onwards, the same relation between RE and Q_{ratio} will be found.

The correlation between the pumping ratio and RE therefore holds, but the relation is only valid under certain conditions. These conditions are the absolute pumping rate of HDDW2 (which may limit RE by abstracting a significant portion of freshwater) and the geometry of the freshwater lens (which may limit the RE if the initial fresh-saltwater interface is shallow in the proximity of the Freshmaker, such as the presence of the saltwater cone under the ditch in Ovezande). The Q_{ratio} that corresponded to the highest recoverable volume was 1.5.

In order to achieve maximum freshwater production it is important to have insight in the geometry of the targeted freshwater lens before the Freshmaker is installed. If the site allows freedom to choose a specific spot for the installation of the Freshmaker, it must be installed at the location where the fresh-saltwater interface is as horizontal as locally possible to limit lateral inflow of saltwater from locations where the fresh-saltwater interface is more shallow. The second criterion to achieve maximum freshwater production at a given Freshmaker site is proper operation management of HDDW2. This will be discussed in detail in the next section.

5.4.3 Operation management of HDDW2

It was discussed in the previous Section (Section 5.4.2) that a lower pumping rate of HDDW2 increases the pumping ratio which corresponds to a lower RE. However, simulation of a potential failure of HDDW2 during various ASR phases (Section 4.3.4) shed more light on this phenomena. Corresponding to the pumping ratio hypothesis, the RE decreased when HDDW2 failure duration increased during the storage and recovery phase. However, the RE increased when HDDW2 failed during the injection phase indicating that a large portion of the freshwater was short circuited by HDDW2.

This shows again that good management of HDDW2 is important for successful application of the Freshmaker. In all model simulations, the abstraction rate of HDDW2 was constant during the different ASR-phases. However, the RE is clearly not only sensitive to the absolute pumping rate of HDDW2 but also the timing of abstraction by HDDW2.

Based on the current simulations it is not yet possible to determine the exact pumping rates needed at HDDW2. However, some qualitative insight was gained from the simulation outcomes from which it was possible to deduce some basic guidelines for the operation management of HDDW2. It is clear that the pumping rate of HDDW2 should be managed such that HDDW2 will not short-circuit freshwater. If an EC-sensor is installed in the pump of HDDW2, the EC of the abstracted water can be used as a proxy for the salinity of the abstracted water and possible short-circuiting can be detected. A possible HDDW2 operation management scheme based on the EC of water abstracted by HDDW2 is shown in Figure 5.8.

In all phases, HDDW2 abstractions should be terminated if the EC_{HDDW2} falls below a certain threshold value indicating short-circuiting of freshwater. However, HDDW2 should always abstract a little water in order to be able to measure the EC_{HDDW2} at the outlet. In the injection phase HDDW2 should abstract at a rate equal to HDDW1 to support the growth of the injected freshwater lens in the vertical direction. The abstraction rate that is needed in the storage phase has to be high enough to avoid movement of the fresh-saltwater interface due to density dependent flow. A pumping rate of about 50% of the HDDW1 pumping rate should be sufficient but more research is needed to quantify the free convective flow rate during the storage phase. During the recovery phase, HDDW2 abstraction rates need to be at least as high as during the storage phase or be increased to keep the pumping ratio of HDDW1 and 2 below a certain threshold value. This threshold value has to be based on the ideal pumping ratio (which was 1.5 for the Freshmaker in Ovezande). During the idle phase, abstraction by HDDW2 should continue in order to keep the fresh-saltwater interface a depth.

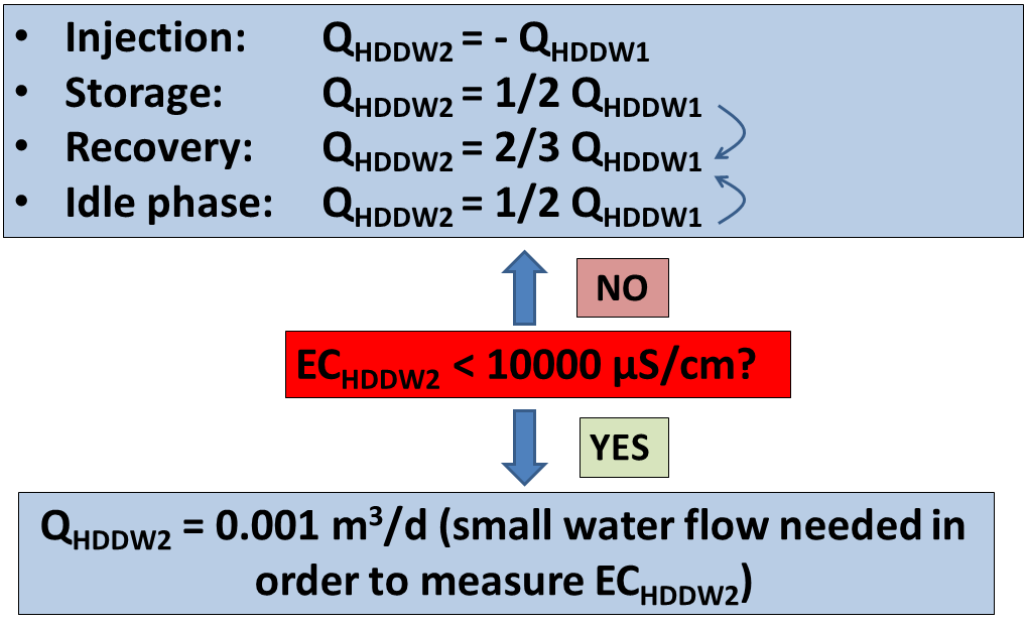

Figure 5.8 – Basic HDDW2 operation management scheme based on a limiting EC of 10000 μS/cm. This corresponds to a chloride concentration of about 4000 mg/l but other EC values can also be proposed. Since HDDW2 will always abstract saline water from below (which will mix with the abstracted freshwater) the value of the threshold EC but must such that the EC sensor is be able to detect short-circuiting of freshwater. Note that during the storage and recovery phases HDDW1 is not activated, so Q_{HDDW1} shown corresponds to the Q_{HDDW1} of the recovery phase.

5.4.4 Sensitivity to installation errors and HDDW2 failure

The results discussed in Section 4.3.6, which showed different possible locations of HDDW1, can also be explained in terms of possible locations of HDDW2. It is all about the relative horizontal distance between HDDW1 and 2.

It was shown that all scenarios where the wells were horizontally moved were able to achieve 100% RE, after the upconing under the ditch was sufficiently removed. This implies that the Freshmaker is not sensitive to horizontal well placement variations (to some extent). This is important since it means that possible calculation mistakes during Freshmaker installation, which may result in improper vertical placement of the wells, will not negatively affect Freshmaker performance. Obviously, the performance will decrease if the mistakes are too large but mistakes in a range of 1 - 2 m will be acceptable.

Whether it is due to well clogging or other causes, as with all other groundwater wells, the HDDWs of the Freshmaker may fail. HDDW2 is very important as it intercepts saline water and therefore failure of HDDW2 will reduce the RE of the Freshmaker. The results discussed in Section 4.3.4, showed that the RE of the Freshmaker in Ovezande decreased with about the same rate in the storage phase as in the recovery phase. The largest RE decrease rate was observed in the early phase (first week) of HDDW2 failure (-1% RE/day) and was slightly lower after a month of HDDW2 failure (-0.5% RE/day). In the modelling simulations a freshwater production of 4.000 m^3 was targeted and the abstraction rate of HDDW1 (Q_{HDDW1}) was kept constant during the recovery phase. However, if Q_{HDDW1} would be larger, for instance, because the same volume was to be abstracted in a shorter time, or because a larger freshwater production is desired, the RE decrease rate would be very different.

As discussed in Section 5.3, the maximum freshwater production of the Freshmaker in Ovezande is about 6.000 m^3. However, increasing the production will also increase the sensitivity to HDDW2 failure. Before trying to produce 6.000 m^3 annually, it is important to make a well-balanced decision that is not only based on the increase in freshwater production, but also acknowledges the increased vulnerability to HDDW2 failure. It is therefore advised that a relation between the RE decrease rate due to HDDW2 failure and the desired freshwater production is derived. This can be done with the FAP-model.

5.4.5 Upscaling

Upscaling is a solution to increase the production of the Freshmaker. However, the results discussed in Section 4.3.6 identified that the feasibility depends on the configuration of the Freshmaker well field and on how the wells are operated simultaneously.

5.4.5.1 *Configuration of the well field*

Various possible upscaling configuration were simulated. One important finding was that upscaling was most effective if the same number of ASR-wells and interception wells were used and they were placed vertically above each other. Upscaling using one less interception well and placing them not vertically only became effective when the Freshmaker was scaled up 4 times. However, only one ASR-cycle was studied. It is not known whether multiple ASR-cycles will decrease the relative advantage of using the same number of ASR as interception wells. Furthermore, in the limit the results of upscaling with one less interception well as ASR-wells will be identical (equation 5.1). This can also be seen when the upscaling results of Table 4.2 are plotted (Figure 5.9). It can be seen that upscaling using one ASR-well more than interception wells can indeed not achieve the same RE as using an identical number of ASR and interception wells but after sufficient upscaling, the differences will be negligible.

$$\lim_{n\to\infty} \frac{n}{n-1} = 1 \qquad (5.1)$$

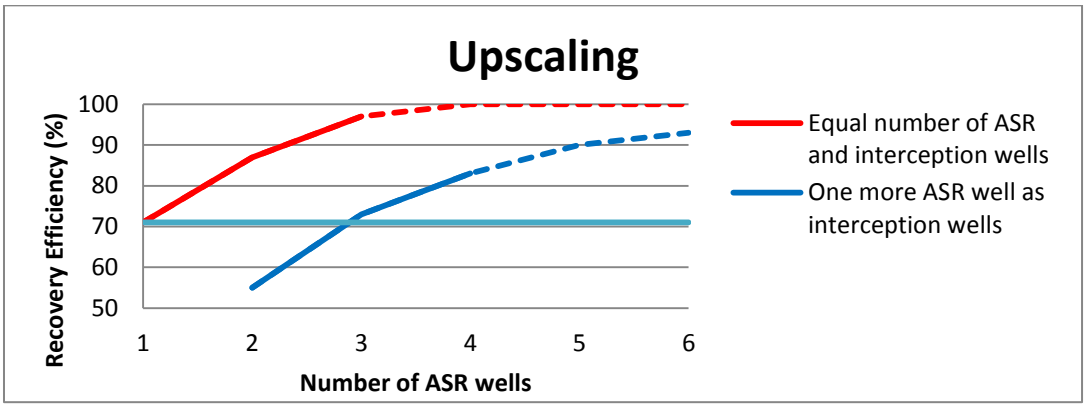

Figure 5.9 – Influence of upscaling on the RE. The solid lines are results from the simulations, derived according to method 2. The dashed lines represent a hypothetical expansion of the results. The horizontal curve is the RE obtained without upscaling (71%).

Although the results showed that the RE increased when the same number of ASR wells and interception wells were used, the driving mechanisms were not well understood. There are two potential driving mechanisms. The first mechanism is that the use of an extra interception well results in a larger volume of saltwater that will be intercepted from below since the pumping rates of the interception wells were not varied. The other mechanism is that installing a larger number of interception wells means that the saltwater interception covered a larger area and hence the fresh-saltwater interface was brought down over a larger area, making the "freshening" of the aquifer more effective.

The pumping rates of the interception wells were not varied in the scenarios, except in Scenario 6B. The simulation of Scenario 6B, which simulated one ASR-well underlain by two interception wells abstracting both at 50% of the reference pumping rate, showed that higher REs could be obtained if the area over which saltwater is intercepted is increased. This confirms that mechanism two is plausible. However, based on the current simulations it is not yet possible to determine which of the two mechanisms is the dominant driving mechanism. More model simulations, with varying pumping rates of the interception wells, should be performed in order to determine the dominant driving mechanism behind the observed higher RE for the upscaling scenarios using the same number of interception wells as ASR-wells.

Despite the fact that the dominant driving mechanism is not known yet, it was shown that the area over which the saltwater interception takes place is an important design parameter for an up-scaled Freshmaker. This means that other interception well configurations than simulated in this research might perform even better. Such as the use of one deeper interception well in the middle, abstracting saline water at a high rate cope with upconing from below and two more outwards (relative to the outer ASR-wells), to cope with upconing at the sides (Figure 5.10). For a proper design of the well-field configuration it is important to gain more insight in the relative influence of upconing from the sides or from below and more research is therefore needed.

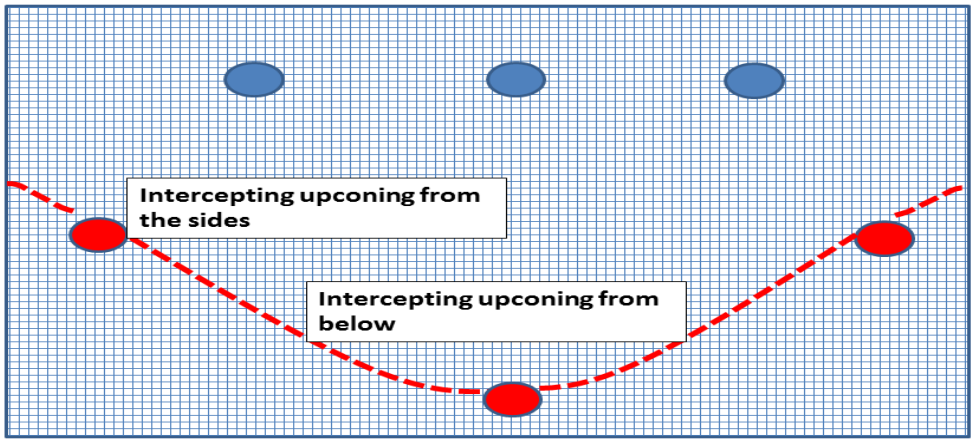

Figure 5.10 - Possible upscaling configuration which may increase Freshmaker production. The blue circles are the ASR-wells, the red circles are the interception wells. The red dotted line represents the fresh-saltwater interface.

5.4.5.2 *Operation management in case of upscaling*

For an up scaled version of the Freshmaker it is important to carefully operate the wells simultaneously and determine how to terminate pumping if the salinity exceeds the maximum allowed limit. Highest RE can be achieved if the water of all ASR wells is directed to a collector pipe. EC loggers should be installed at the outlet of the main pipe and at the pipe of each individual ASR well. If the reference EC corresponding to maximum allowable salinity limit is exceeded, abstractions from the ASR well with the highest EC should be terminated which brings down the average salinity. This process can continue until all ASR wells stopped pumping.

Although not studied with the model, it is likely that the salinity in the groundwater nearby the ASR well that had to be terminated due to salinization will decrease when abstraction stopped. It is therefore possible that the ASR well can be activated at a later time. However, this would require additional EC loggers in several monitoring wells near each ASR well which may significantly increase construction costs.

5.5 Hydrogeological parameters

5.5.1 Hydraulic conductivity

The results have shown that the RE of the Freshmaker is higher when applied in aquifers with a lower hydraulic conductivity. This is all dependent on fresh-saltwater interface dynamics. The fresh-saltwater interface moves down during the injection phase, is held in place during the storage phase and moves up during the recovery phase. The speed at which the interface moves up and down is determined by the flow velocity which depends on the hydraulic conductivity. For this reason it is clear there is a strong correlation between the hydraulic conductivity and the RE.

However, the fresh-saltwater interface moves down at a higher rate than it moves up. This is caused by the fact that during the injection phase, injection by HDDW1 and abstraction by HDDW2 reinforce each other, while during the recovery phase they oppose each other. During the recovery phase the interface did start to move back up, but this went less fast as abstraction by HDDW1 and HDDW2 now opposed each other. Apparently, in the scenarios with a low hydraulic conductivity the interface movement was sufficiently slow that it was possible to achieve 100% RE. While in the scenarios with a higher hydraulic conductivity the upward movement of the interface was too fast, leading to salinization of HDDW1, despite the opposing behaviors of HDDW1 and HDDW2.

Nevertheless, all of the above was discussed for a given pumping rate. In reality, flow velocity and therefore the movement of the fresh-saltwater interface, not only depends on the hydraulic conductivity but also on the pumping rate. So, even though the potential success of the Freshmaker will be higher when applied in aquifers with a lower hydraulic conductivity, the maintained pumping rate ultimately determines whether upconing occurs or not. For each aquifer, with a given hydraulic conductivity, there appears to be some threshold pumping rate at which the RE will fall below 100%. If the hydraulic conductivity is low, this pumping rate can be relatively high and hence the maximum volume of freshwater that can be stored and recovered by the Freshmaker will be large. On the other hand, if the hydraulic conductivity is large, the maximum pumping rate has to remain low and the maximum recoverable volume will be small.

5.5.2 Vertical anisotropy

The reference scenario of the FAT-model (with an isotropic hydraulic conductivity of 10 m/d) could not achieve a RE of 100%. However, the results have shown that a VANI of 2 (Scenario II_B) resulted in 100% RE. VANI 2 implies a vertical hydraulic conductivity of 5 m/d, while the horizontal hydraulic conductivity remains 10 m/d. Scenario I_B (in which an isotropic hydraulic conductivity of 5 m/d was simulated) could also achieve a RE of 100%. The reason that a RE of 100% could be achieved in both scenarios was mainly caused by the lower hydraulic conductivity in the vertical direction and less by the lower hydraulic conductivity in the horizontal direction.

Since all anisotropy scenarios (VANI = 2, 4, 10) achieved a RE of 100%, no conclusions could be drawn from the relative influence of the degree of the anisotropy on the RE. Nevertheless, the observed trend was that the anisotropy led to a higher RE. In the previous section was discussed that the maximum recoverable freshwater volume was lower for aquifers with a higher hydraulic conductivity. However, the Freshmaker may recover large volumes of freshwater from high conductivity aquifers if they are anisotropic.

Anisotropy is a common feature in water laid sedimentary deposits, such as, fluvial, glacial outwash, clastic lake, but also deltaic deposits. Traditional ASR techniques are often not feasible in delta systems due to the presence of saline (paleo)groundwater leading to low RE. However, the Freshmaker might have large potential in such systems, as the RE of the Freshmaker increases when aquifers are anisotropic.

5.5.3 Porosity

Injection of 4000 m^3 freshwater was simulated for a porosity range of 0.2 – 0.5. The achieved RE was 25% lower for the 0.2 scenario than for the 0.5 scenario. Despite the significant difference in RE, the simulations showed that reasonable REs (RE>75%) could be obtained for the most likely values of porosity that may be encountered in aquifers which are potential Freshmaker sites (i.e. deltaic systems. Typical porosity values for loose deltaic sediments are 0.2 – 0.4.

A clear relation between RE and porosity was observed in the results. High porosities result in higher REs than low porosities. One of the reasons identified for the low RE with low porosities was that a larger share of the injected freshwater will be short-circuited by HDDW2. It might be possible to eliminate this process by decreasing the injected volume. However, aside from the RE, the maximum volume of freshwater that can be injected and recovered is a major factor determining the successful application of the Freshmaker on a certain location. So, the business case may fail depending on the desired volume of freshwater production by the Freshmaker.

The maximum volume of freshwater that can be stored by the Freshmaker is controlled by the distance between HDDW1 and 2 and the porosity. The optimal distance between HDDW1 and 2 for any targeted freshwater storage volume is therefore strongly determined by the porosity. If the Freshmaker is installed in an aquifer with a low porosity, the distance between HDDW1 and 2 must be larger than if it is installed in an aquifer with a high porosity (if the same volume of freshwater needs to be produced). It is therefore important to have insight in the porosity for a proper design of the Freshmaker setup at a potential site (i.e. determining the appropriate distance between HDDW1 and 2).

5.5.4 Dispersivity

5.5.4.1 *Value of the longitudinal dispersivity*

The simulations have shown that the performance of the Freshmaker is highly sensitive to the value of the longitudinal dispersion. This is caused by the fact that HDDW1 will always be located in near proximity of the interface which means that small changes in the thickness of the mixing zone will have a profound influence on the RE. Underestimation of the value of the longitudinal dispersivity may eventually result in a lower RE than expected.

Gelhar (1986) examined the scale dependency of (macro)dispersion. Based on a large number of field scale dispersivities, he determined a range of possible dispersivity values for a number of scales (Figure 5.11). Lallemand-Barres and Peaudecerf (1978) a similar study and they determined that the longitudinal dispersivity is about 10% of the scale length. The scale of macrodispersion at a Freshmaker site is determined by the amplitude of the upward and downward movement of the fresh-saltwater interface. This movement is in the 1 m – 3 m range.

A longitudinal dispersivity range of 0.1 to 1 m was studied in the sensitivity analysis. However, based on the works of Gelhar (1986) and Lallemand-Barres and Peaudecerf (1978), the longitudinal dispersivity value that is likely to occur at the Freshmaker scale (1 – 3 m) will be in the 0.1 – 0.5 m range. In the calibration procedure of the FAP-model, a longitudinal dispersivity value of 0.33 was determined. This value corresponds well with the proposed range.

The sensitivity analysis showed that the performance of the Freshmaker is very sensitive to the value of the longitudinal dispersivity. However, the dispersivity values that are likely to be encountered at potential Freshmaker scales are low enough to allow successful application of the Freshmaker.

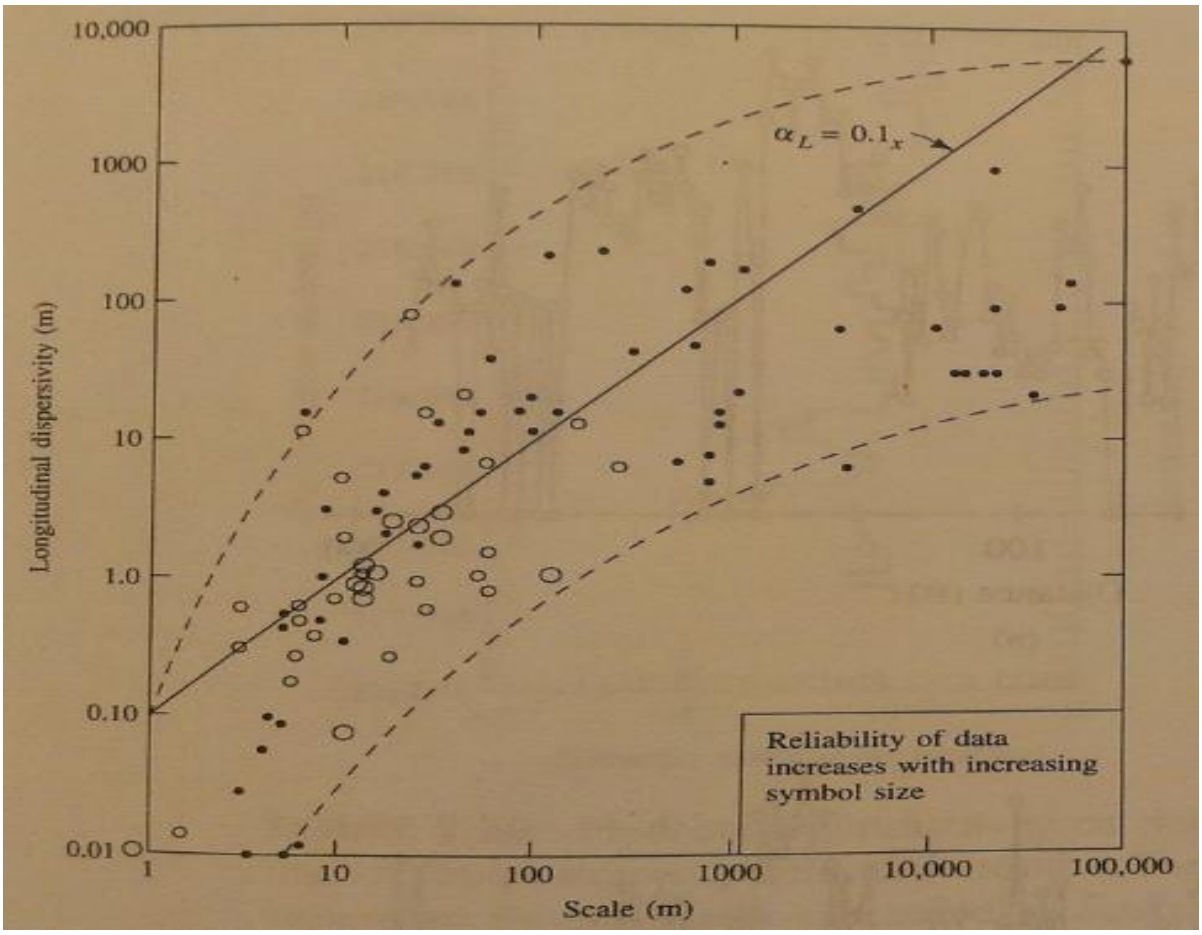

Figure 5.11 Scale dependency of longitudinal dispersion. Source: Gelhar (1986).

5.5.4.2 *Longitudinal dispersion versus transversal dispersion*

In the analysis of the sensitivity of the Freshmaker on dispersion, transversal dispersion was not taken into account. Although the transversal dispersivity was still varying through the different scenarios (since the ratio between the longitudinal and transversal dispersivity remained the same throughout all simulations), it was believed that the relative influence of the transversal dispersion on the decreasing RE was negligible compared to the influence of the longitudinal dispersion. This assumption coincides with the work of Eeman et al. (2011).

Eeman et al. studied the relative contributions of transversal and longitudinal dispersion on the transition zone in a freshwater lens with saline seepage. They showed that the relative influence of each is dependent on the development stage of the freshwater lens. If the freshwater lens is growing, more water flows perpendicular to the fresh-saltwater interface and mixing by longitudinal dispersion is dominant in the transition zone. If the freshwater lens is in dynamic equilibrium, the major flow direction will be parallel to the interface and mixing in the transition zone is dominated by transversal dispersion. Groundwater flow patterns in the freshwater lens at the Ovezande pilot significantly changed under the influence of the Freshmaker. The freshwater lens was no longer in equilibrium as the interface moved up and down during the ASR-cycle. This means flow was no longer parallel, but perpendicular to the interface and therefore not transversal, but longitudinal dispersion was the dominant mixing process. The assumption to neglect the influence of the transversal on the performance of the Freshmaker was therefore correct.

5.5.5 Ambient concentration

5.5.5.1 *The influence of ambient concentration on the RE of the Freshmaker compared to conventional ASR-techniques*

The results showed that the initial RE of the Freshmaker was higher when applied in aquifers with a lower ambient chloride concentration and lower when applied in aquifers with a higher ambient chloride concentration. This means there is a relation between the ambient concentration and the RE. The relation was accounted to density effects (Section 4.4.5). Despite the occurrence of density effects, the Freshmaker was able to achieve high RE (RE>90%) after 3 ASR-cycles. Nevertheless, this was only true for the simulated scenarios, with a targeted freshwater production of 4.000 m^3. Given the fact that density effects led to earlier upconing of saltwater, more freshwater production can be achieved from aquifers with a lower ambient chloride concentration.

Although the potential freshwater production volume of the Freshmaker is influenced by density effects, the sensitivity of the Freshmaker to density effects is smaller than for conventional ASR-systems. The main for this is that the Freshmaker uses the interception well (HDDW2). For conventional ASR-systems in saline aquifers, groundwater flow in the storage phase is dominated by free-convection resulting from density differences. The continued pumping of HDDW2 makes the groundwater flow of the Freshmaker dominated by advection at all times and therefore limits the relative influence of density dependent flow.

Another reason is the use of horizontal instead of vertical wells. The negative effect of a density difference on the performance of the Freshmaker is the tilting of the vertical interface between the injected freshwater and native saline water. The area of the vertical interface is much larger for the vertical well than for the horizontal well. Therefore, although the tilting interface has influence on the RE, this influence is significantly less for the Freshmaker than for conventional ASR-systems.

Overall, it can be concluded that, even though ambient salinity has some influence on the performance of the Freshmaker, the potential for successful application of ASR in saline aquifers is significantly larger for the Freshmaker than for conventional ASR.

5.5.5.2 *Freshmaker performance in brackish/saline aquifers without a freshwater lens*

The Freshmaker simulations were performed in an aquifer which had a freshwater layer floating on top of saline groundwater initially. This was done because the maximum depth at which the Freshmaker can be installed (currently) is about 18 m, which makes unconfined saline aquifers (i.e. aquifers with freshwater lenses) the most likely target locations for the application of the Freshmaker. It is not likely that the Freshmaker will be applied in a confined fully saline aquifer or at a depth, much greater than the depth of the initial fresh saltwater interface. If applied under such conditions, the RE of the Freshmaker will most likely be low. As the Freshmaker uses horizontal wells, the vertical extend of the freshwater bubble will be limited and this increases the possibility that ambient (saline) groundwater will remain above the freshwater bubble. A situation like this is highly unstable and will result in fingered mixing due to density differences which may decrease the RE of the Freshmaker. The higher the ambient concentration, the more unstable the situation and hence the more likely the RE will decrease because of density dependent flow. Successful application of the Freshmaker in such situations can only be achieved provided that the top of the freshwater bubble reaches the groundwater level, or the top of the overlaying aquitard.

5.5.6 Heterogeneity

5.5.6.1 *The influence of clay and gravel heterogeneities*

The effect of aquifer heterogeneity on groundwater flow was found to be different for clay or gravel heterogeneities. However, for the scenarios with the clay or gravel lenses, the differences were insignificant compared to the scenarios with the clay or gravel layers.

Whereas clay lenses functioned as extra resistances to flow and became sources of saline water in the first ASR-cycles, gravel lenses functioned as zones through which saline water could flow at high velocities, quickly salinizing the Freshmaker. Nevertheless, both for the scenarios with clay and gravel lenses, after several ASR-cycles the RE was no longer significantly lower than the homogeneous scenario. This means that

lower REs should not necessarily be expected if the Freshmaker will be installed in an aquifer and some gravel or clay heterogeneities were not discovered during drillings and aquifer characterization. Although clay lenses will function as salt water sources initially, the salt water will be flushed out. In fact, the presence of clay lenses in an aquifer may be beneficial for the potential performance of the Freshmaker since the results showed that the Freshmaker was able to achieve higher REs in an aquifer with clay heterogeneities.

Modeling simulation identified that the RE of the Freshmaker is more sensitive to the potential presence of clay or gravel layers, which had significant and opposite effects on the RE. The potential presence of a clay layer increases the anisotropy of the aquifer which, as discussed in Section 5.5.2, increases RE. However, because of their high hydraulic conductivity, gravel layers will function as a preferential flow-path for saline water. The RE in the modeled scenario became lower with every passing ASR-cycle as more and more saline water was drawn into the gravel layer. This preferential flow phenomena was also observed by Missimer (2002) for traditional ASR-systems. Although the effect of preferential flow was identical for traditional ASR as for the Freshmaker (saline water entering the high transmissivity zone, leading to low RE), the mechanisms are slightly different. They found that saline water entered the high transmissivity zones due to density fingering. Though entrance of saline water in a high transmissivity zone due to density fingering may also occur for the Freshmaker, the major difference is the continued pumping of HDDW2. Due to abstractions by HDDW2, and thus a net abstraction of the Freshmaker, saline water was drawn into the high transmissivity zone leading to lower RE with every passing ASR-cycle.

It can be concluded that the performance of the Freshmaker is significantly sensitive to the presence of clay layers (which increase the RE) or gravel layers (which decrease the RE) but not sensitive to the presence of either clay or gravel lenses.

5.5.6.2 *Application of the Freshmaker in dual-porosity aquifers.*

One special case of heterogeneous aquifer systems are so called dual-porosity aquifers. Van der Linde (2012) has shown that neglecting the dual porosity character of limestone aquifers will lead to significant underestimation of the transport of contaminants to drinking water wells. Although not modelled in this study, dual-porosity may also significantly influence the performance of the Freshmaker. In the Netherlands, dual-porosity aquifers are only found in the province of Limburg (Chalk aquifers). However, many coastal aquifers in the world have a dual porosity system (e.g. limestone aquifers in Denmark, the United Kingdom, Northern France, Israel, Poland, Florida) and care must be taken when the Freshmaker is projected there. The influence of dual-porosity on the performance of the Freshmaker is explained below and conceptualized in Figure 5.12.

In a dual porosity aquifer there are two distinct, but overlapping, pore systems. The porosity of the rock matrix is called the primary porosity, here water is more or less stagnant. In the case of a saline aquifer, the rock matrix will be filled with saline groundwater. A secondary porosity is caused by the presence of conduits in the rocks due to fractures or matrix dissolution. The freshwater, injected by the Freshmaker, will only displace the saline water initially present in the conduits. However, since the saline water in the rock matrix will not be displaced, the matrix will function as a major source of salt during the storage phase. Both due to density effects and diffusion, salt will enter the freshwater present in the conduits. If the Freshmaker is installed in such an aquifer it is therefore important to take dual porosity into account to avoid disappointing results.

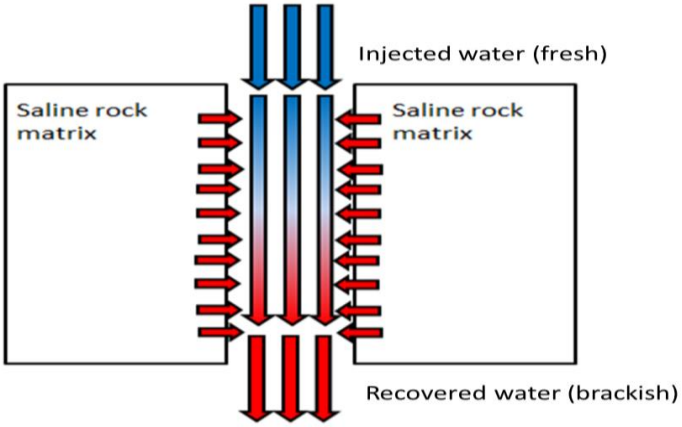

Figure 5.12 - Effect of dual porosity on ASR performance. Injected freshwater becomes contaminated by saline water present in the rock matrix due to diffusion.

5.5.7 Lateral flow

5.5.7.1 *The Freshmaker and lateral flow*

The fact that lateral flow decreases the performance of traditional ASR-systems in brackish and saline aquifers has been acknowledged by many authors (e.g. Bear and Jacobs, 1965; Pavelic et al., 2002; Ward et al., 2008) and has been discussed in Chapter 2 in detail. However, there were two observations that made the simulation results of the Freshmaker with lateral flow significantly different from the simulation results of traditional ASR-systems with lateral flow.

The first result that was different was observed for a lateral flow velocity of 0.03 m/d. While the whole injected freshwater bubble drifted downstream, the RE was not lower than the scenarios without lateral flow. Traditional ASR-systems in brackish/saline aquifers would most likely have seen a decrease in the RE as the freshwater bubble would have been displaced by water with a higher salinity. Vertical ASR-systems are only unaffected by lateral flow if applied in freshwater aquifers. This highlights the main reason why the Freshmaker is able to achieve high RE in brackish/saline aquifers. The abstraction by the interception well (HDDW2) effectively keeps the fresh-saltwater interface at depth which allows the ASR well (HDDW1) to operate in the fresh part of the aquifer.

The second observation was that the RE kept decreasing from ASR-cycle 1 to 3 if the lateral flow was high ($v_{lateral}$ > 0.15 m/d), while with traditional ASR the RE would initially be low but would show some increase to an asymptotic value after sufficient ASR-cycles. When the results were analyzed it was found that the decreasing REs were caused by the fresh-saltwater interface that moved up from ASR-cycle 1 to 3.

The use of the interception well in the Freshmaker-setup increases the potential of successful application of ASR in brackish aquifers with lateral flow where traditional ASR-systems will fail. However, the performance of the Freshmaker is sensitive to the lateral flow velocities. If the lateral flow velocity is low (<0.05 m/d) high RE (RE >75%) could be achieved but the RE decreased when the flow velocity got higher. Note that simulations were done with a fixed distance between HDDW1 and 2. Higher REs might be possible if this distance is increased.

5.5.7.2 *The fresh-saltwater interface upstream of the HDDWs moves up*

There are two mechanisms that explain the upward movement of the fresh-salt water interface upstream of the HDDWs. The first mechanism has to do with density effects and the second mechanism with the size of the capture zone of HDDW1. Both processes are illustrated in Figure 5.13.

Mechanism 1 (upper figure in Figure 5.13)

Due to the high lateral flow rate, all water abstracted by HDDW2 water originates upstream and the capture zone is therefore elliptical. Upstream, the abstracted water comes from a freshwater zone and a saltwater zone. However, since the density of the saltwater is significantly higher than the density of the freshwater, the freshwater is more easily displaced. As a result a larger portion of abstraction water will originate from

the freshwater zone ($Q_{fresh} > Q_{saline}$) . This means that the pressure above the fresh-saltwater interface decreases relative to the pressure below the fresh-saltwater interface. The pressure difference above and below the interface is resulting in an upward movement of the fresh-saltwater interface upstream of the HDDWs.

Mechanism 2 (lower figure in Figure 5.13)
The second mechanism is only active in the recovery phases. The capture zone of HDDW1 is larger than the freshwater zone and crosses the fresh-saltwater interface. Since HDDW1 is located above the fresh-saltwater interface, the interface moves upwards, towards HDDW1.

The result of the upward movement of the fresh-saltwater interface due to mechanisms 1 and 2 is that saltwater is abstracted earlier with every passing ASR-cycle. This explains the decreasing RE from ASR-cycle 1-3.

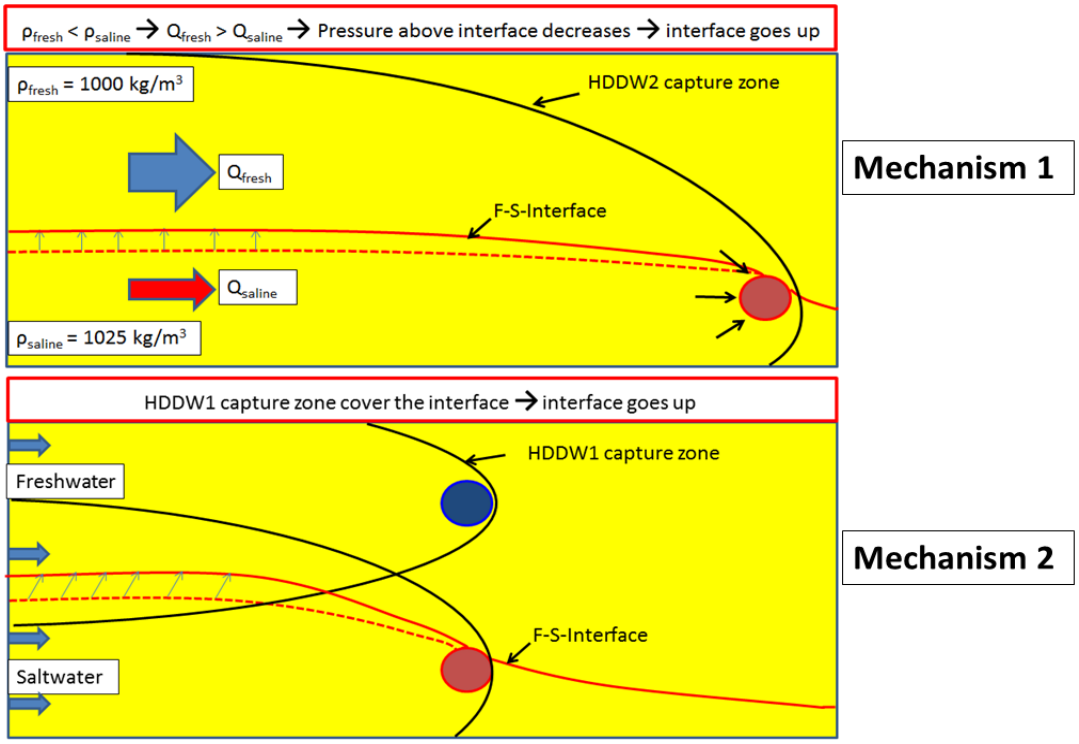

Figure 5.13 – Conceptual representation of the two mechanisms that were thought to be responsible for the upward movement of the fresh-saltwater interface, upstream of the HDDWs. Note that HDDW1 (blue well) is not shown in the upper figure. The upper figure therefore represent the storage and idle phases. The lower figure represent the recovery phase. Not to scale.

5.5.7.3 *Orientation of the Freshmaker with respect to the background gradient*

Although not explicitly modeled, the direction of the background flow is an important design criteria too. The simulations were only performed for a hydraulic gradient perpendicular on the length of the Freshmaker. Although the effects described above will occur for any direction in which the Freshmaker will be installed its relative importance will be significantly smaller when the Freshmaker is installed parallel to the background flow. Figure 5.14 illustrates the two possible directions in which the Freshmaker may be installed. The front where the fresh-saltwater interface will be moving up will be significantly smaller if the Freshmaker is installed parallel to the background flow. Furthermore, installation of the Freshmaker in the direction of flow results in a larger share of the injected freshwater bubble that can be abstracted again and does not get lost by lateral flow. This may be advisable if the water quality is stringent.

If the Freshmaker is installed parallel to the direction of flow one more design criteria needs to be taken into account. Although the area over which the fresh-saltwater interface moves up is smaller, it will still be abstracted by the outer end of HDDW1 that faces the lateral flow (1st 3D effect, discussed in Section 5.1.2.1).

Even if the outer end is only 10% of the total HDDW length (i.e. the volume of abstracted saltwater = 10% of total abstracted water volume), freshwater production may still be terminated as the chloride concentrations of brackish/saline water are more than an order of magnitude larger than the maximum allow chloride concentration limit (250 mg/l). The same design modification as proposed in Section 5.2 is proposed here: increasing the length of HDDW2 relative to HDDW1 (Figure 5.6). This may limit the volume of saltwater that is abstracted by the outer end of HDDW1 facing lateral flow.

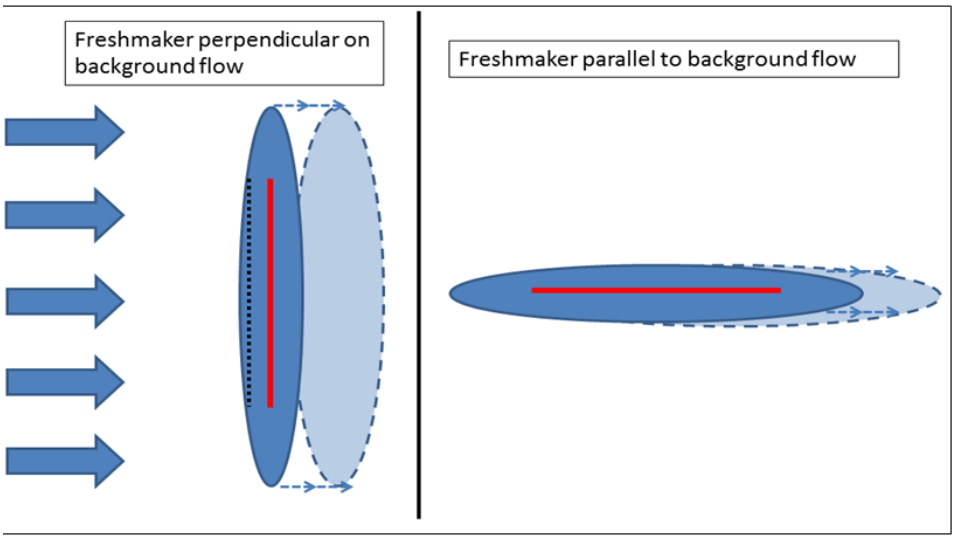

Figure 5.14 – Effect of lateral flow on the displacement of the injected freshwater. The figure illustrates the two possible directions in which the Freshmaker may be installed: perpendicular (left) or parallel (right). Not to scale.

5.6 Research questions

The following research questions were answered during this MSc research:

What is the significance of effects on the outer ends of the Freshmaker?
Groundwater flow on the outer ends of the Freshmaker is three dimensional and can therefore only be captured with a 3D-model. The fresh-saltwater interface is lowered less at the outer ends which leads to upconing of saline water during the recovery phase. For the Freshmaker in Ovezande, the increase of chloride concentrations at the outer ends was restricted to a section of 5 m of each outer end.

The majority of upconing occurred in the central part of the HDDWs since the hydraulic heads gradients were larger in the central part of the HDDWs. Furthermore, groundwater flow in the central part was 2D which resulted in shorter flow-lines from the fresh-saltwater interface towards the middle of the HDDWs than towards the outer ends of the HDDWs. The assumption that the outer ends of the Freshmaker could be neglected was therefore correct. However, for shorter HDDW lengths the influence of the outer ends might be more significant.

What is the maximum freshwater storage capacity of the Freshmaker in the current Ovezande setup and how can this be increased?
The maximum freshwater storage capacity (or maximum recoverable volume of freshwater) of the Freshmaker in Ovezande is about 6.000 m^3 and may be even higher if HDDW2 is deactivated during the injection phase.

The storage capacity was found to be highly sensitive to the abstraction ratio of HDDW1 and HDDW2 (Q_{ratio}) during the recovery phase. A correlation was found between Q_{ratio} and RE, but the relation is only valid under certain conditions. These conditions are the absolute pumping rate of HDDW2 during the injection phase (which may limit RE by abstraction of a significant portion of freshwater) and the geometry of the freshwater lens (which may limit RE if the initial fresh-saltwater interface is shallow in the proximity of the Freshmaker). The maximum recovered freshwater volume was obtained with a pumping ratio of 1.5.

What will happen if the interception well abstraction rates fall for a long period due to well clogging or other errors?
The hypothesis that in a case of significant well clogging or failure the effectiveness of the Freshmaker is only negatively impacted in the recovery phase, not during the injection and storage phases was not correct. The RE of the Freshmaker was also negatively when HDDW2 was not active during the storage phase. However, failure in the injection phase had a positive effect on the RE since less water was short-circuited by HDDW2. For a targeted freshwater production of 4000 m^3 the decrease in RE due to HDDW2 failure in the recovery and storage phase is about 0.5% - 1% per day.

What is the effect of upscaling, i.e. increasing the number of Freshmakers in one aquifer?
The hypothesis that upscaling will lead to a RE is correct. However, upscaling was only effective if the same number of ASR wells and interception wells were used and they were placed vertically above each other. Upscaling using one less interception well than ASR wells only became effective when the Freshmaker was scaled up 4 times.

For an upscaled version of the Freshmaker it is important to carefully operate the wells simultaneously and determine how to terminate pumping if the salinity exceeds the maximum allowed limit. Highest RE can be achieved if the water of all ASR wells is directed to one collector pipe and individual ASR wells are terminated if the average Freshmaker concentration exceeds the limit.

What is the sensitivity of different operational variables on the RE of the Freshmaker?

- The RE of the Freshmaker is sensitive to the targeted volume of abstracted freshwater. In the Ovezande pilot, a RE of 100% was achievable up to a target volume of 6.000 m^3 . Target volumes larger than 6.000 m^3 lead to significantly decreasing REs and result in less freshwater production than 6.000 m^3.
- The length of the recovery phase is strongly correlated to the RE of the Freshmaker. Longer recovery phases result in higher RE because of the lower Q_{ratio}.

- The RE of the Freshmaker is sensitive to the pumping rates of HDDW2. The RE is not only sensitive to the absolute pumping rate of HDDW2 but also the timing of abstraction by HDDW2. It is clear that the pumping rate of HDDW2 during the injection phase should be minimised to prevent short-circuiting of freshwater. In the storage phase, HDDW2 needs to remain activated to avoid movement of the fresh-saltwater interface due to density dependent flow. During the recovery phase, HDDW2 pumping rates need to be increased according to the abstraction rate of HDDW1 to keep the Q_{ratio} at a certain threshold value. For Ovezande, this ratio was determined at 1.5.

How well does the Freshmaker perform in a different hydrogeological context?

- The RE of the Freshmaker was negatively correlated with the hydraulic conductivity. The Freshmaker can abstract larger volumes of freshwater from aquifers with a low hydraulic conductivity.
- Anisotropy strongly influenced the RE of the Freshmaker. The Freshmaker performs better in aquifers which have anisotropy.
- The higher the porosity of the aquifer, the higher the RE and the recoverable volume of freshwater.
- The Freshmaker is very sensitive to the value of the longitudinal dispersivity since the ASR well is located relatively close to the fresh-saltwater interface. The Freshmaker performs best in aquifers with a low longitudinal dispersivity. The influence of transversal dispersion is negligible compared to the influence of longitudinal dispersion.
- The performance of the Freshmaker is sensitive to the ambient chloride concentration. Nevertheless, the Freshmaker is significantly less sensitive to the ambient chloride concentration as conventional ASR-techniques. Reasonable freshwater productions (>4000 m^3) can be achieved in saline aquifers (20.000 mg Cl/l).
- The Freshmaker is relatively insensitive to heterogeneities occurring as lenses, but highly sensitive to heterogeneities occurring as layers. The RE of the Freshmaker is higher when installed in an aquifer which have layers with a low conductivity. The RE of the Freshmaker decreases when installed in an aquifer with highly conductive layers due to the occurrence of preferential flow.
- The performance of the Freshmaker is very sensitive to lateral flow. It is important that the orientation of the Freshmaker with respect to the background hydraulic gradient is taken into account since it is expected that higher REs can be achieved when the Freshmaker is installed parallel to the flow direction.

6 Conclusions

The performance of the Freshmaker was studied during this MSc research. This study analysed the performance of the Freshmaker at a pilot location in Ovezande and further identified the influence of several hydrogeological and operational parameters on the performance of the Freshmaker in general. The implications of these findings on the current and future application of the Freshmaker are described for the Ovezande pilot, the hydrogeological parameters, and the operational parameters in separate subsections below.

Ovezande Pilot

Field data were used to construct and calibrate a groundwater model for the Freshmaker in Ovezande. Both field data and modelling results of the Ovezande pilot verified the expectations of Zuurbier et al. (2014) that the Freshmaker is an effective ASR-technique, applicable in saline aquifers with freshwater lenses.

However, simulations also showed that the recovery efficiency (RE) of the Freshmaker in Ovezande might be lower in the coming (third) ASR-cycle due to a nearby draining ditch, under which a cone of brackish/saline water is present. This saltwater cone sinks due to activity of the Freshmaker. However, as the cone sinks, it leads to some upconing of saline water during the first three recovery phases. Fortunately, the upconing under the ditch will decrease after 3 completed ASR-cycles with an injected freshwater volume of 4.000 m^3. With the removal of the salt water cone, the potential freshwater abstraction capacity of the Freshmaker in Ovezande increases. The maximum freshwater production of the Freshmaker in Ovezande was derived at approximately 6.000 m^3.

HDDW2 was observed to abstract injected freshwater. This process (which was called short-circuiting of freshwater) decreased the size of the freshwater lens and therefore the RE.

Two 3D-effects that influenced the chloride concentration in the abstracted water of the Freshmaker, and therefore the performance of the Freshmaker, were identified:

1. Upconing of saline water at the outer ends of the Freshmaker due to the limited length of HDDW2 with respect to HDDW1
2. Greater movement of the fresh-saltwater interface in the middle part of the Freshmaker due to greater hydraulic head gradients and 2D flow.

It was shown that despite the occurrence of the observed 3D-effects, the assumption to neglect the influence of the outer ends and study the 70 m long HDDWs with a 2D model was valid.

Operational Parameters

There is a strong correlation between the pumping ratio of HDDW1 and HDDW2 during the recovery phase (Q_{HDDW1}/Q_{HDDW2}) and the RE. If the pumping ratio increases, the RE decreases. However, the relation is only valid under two conditions. These conditions are the absolute pumping rate of HDDW2 during the injection phase (which may limit RE by short-circuiting freshwater) and the geometry of the freshwater lens (which may limit RE if the initial fresh-saltwater interface is shallow in the proximity of the Freshmaker, as was the case with the nearby saltwater cone in Ovezande). The pumping ratio that will produce the maximum recoverable freshwater volume at Ovezande was determined at 1.5.

Good management of the pumping rate of HDDW2 is important for successful application of the Freshmaker. The RE is not just sensitive to the absolute pumping rate of HDDW2 but also to the timing of abstraction by HDDW2. It became clear that the pumping rate of HDDW2 during the injection phase should be minimised to prevent short-circuiting of injection water which can be prevented by installing an EC-sensor at the outlet of HDDW2. During the storage phase HDDW2 needs to abstract some water to avoid movement of the fresh-saltwater interface due to density dependent flow. The pumping rate during the recovery phase needs to be such that the Q_{ratio} remains at a certain threshold value (1.5 for Ovezande).

For a targeted freshwater production of 4000 m^3 the decrease in RE due to HDDW2 failure in the recovery and storage phase is about 0.5% - 1% per day. However, the RE decrease rates will be larger if larger freshwater productions are desired.

The Freshmaker is not sensitive to horizontal well placement variations as long as the variations stay within a range of 1 - 2 m. This means that possible mistakes during Freshmaker installation, which may result in improper vertical superposition of the wells, will not negatively affect Freshmaker performance.

Upscaling can increase the total RE and therefore production of the Freshmaker. However, upscaling was only effective if the same number of ASR-wells and interception wells were used and they were placed vertically above each other. For an upscaled version of the Freshmaker it is important to carefully operate the wells simultaneously. The following operation management procedure is proposed: lead all the abstracted freshwater through one main pipe. Abort abstraction of the ASR-well that abstracts groundwater with the highest EC, if the salinity in the main pipe (i.e. average concentration of all ASR-wells) exceeds the maximum allowed limit.

Hydrogeological parameters

Detailed characterization of the aquifer in which a potential Freshmaker is installed was found to be of great importance to achieve the highest freshwater production. Although the Freshmaker may achieve a RE of 100% in most hydrogeological settings, the maximum recoverable freshwater volume significantly varies. Larger recoverable volumes of freshwater can be achieved from low hydraulic conductivity aquifers, anisotropic aquifers and highly porous aquifers.

Aquifer heterogeneities occurring as lenses do not have a distinct influence on the performance of the Freshmaker. However, heterogeneities occurring as layers do. The RE of the Freshmaker is higher if installed in an aquifer which has layers with a low conductivity but decreases if installed in an aquifer with highly conductive layers.

The Freshmaker is sensitive to the value of the longitudinal dispersivity since the ASR well is located relatively close to the fresh-saltwater interface. The Freshmaker performs best in aquifers with a small longitudinal dispersivity. However, for commonly found dispersivity values at the Freshmaker scale (0.1 – 0.5 m), the Freshmaker performs well.

The performance of the Freshmaker is sensitive to the ambient chloride concentration. Nevertheless, the Freshmaker is significantly less sensitive to the ambient chloride concentration as conventional ASR-techniques. Reasonable freshwater productions (>4000 m3) can be achieved in saline aquifers (20.000 mg Cl/l).

Lateral flow significantly influences the RE of the Freshmaker. If the lateral flow velocity is low (<0.05 m/d) high RE (RE >75%) can be achieved. However, the fresh-saltwater interface upstream of the HDDWs slowly moves up at higher lateral flow velocities. As a result the REs decreases with every completed ASR-cycle. It is important that the orientation of the Freshmaker with respect to the background hydraulic gradient is taken into account since higher REs might be achieved when the Freshmaker is installed parallel to the flow direction.

7 Recommendations

It was shown that freshwater was being short-circuited by HDDW2 at the Freshmaker pilot in Ovezande. It is advised that the abstraction rate of HDDW2 is decreased since this would increase the RE of the Freshmaker. In order to optimize HDDW2 operations, a management scheme was developed in Section 5.4.3. It is advised that this scheme is followed to optimize the Freshmaker performance in Ovezande (Figure 7.1).

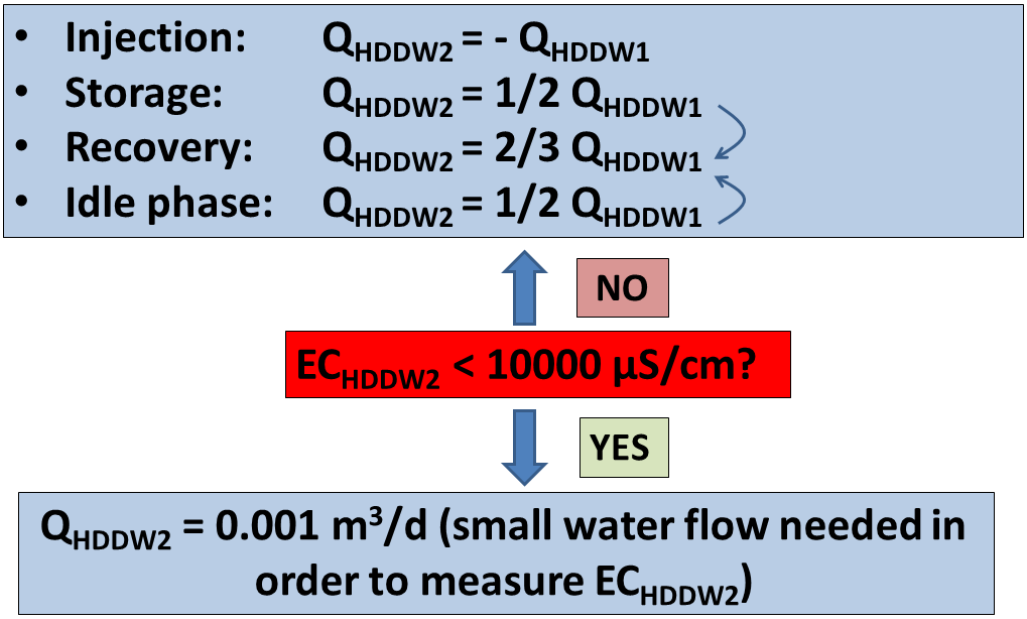

Figure 7.1 – Basic HDDW2 operation management scheme based on a limiting EC of 10000 μS/cm. This corresponds to a chloride concentration of about 4000 mg/l but other EC values can also be proposed. Since HDDW2 will always abstract saline water from below (which will mix with the abstracted freshwater) the value of the threshold EC but must such that the EC sensor is be able to detect short-circuiting of freshwater. Note that during the storage and recovery phases HDDW1 is not activated, so Q_{HDDW1} shown corresponds to the Q_{HDDW1} of the recovery phase.

Numerical modelling showed that the saline water under the ditch is drawn towards the Freshmaker which may negatively affect the recovery efficiency (RE) of the Freshmaker in the Ovezande pilot. It was also shown that the RE of the coming (3rd) ASR-cycle might be lower than the previous two ASR-cycles. For this reason it is strongly recommended that a significantly larger freshwater volume is injected than probably needed this year. Given the fact that the RE will be 25% lower in the worst case scenario, it is advised that 25% more freshwater will be stored than scheduled. This makes sure there is enough freshwater available in summer 2015 may the RE fall below 100%. More important, the larger injected freshwater volume may significantly accelerate the process of thinning the saline water cone, drawn towards the Freshmaker and avoid low RE.

The hypothesis that ASR-cycle III might experience lower RE and that this can be avoided by injecting extra freshwater have to be validated with the 2D-FAP model. Simulations of the Ovezande were run until August 2014, but can be extended for several months as more pumping data has become available.

The saline water movement in the saltwater cone under the draining ditch could not yet be validated from field data as they were not available. Given the importance of this phenomena it is advised that two monitoring wells are installed between the Freshmaker and the ditch: one, equidistant from MW1 and the ditch and one, equidistant from MW4 and the ditch. The diameter of the monitoring wells should be wide enough to allow EM39 measurements. Regular monitoring should provide the necessary insights in the dynamics of the saline water under the ditch. Furthermore, it will be highly informative if a second CVES campaign is undertaken. The CVES results can then be compared to results of the 1st CVES campaign and this MSc research.

This study had a strong focus on the performance of the Freshmaker with respect to the RE and movement of the fresh-saltwater interface. Although attention was given to the influence of the Freshmaker on local groundwater flow, more research needs to be done on the large scale influence of the Freshmaker. The regional hydrological influence of the Freshmaker might be significant since there is a net abstraction by the Freshmaker. It is advised that water budget and particle tracking studies are performed to gain more insight in the regional hydrological influence of the Freshmaker and the relative importance of vertical flow and lateral flow. It is recommended that this is done with the 3D FAP-model.

Some design modifications were proposed in Section 5.3. If the HDDW2 filter is made longer than the HDDW1 filter, the influence of upconing at the outer ends of the HDDWs will be limited (Figure 7.1). Another modification is using a different distribution of holes in the HDDWs (Figure 7.2). This may reduce the differences between the hydraulic head variations at the outer ends and at the centre of the HDDWs. The hydraulic head variations were responsible for increased chloride concentrations.

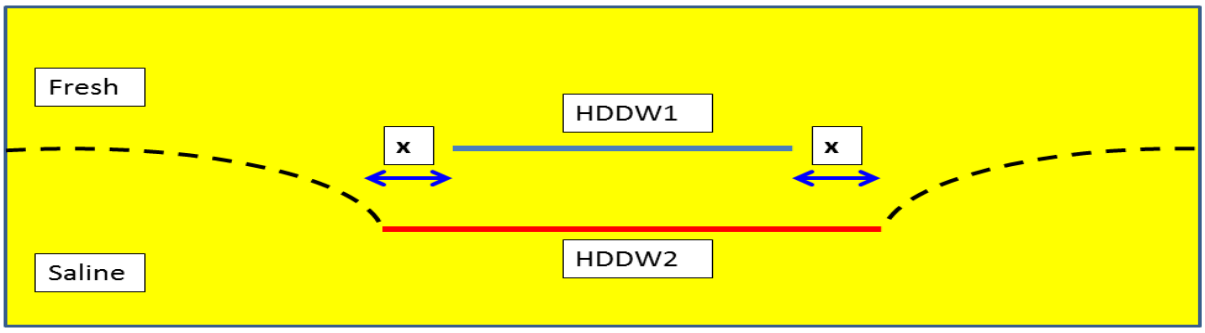

Figure 7.2 – A proposed design modification of the current Freshmaker design: increasing HDDW2 with a length X. This will increase the area over which the fresh-saltwater interface can be lowered.

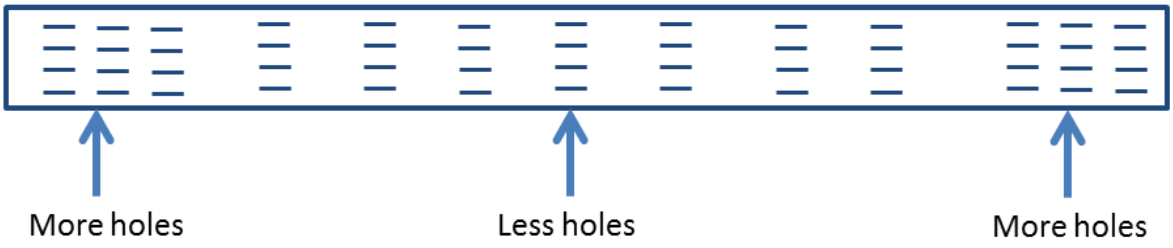

Figure 7.3 - Proposed design modification to decrease the differences in hydraulic head variations between the outer ends and the central part of the HDDWs.

References

Acacia (2014) – Veldonderzoek zoet en zout grondwater Koegraspolder. End report Acacia Water. Projectnumber: N20140550.

Allen, R.G., Pereira, L.S., Raes, D., Smith, M. (1998). Crop evapotranspiration – guidelines for computing crop water requirements – FAO Irrigation and Drainage Paper 56. FAO, 1998. ISBN 92-5-104219-5.

Archie, G.E. (1942). The electrical resistivity log as an aid in determining some reservoir characteristics. Petroleum Transactions of AIME 146, 54–62.

Bakker, M. (2010). Radial Dupuit interface flow to assess the aquifer storage and recovery potential of saltwater aquifers. Hydrogeology Journal 18, 107 – 115.

Bear, J. and Jacobs, M. (1965). On the movement of water bodies injected into aquifers. Journal of Hydrology 3, 37–57.

Brown, C. J. (2005). Planning Decision Framework for Brackish Water Aquifer, Storage and Recovery (ASR) Projects. University of Florida. Ph.D. Thesis, 415 pp.

Cederstrom, D. J. (1947). Artificial Recharge of a Brackish Water Well, Vol. 14 (No. 14), 31-73. Richmond: Virginia Chamber Commerce.

Circel, D. G., van der Wens, P, Rothuizen, R. D. and Kooiman, J. W. (2010). Water extraction with HDD drillings – one horizontal well for multiple vertical wells. Land+Water, access via www.hddw.nl.

Eeman, S., Leijnse, A., Raats, P. A. C. and van der Zee, S. E. A. T. M. (2010). Analysis of the thickness of a freshwater lens and of the transition zone between this lens and upwelling saline water. Advances in Water Resources 34, 291 – 302.

Esmail, O. J. and Kimbler, O.K. (1967). Investigation of the technical feasibility of storing freshwater in saline aquifers. Water Resources Research 3 (3), 683 - 695.

Fedoroff, N.V., Battisti, D.S., Beachy, R.N., Cooper, P.J.M., Fischhoff, D.A., Hodges, C.N., Knauf, V.C., Lobell, D., Mazur, B.J., Molden, D., Reynolds, M.P., Ronald, P.C., Rosegrant, M.W., Sanchez, P.A., Vonshak, A. and Zhu, J.-K. (2010). Radically rethinking agriculture for the 21st century. Science 327 (5967), 833–834.

Gelhar, L. W. (1986). Stochastic subsurface hydrology from theory to applications. Water Resources Research 22 (9), 135 -145.

Gleick, P.H. (2003). Global freshwater resources: soft-path solutions for the 21st century. Science 302 (28), 1524–1528.

Goes, B. J. M., Oude Essink, G. H. P., Vernes, R. W. and Sergi, F. (2009). Estimating the depth of fresh and brackish groundwater in a predominantly saline region using geophysical and hydrological methods, Zeeland, the Netherlands. Near Surface Geophysics, 401-412.

Guo, W. and Langevin, C.D. (2002). User's guide to SEAWAT: A computer program for simulation of threedimensional variable-density ground-water flow: U.S. Geological Survey Techniques of Water-Resources Investigations, Book 6, Chap. A7.

Kimbler, O. K., Kazmann, R. G. and Whitehead, W. R. (1975). Cyclic Storage of Freshwater in Saline Aquifers. Louoisana State University, Baton Rouge, LA.

Kundzewicz, Z.W., Mata L.J., Arnell N.W., Döll P., Kabat P., Jiménez B., Miller K.A., Oki T., Sen, Z. and Shiklomanov, I.A. (2007). Freshwater resources and their management. Climate Change 2007: Impacts, Adaptation and Vulnerability. Contribution of Working Group II to the Fourth Assessment Report of the

Intergovernmental Panel on Climate Change, Parry, M. L., Canziani O.F., Palutikof J.P., van der Linden P.J. and Hanson C.E., Eds., Cambridge University Press, Cambridge, UK, 173-210.

Kundzewicz, Z.W., Mata L.J., Arnell N.W., Döll P., Kabat P., Jiménez B., Miller K.A., Oki T., Sen, Z. and Shiklomanov, I.A. (2008). The implications of projected climate change for freshwater resources and their management, Hydrological Sciences Journal 53 (1), 3-10

Lallemand-Barres, P. and Peaudecerf, P. (1978). Recherche des relations entre la valeur de la dispersivite macroscopique d'un milieu aquifer, ses autres caracteristiques et les conditions de mesure, etude bibliographique. In: Fetter, C. W. (ed.), Contaminant Hydrogeology (2nd edition), p 82. Long Grove, Illinois: Waveland Press.

de Louw, P. G. B., Eeman, S., Siemon, B., Voortman, B. R., Gunnink, J., van Baaren, E. S. and Oude Essink, G. H. P. (2011). Shallow rainwater lenses in deltaic areas with saline seepage. Hydrology and Earth System Sciences 15, 3659 – 3678.

Lenton, R. (2004). Water and climate variability: development impacts and coping strategies. Water Science Technology 49 (7), 17-24.

van der Linde, S. J. (2012). BSc Thesis: A study into the fate of nitrate in the Chalk of Southern Limburg. Utrecht University.

Maliva, R. G., Guo, W. and Missimer, T. M. (2006). Aquifer Storage and Recovery: Recent Hydrogeological Advances and System Performance. Water Environment. Res. 78 (13), 2438 – 2435.

Missimer, T. M., Guo,W., Walker, C.W., Maliva, R.G., (2002). Hydraulic and density considerations in the design of aquifer storage and recovery systems. Florida Water Resources Journal (February), 31-35.

Missimer, T. M. and Guo,W. (1999). Theoretical considerations in the design of aquifer storage and recovery wells proposed in the Everglades restudy: National groundwater Association, The 1999 Southeast Focus Groundwater Conference Official Program, p. 21 (abs.).

Mulder, J. R and Spoelstra, J. (1995). Een geohydrologische systeembeschrijving van het noordelijk deel van het herinrichtingsgebied Bergen-Schoorl, sc-dlo Wageningen.

Molden, D., Oweis, T.Y., Steduto, P., Kijne, J.W., Hanjra, M.A., Bindraban, P.S., Bouman, B.A.M., Cook, S., Erenstein, O., Farahani, H., Hachum, A., Hoogeveen, J., Mahoo, H., Nangia, V., Peden, D., Sikka, A., Silva, P., Turral, H., Upadhyaya, A. and Zwart, S. (2007). Pathways for increasing agricultural water productivity. In: Molden, D. (Ed.), Comprehensive Assessment of Water Management in Agriculture, Water for Food, Water for Life: A Comprehensive Assessment of Water Management in Agriculture. International Water Management Institute, London: Earthscan, Colombo.

Pavelic, P., Dillon, P. J. and Simmons, C. T. (2002). Lumped parameter estimation of initial recovery efficiency during aquifer storage and recovery. In: Dillon, P.J. (Ed.), Management of Aquifer Recharge for Sustainability, Proceedings of the fourth International Symposium on Artificial Recharge (ISAR4), Adelaide, September 22-26 2002, Swets & Zeitlinger, Lisse, ISBN. 90 5809 527 4, pp. 285-290.

Peters, J. H. (1983). The movement of freshwater injected in salaquifers. Geologia Applicata e Idrogeologia 18 (2), 144-155.

Post, V. E. A. (2004). Groundwater salinization processes in the coastal area of The Netherlands due to transgressions during the Holocene, Ph. D. thesis, Free University Amsterdam.

Pyne, R. D. G. (2005). Aquifer Storage Recovery: A Guide to Groundwater Recharge Through Wells, 2nd edition. ASR Press, Gainesville, Florida, ISBN 09 7743 370 6.

Ranjan, P., Kazama, S., Sawamoto, M. and Sana, A. (2009). Global scale evaluation of coastal fresh groundwater resources. Ocean & Coastal Management 52, 197 – 206.

Reese, R. S. (2004). Review of Aquifer Storage and Recovery in the Floridan Aquifer System of Southern Florida. U. S. Geological Survey Water Resources Investigation Report 2004-3128. 4 p.

Schuurman, J. M. and Droogers, P. (2009). Penman-Monteith referentieverdamping: inventarisatie beschikbaarheid en mogelijkheden to regionalisatie. Future Water Report 86.

Serageldin, I. (2001). Assuring water for food: the challenge of the coming generation. Water Resources Development 17 (4), 521–525.

Smith, S. H. (1962). Temperature correction in conductivity measurements. Limnology and Oceanography 7 (3), 330 – 334.

Simmons, C.T., Narayan, K.A., Wooding, R.A. (1999). On a test case for density-dependent groundwater flow and solute transport models: the salt lake problem. Water Resources Research 35 (12), 3607–3620.

United Nations, Department of Economic and Social Affairs, Population Division (2014). World Urbanization Prospects: The 2014 Revision, Highlights (ST/ESA/SER.A/352).

Unsal, B., Yagbasan, O. and Yazicigil, H. (2014). Assessing the impacts of climate change on sustainable management of coastal aquifers. Environmental Earth Sciences 72 (6), 2183 – 2193.

Vos, P. and Zeiler, F. (2008). Holocene transgressions of southwestern Netherlands, interaction between natural and antrophogenic processes, Grondboor & Hamer, 3-4 (in Dutch).

Ward, J. D., Simmons, C. T. and Dillon, P. J. (2007). A theoretical analysis of mixed convection in aquifer storage and recovery: how important are density effects? Journal of Hydrology 343 (3–4), 169–186.

Ward, J. D., Simmons, C. T. and Dillon, P. J. (2008). Variable-density modelling of multiple-cycle aquifer storage and recovery (ASR): importance of anisotropy and layered heterogeneity in brackish aquifers. Journal of Hydrology 356, 93–105.

Ward, J. D., Simmons, C. T., Dillon, P. J and Pavelic, P. (2009). Integrated assessment of lateral flow, density effects and dispersion in aquifer storage and recovery. Journal of Hydrology 370, 83-99.

Zheng, CC, and Wang, P.P., 1999. MT3DMS, a modular three-dimensional multispecies model for simulation of advection, dispersion and chemical reactions of contaminants in groundwater systems: Documentation and user's guide. US Army Engineer Research and Development Center, Contract Report SERDP-99-1. Vicksburg, Mississippi: USAERDC.

Zuurbier, K. G., Bakker, M., Zaadnoordijk, W. J. and Stuyfzand, P. (2013). Identification of potential sites for aquifer storage and recovery (ASR) in coastal areas using ASR performance estimation methods. Hydrogeology Journal 21 (6), 1373-1383.

Zuurbier, K. G., Zaadnoordijk, W. J. and Stuyfzand, P. (2014). How multiple partially penetrating wells improve the freshwater reocvery of coastal aquifer storage and recovery (ASR) systems: A field and modeling study. Journal of Hydrology 509 (0), 430 – 411.

Zuurbier, K. G. Kooiman, J. W., Groen, M. M. A., Maas, B. and Stuyfzand, P. J. (2014). Enabling successful aquifer storage and recovery (ASR) of freshwater using horizontal directional drilled wells (HDDWs) in coastal aquifers. Journal of Hydrologic Engineering. DOI:10.1061/(ASCE)HE.1943-5584.0000990, B4014003.

Appendices

A: Derivation of the dimensionless numbers

B: Description of the groundwater models (incl. FAP-model calibration)

C: Field data analysis

D: Meteorological data analysis

Appendix A: Derivation of the dimensionless numbers

Two dimensionless numbers were introduced in Chapter 2 but they were not derived. The derivation of the numbers is shown in this Appendix. Section A1 shows the derivation of the mixed convection ratio. The derivation of the Rayleigh number is shown in Section A2.

A1. Mixed convection ratio

The mixed convection ratio, M, is a dimensionless parameter to assess the relative influence of forced convection (due to pumping) and free convection (due to density dependent flow) of the fresh-saltwater interface (Ward et al., 2007). The mixed convection ratio is defined as:

$$M = \frac{v_{free}}{v_{forced}} \quad (1)$$

In order to derive an expression for M, two individual expressions need to be determined.

Forced convection term

Assume a fully penetrating well in a confined aquifer. Freshwater injected in this well can be conceptualized as a cylinder with radius r and height B (which is the thickness of the aquifer). The volume of water in this cylinder is given by the following expression:

$$V = \pi r^2 \theta B \quad (2)$$

Where:
V = volume [m^3]
r = radius of the cylinder [m]
θ= porosity [-]
B = thickness of the aquifer [m]

The pumping rate, Q, can be expressed in terms of time rate of change of volume and can therefore be expressed as a function of the bubble radius:

$$Q = \frac{dV}{dt} = \frac{d(\pi r^2 \theta B)}{dt} = 2\pi r \frac{dr}{dt} \theta B \quad (3)$$

v_{forced} is the radial velocity of the outer end of the cylinder from the well which varies due to puming. The radial velocity equals the time rate of change of the radius of the cylinder:

$$v_{forced} = \frac{dr}{dt} = \frac{Q}{2\pi r \theta B} \quad (4)$$

Free convection term

The free convection term is derived from Darcy's Law. Darcy's Law written in terms of head and for the three dimensions separately is given by:

$$q_x = -K_x \frac{\partial h}{\partial x} \quad (5)$$

$$q_y = -K_y \frac{\partial h}{\partial y} \quad (6)$$

$$q_z = -K_z \left[\frac{\partial h}{\partial z} + \frac{\rho(C_s) - \rho_0}{\rho_0}\right] \quad (7)$$

Where:
$Q_{x,y,z}$ = Darcy velocity in three dimensions [m/d]
$K_{x,y,z}$ = Hydraulic conductivity in three dimensions [m/d]
h = hydraulic head
$\rho(C_s)$ = ambient water density for a concentration C_s [kg/m^3]
ρ_0 = freshwater density [kg/m^3]

Since we are dealing with a situation without pumping, there are no head variations. So ∇h is 0 and can be neglected. The free convection term can therefore be written as:

$$v_{free} = \frac{q}{\theta} = \frac{K_z \frac{\rho(C_s)-\rho_0}{\rho_0}}{\theta} \quad (8)$$

Note that Equation (8) is a conservative proxy for the real free convection of the fresh-saltwater interface since dispersion is not taken into account. The interface between fresh and salt water is assumed to be sharp. In reality dispersion will result in a smeared interface decreasing the density gradient and hence reducing the free convective flow.

Putting it all together

Substitution of the expressions for the forced and free convection terms ((4) and (8)) in the equation for the mixed convection ratio (1) gives the formula for the mixed convection ratio as introduced in Section 2.4.2:

$$M = \frac{v_{free}}{v_{forced}} = \frac{K_z \frac{\rho(C_s)-\rho_0}{\rho_0}}{\frac{Q}{2\pi r\theta B}} = \frac{2\pi r K_z B}{Q}\frac{\rho(C_s)-\rho_0}{\rho_0} \quad (9)$$

A2. Rayleigh number

The Rayleigh number is defined similar to Simmons et al. (1999), as the ratio of convective velocity (multiplied by an appropriate length scale, which in this case is the thickness of the confined aquifer B) to mechanical dispersion (diffusion + dispersion). The convective velocity is the same as the free convection which was already derived above (Equation (8)). The Rayleigh number can therefore be written as:

$$Ra = \frac{K_z B \frac{\rho(C_s)-\rho_0}{\rho_0}}{(D_d+\beta_l v)\theta} \quad (10)$$

Where:
D_d = the molecular diffusivity [m^2/s]
β_l = the longitudinal dispersivity [m]
v = velocity

It is convenient to write the density difference ratio as an individual parameter α:

$$\alpha = \frac{\rho(C_s)-\rho_0}{\rho_0} \quad (11)$$

The velocity, v, is the idealized average velocity at the outer edge of the plume at the end of injection. This is equal to the forced convection velocity (Equation (4)). At the ASR scale, mixing by molecular diffusion is negligible compared to the mixing due to dispersion that has occurred during pumping. The Rayleigh number, after neglecting diffusion and substitution of Equation (4) and (11) becomes:

$$Ra = \frac{K_z B\,\alpha}{\beta_l \theta \frac{Q}{2\pi r\theta B}} = \frac{2\pi r K_z B^2 \alpha}{\beta_l Q} \quad (12)$$

The parameter r is the radial extent of the plume in the aquifer after injection for duration t at the nonzero pumping rate Q and can be written as:

$$r = \sqrt{\frac{Qt}{\pi B\theta}} \tag{13}$$

Substitution of Equation (13) in equation (12) and rewriting gives:

$$Ra = \frac{2\pi K_z B^2 \alpha}{\beta_l Q}\sqrt{\frac{Qt}{\pi B\theta}} = \frac{2K_z\alpha}{\beta_l}\sqrt{\frac{\pi^2 QB^4 t}{Q^2 B\theta\pi}} = \frac{2K_z\alpha}{\beta_l}\sqrt{\frac{\pi B^3 t}{Q\theta}} = \frac{2K_z\alpha\sqrt{\pi B^3 t}}{\beta_L\sqrt{Q\theta}} \tag{14}$$

Back substitution of the density difference ratio (Equation 11) gives the Rayleigh number as given in the main text in Section 2.4.3.

Appendix B - Description of the Groundwater models

This appendix describes the groundwater models used in the MSc research. Three models were constructed:

1. Freshmaker Applied in Practice 2D and 3D (2D and 3D FAP-model), described in Section B2, and
2. Freshmaker Applied in Theory (FAT-model), described in Section B4.

All models were build and simulated using the SEAWAT code in the modelling environment of PMWIN (version 8). The next section explains SEAWAT and why SEAWAT was chosen to simulate the Freshmaker.

B1. SEAWAT

B1.1 Why SEAWAT

Density variations in groundwater are important aspects to consider when modelling the effect of the Freshmaker and freshwater lenses in general and therefore the basic MODFLOW code cannot be used. To solve flow problems in MODFLOW, Darcy's Law for groundwater flow in three directions is used:

$$\boldsymbol{q} = -\frac{\boldsymbol{k}}{\mu}\nabla \boldsymbol{P} \qquad (1)$$

Where:
$\boldsymbol{q}$ = specific discharge vector [L/T]
$\mathbf{k}$ = intrinsic permeability tensor [L^2]
μ = dynamic viscosity [Pa*T]
$\nabla \boldsymbol{P}$ = pressure gradient vector [Pa/L].

When Equation 1 is written for each direction separately, it can be seen that density changes affects the vertical (z) component of Darcy's Law:

$$q_x = -\frac{k_x}{\mu}\frac{dP}{dx} \qquad (2)$$

$$q_y = -\frac{k_y}{\mu}\frac{dP}{dy} \qquad (3)$$

$$q_z = -\frac{k_z}{\mu}\left[\frac{dP}{dz} + \rho g\right] \qquad (4)$$

Where the subscripts x,y,z denote the individual components of specific discharge and intrinsic permeability in the principal directions.

When water densities are variable the vertical flow term becomes variable too, which is something that MODFLOW does not take into account. Since water densities are highly variable at the Freshmaker pilot site, the SEAWAT code has been used as SEAWAT is able to deal with variable density in the vertical flux term.

B1.2 Governing equations used in SEAWAT

SEAWAT (Guo and Langevin, 2002) has been developed at the U.S. Geological survey. In this research SEAWAT version 4 has been used. SEAWAT is a coupled version of MODFLOW-2000 and MT3DMS with a variable-density flow package. It has been designed to simulate three-dimensional, variable-density, multi-species saturated groundwater flow. In SEAWAT the variable density groundwater flow equation is developed in terms of equivalent freshwater head, rather than in pressure, or head. The "normal" equation for head is given by:

$$\mathrm{h} = \frac{P}{\rho g} + z \qquad (5)$$

Where:
h = head [m]
P = pressure [Pa],
ρ = density [M/L^3]
g = acceleration by gravity [L/T^2]
z = elevation above a certain datum (L)

As can be seen from Equation 5, head does not only depend on pressure or elevation. Head also depends on the density. This implies that two points having the same elevation above a certain reference level and experiencing the same pressure but with different densities will have two different values of hydraulic head. When the flow problem is solved in terms of local density it results in cumbersome equations and the results become numerically less stable. For this reason SEAWAT uses the so called "equivalent freshwater head". The freshwater head is related to "normal" head by the following relationship:

$$h_f = \frac{\rho}{\rho_f} h + \frac{\rho - \rho_f}{\rho} z \qquad (6)$$

Where:
h_f = equivalent freshwater head (L)
h = local head [L]
ρ_f = freshwater density (M/L^3)
ρ = local water density (M/L^3)

It follows from Equation 6 that when the density of the groundwater at a certain location equals ρ_f, equivalent freshwater head becomes equal to actual (local) head.

The two resulting governing equations, in terms of equivalent freshwater head, for flow and transport as used in the SEAWAT code are (Zheng and Wang., 1999; Guo and Langevin., 2002):

- For groundwater flow:

$$\nabla \left[\rho \boldsymbol{K} \left(\nabla h_f + \frac{\rho - \rho_f}{\rho_f} \nabla z \right) \right] = \rho S_s \frac{\delta h_f}{\delta t} + \theta \frac{\delta \rho}{\delta C} \frac{\delta C}{\delta t} - \rho_s q_s \qquad (7)$$

Where:
S_s = specific storage, which is defined as the volume of freshwater released from storage per unit decline of h_f [1/L]
K = hydraulic conductivity tensor [L/T]
t = time [T]
θ = porosity [-]
C = solute concentration [M/L^3]
q_s = a source or sink [1/T]
ρ_s = source or sink fluid density [M/L^3].

- For solute transport:

$$\frac{\delta C}{\delta t} = \nabla \cdot (D \cdot \nabla C) - \nabla \cdot (vC) - \frac{q_s}{\theta} C_s + \sum_{k=1}^{N} R_k \qquad (8)$$

Where:
D = hydrodynamic dispersion coefficient [L^2/T],
v = fluid velocity [L/T],
C_s = solute concentration of water entering from sources or sinks [M/L^3], and
R_k = rate of solute production or decay in reaction *k* of *N* different reactions [M/L^3/T].

The two equations are used in a coupled way. For each calculation time step a flow field is calculated from Equation 7 based on the density distribution at the start of the time step. From this flow field a fluid velocity is derived which is then used as input in the solute transport equation (Equation 8). At the end of the time step, the resulting concentration distribution is used to derive a new density distribution which is then used to calculate the new flow field in the next time step.

B1.3 An Equation of State for the Freshmaker pilot site

As can be seen from the coupling process in the previous section, a formula is needed to derive water density (used in the flow equation) from the solute concentration (used in the transport equation). However, in reality, the density of water is not just a function of solute concentration (or salinity) but also of the water temperature and pressure:

$$\rho = f(P, T, S) \qquad (9)$$

Where:
ρ = density (M/L^3)
P = pressure ($M/L/T^2$)
T = temperature (˚C)
S = salinity (ppt) or TDS concentration (M/L^3).

In the literature there are many conversion formulas relating density to salinity, pressure and temperature. Such a formula is called an "equation of state". For most hydrogeological systems, density changes due to pressure changes with depth are negligible so the density only depends on T and S. For many groundwater applications the influence of temperature variations on density may be assumed to be negligible too. Nevertheless, since there are differences between the injected freshwater water temperature and native groundwater temperature, this has to be validated first.

The measured temperature range at the Freshmaker pilot site is between 10˚C and 13˚C at the depth of the HDDWs and between 5˚C and 16˚C in the semi-confining layer, while measured TDS concentrations vary from 1100 to 30500 mg/L. Graphs showing water density as a function of temperature or TDS concentration are given in Figure B1 and B2. From the figures can be seen that, in relative terms, the maximum difference in water density due to temperature differences at the Freshmaker site is significantly smaller than due to differences in TDS concentration (0.93<<21.43). Furthermore, in groundwater, temperature gradients are usually smoother then concentration gradients since conduction in a porous medium occurs much faster than molecular diffusion. This means that for this research the effect of differences in temperature on groundwater flow can be safely neglected. The equation of state used in this research is therefore a function with solute concentration as the only variable. The following linear relation was used (Guo and Langevin, 2002):

$$\rho = \rho_f + EC \qquad (10)$$

Where:
ρ = water density [M/L^3],
ρ_f = freshwater density [M/L^3],
E = density gradient, a dimensionless constant equal to $\frac{\partial \rho}{\partial c}$. If TDS concentrations are used in mg/l the value of E becomes 0.0007143,
C = TDS concentration [M/L^3].

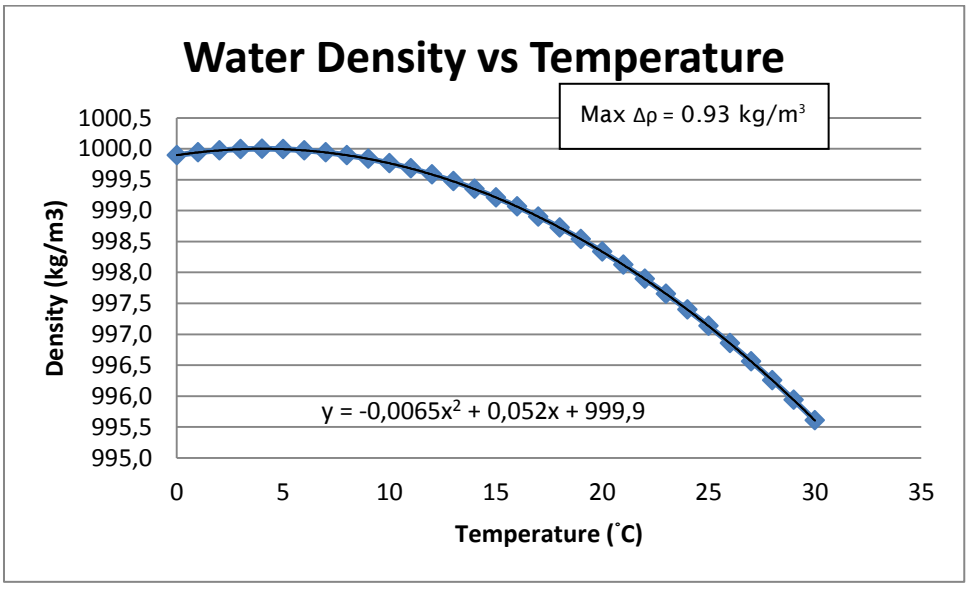

Figure B1 - Water density as a function of temperature.

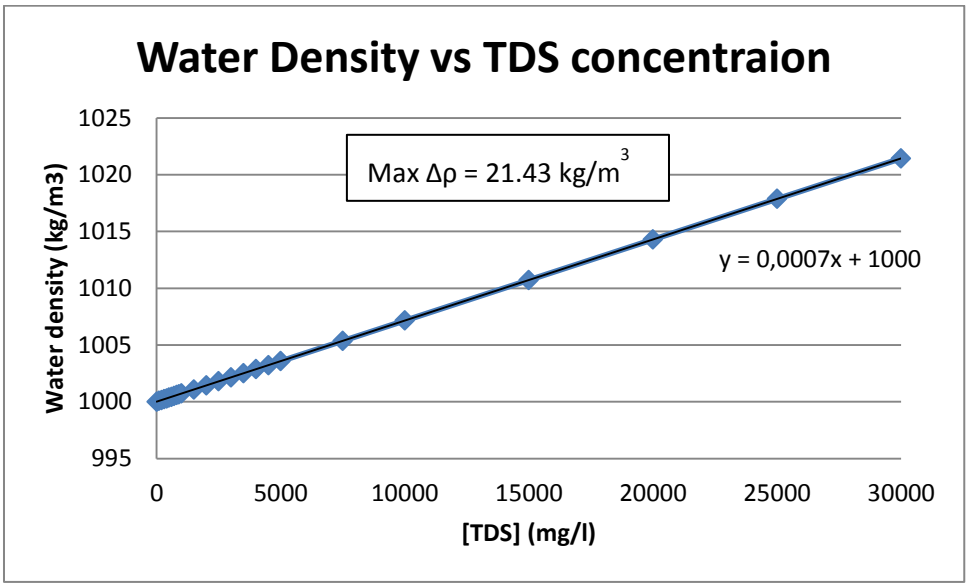

Figure B2 – Water density as a function of TDS concentration. The temperature was fixed on 10°C.

B2. FAP-model: Freshmaker Applied in Practice (2D & 3D)

Zuurbier et al. (2014) built a cross-sectional SEAWAT model prior to the installation of the HDDWs in order to estimate the required pumping rates during operation and the distance that was needed between the two HDDWs. This basic 2D model was used as a starting point and was validated and further developed in this MSc research. The resulting model was called the 2D FAP-model. Before the 2D FAP-model could be used to study the Freshmaker in the current setup and for simulating hypothetical scenarios, it had to be calibrated. The model results could only be used to reliably analyse the concept of the Freshmaker when it was able to generate output corresponding to reality. The calibration process is described in Section B3. The 2D FAP-model is described in Section B2.1 and the 3D FAP-model in Section B2.2.

B2.1 – 2D FAP-model

Model configuration

The cross-sectional model of the Freshmaker consists of 10 m thick slice of the HDDW pair. It was assumed that effects on the edges of the wells do not influence model outcomes. The location of the model is shown in Figure B3, the resulting calculation grid in Figure B4. The properties of the model are shown in Table B1. The hydrogeological properties were obtained in the calibration (Section B3). As can be seen in Figure B4, the model is refined near the location of the Freshmaker. Cell widths vary from 110 m at the boundary to 1 m in the middle, near the Freshmaker. Layer thicknesses are increasing from 20 m at the bottom to 0.5 m at the top. Model top elevations follow the local topography and all elevations are related to sea level. The surface elevation at the creek ridge is 1.50 m-ASL, in the drained polder North of the field site 0.60 m-BSL, and at the field site 0.75 m-ASL. HDDW1 was placed at -6.75-BSL and HDDW2 at -14.25 m-BSL

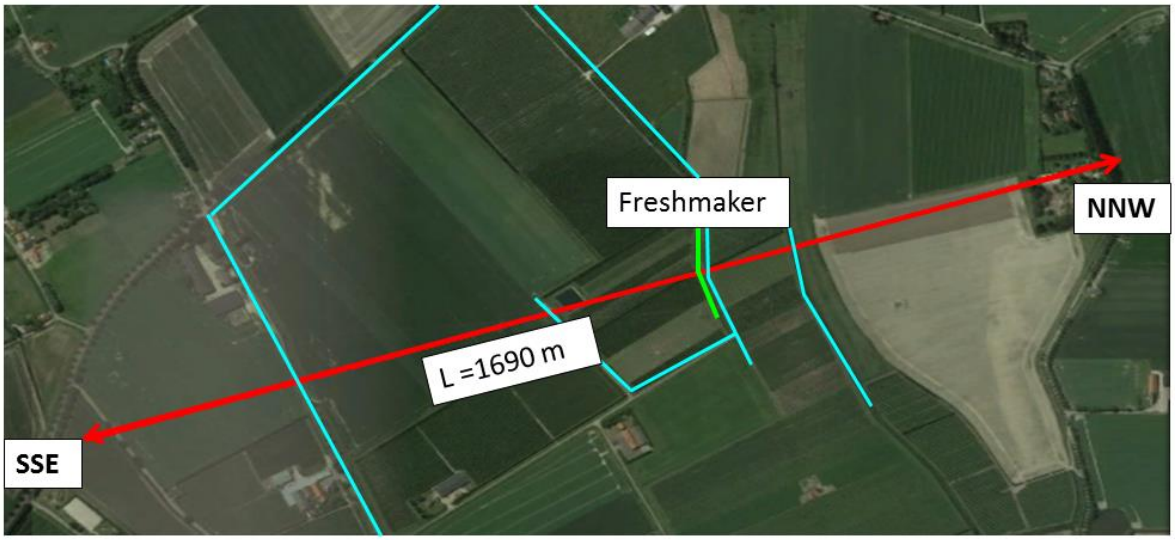

Figure B3 – Location of the model. Red: cross Section length, green: Freshmaker, and blue: water bodies.

Solute transport

The FAP-model was used to simulate chloride transport. However, as described in Appendix C, it was not possible to obtain chloride measurements that could be used for model calibration. For this reason, the model was calibrated using TDS measurements instead. TDS was selected as the species whose concentration influences water density and therefore flow. Since the model was calibrated on TDS for flow, chloride was simulated as a species that was transported along with that flow.

Boundary conditions

Since the polder is drained, a constant head boundary of -0.40 m was applied at the top cells there. These cells also have a constant concentration boundary condition of 1100 mg TDS/l and 50 mg Cl/l. A hydrostatic boundary condition was applied at the left and right boundaries with a hydraulic head of -0.53 m and a concentration of 30500 mg TDS/l and 16800 mg Cl/l. The region experiences saline seepage, therefore, a constant head of -0.53 m and a constant concentration of 30500 mg TDS/l and 16800 mg Cl/l was applied

along the bottom of the model. Four ditches were simulated with MODFLOW's river package with constant water levels of -0.65 m. The locations of the ditches and the constant head and concentration boundaries are shown in Figure B4.

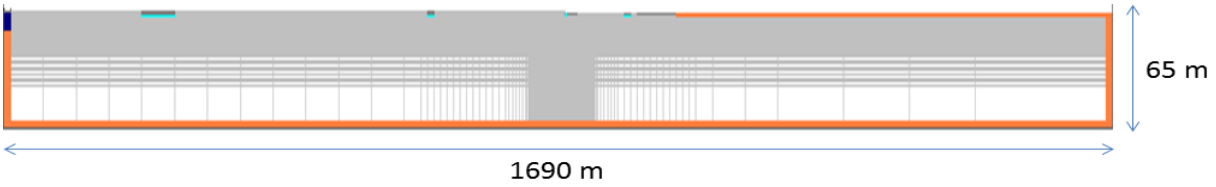

Figure B4 – Model calculation grid of the 2D FAP-model. Ditches are shown in light blue. Constant head and concentration boundary conditions shown in orange.

Initial conditions

As explained in Section B1, solute concentrations and heads are interconnected in SEAWAT and they must be in steady state before Freshmaker simulations start. Otherwise there will be movement of the fresh-saltwater interface induced by the non-equilibrium between hydraulic head and solute concentration which will lead to interpretation errors of the results. The initial solute concentrations and hydraulic head distribution was obtained by starting with a model that contained the maximum measured TDS and Chloride concentrations (30500 and 16800 mg/l respectively) and had a hydraulic head of -0.53 m everywhere. The model was run with a realistic average recharge of 0.46 mm/d and a concentration of 1100 mg TDS/l and 50 mg Cl/l. Simulation of 300 years was found to be sufficient to reach equilibrium. The recharge rate was derived from KNMI data (Royal Dutch Meteorological Institute) (Appendix D) and the TDS concentration from measurements (Appendix D). The resulting TDS and Chloride concentrations, and hydraulic head distributions were saved as ASCII matrix files and used as initial conditions in the SEAWAT model. Figure B5 shows the resulting initial TDS concentration. To solve the transport equation, the HMOC numerical scheme was used. The solver configurations are given in Table B2 and B3.

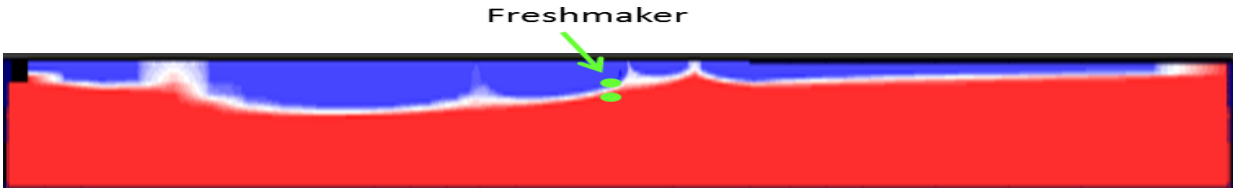

Figure B5 – Initial TDS concentration. Concentrations ranging from 1100 mg/l (blue) to 30500 mg/l (red).

Table B1 – FAP-model properties (after model calibration)

Model property	Value
Top elevation (m)	Varies between 1.5 and -0.16 m
Bottom elevation (m)	-63.5
Thickness of the cross sectional model slice (m)	10
Horizontal extent (m)	1690
Hydraulic conductivity of the semi confining layer (m/d)	0.45
Hydraulic conductivity of aquifer 1 (m/d)	2.5
Resistance of the clay aquitard (d)	4000
Hydraulic conductivity of aquifer 2 (m/d)	2.5
Porosity (-)	0.3
Specific Yield (-)	0.25
Storativity (m^{-1})	0.0001
Vertical anisotropy (-)	1
Conductance river bottom (m^2/d) (river 1,2,3,4)	1000, 2, 10, 33

Table B2 – Generalized Conjugate Gradient (GCG) solver for transport

Property	Value
Preconditioning method	Jacobi
Max. number of Outer iterations	1
Max. number of inner iterations	100
Relaxation factor	1
Concentration closure criterion	0.00001

Table B3 – Strongly Implicit Procedure (SIP) solver for flow

Property	Value
Maximum allowed iterations	2000
Printout interval	1
No. of iteration parameters	5
Acceleration parameter	1
Head convergence criterion (m)	0.1

B2.2 – 3D FAP-model

The 3D FAP-model was based on the calibrated 2D model. It simulates the same freshwater lens as the 2D FAP-model however, this lens was now simulated in 3D. The model domain and hydrogeological parameters were identical to the 2D-FAP model. Since the Freshmaker consists of horizontal wells, an axis of symmetry exists in the middle of the HDDW pair. This symmetrical plane was used for the eastern model boundary with a Neuman boundary condition (i.e no-flow boundary), so the 3D model simulates one half of the HDDW pair. The western model boundary had a Dirichlet boundary condition and was placed sufficiently far from the eastern boundary such that the bottom of the freshwater lens was horizontal at the location of the HDDWs.

Furthermore, the western boundary was placed out of the area of influence of the HDDWs, to avoid hydraulic heads to be "hanging" on the western boundary when the Freshmaker was active. Recharge was applied at the top, with a constant recharge rate derived from KNMI data. For details, refer to Appendix D. As in the 2D model, a constant head boundary was applied at the bottom in order to simulate saline seepage from aquifer 2 into aquifer 1.

The resulting 3D-model grid is shown in Figure B6 and close up of the HDDWs in figure B7. The HDDWs were simulated by a string of 6 grid cells of each 5 m width and an outer end of 5 model cells of 1 m, resulting in a total well length of 35 m (i.e. ½ HDDW length). Each well node was given a pumping rate corrected for the width of the model cell relative to the total Freshmaker pumping rate.

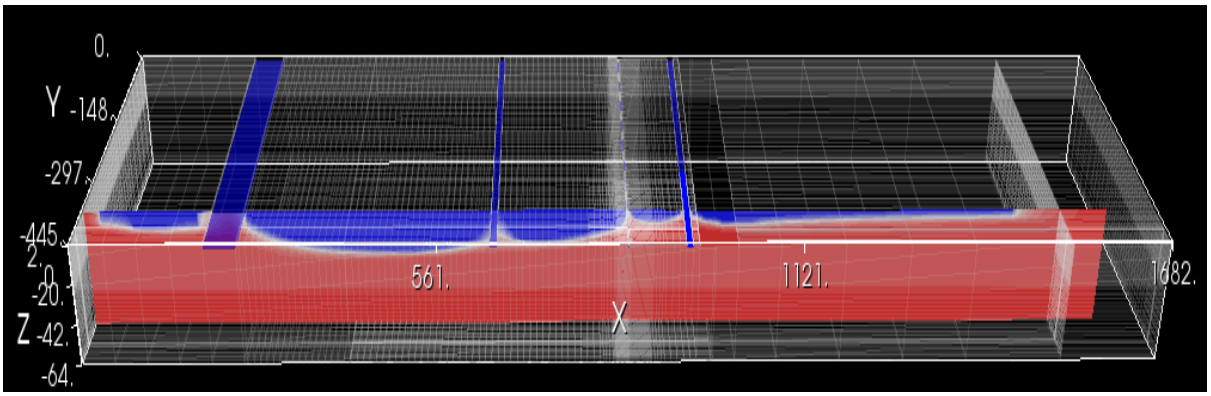

Figure B6 – 3D FAP-model calculation grid and initial chloride concentration distribution.

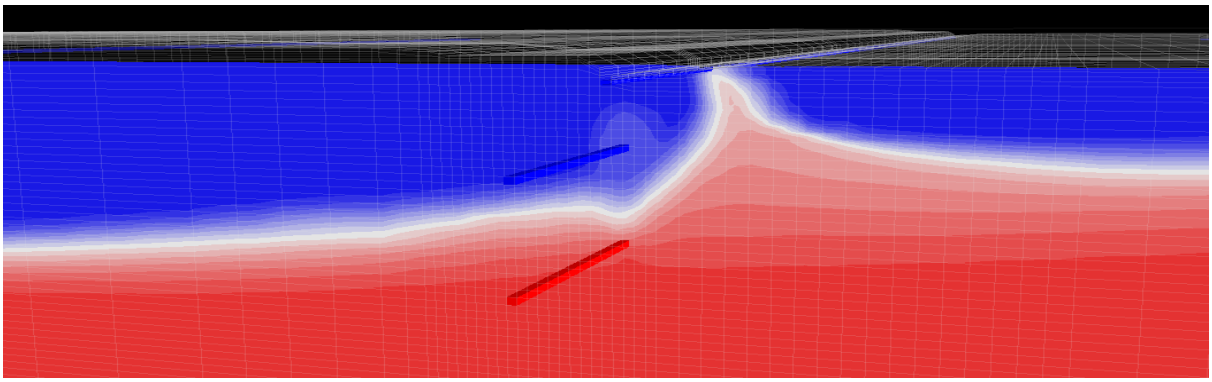

Figure B7 – Close-up of the HDDW pair. Both wells are representing ½ of the total Freshmaker length. In blue: HDDW1, in red: HDDW2.

B3 - 2D FAP-model calibration

B3.1 – Initial model performance

The uncalibrated FAP-model was ran from 01/02/2013 till 13/08/2014 with stress periods of 7 days and transport steps of 1 day. A total of 81 stress periods were simulated. The Freshmaker wells were injecting and/or abstracting at the actual pumping rates as derived in the data analysis (Appendix C) and since the model consists of a 10 m thick slice of the 70 m long HDDW pair, the model was simulated with 1/7th of the real pumping rate. The initial model had hydraulic conductivities estimated from grain size distributions using Bear (1972) and a river bed conductance which was modified until the model produced the salinity distribution of the reference CVES results (Zuurbier et al., 2014).

Simulation results were compared to TDS measurements which showed a poor fit (Figure B8). It can be seen that the fresh-saltwater interface is modelled at a lower depth than at which it is in reality. Also, the measurements show the interface is moving upwards during the recovery phases while this dynamic is clearly not correctly captured in the model. The cause behind the poor fit was first sought in parameters that influence vertical flow: hydraulic conductivity, vertical anisotropy, porosity and specific storage. However, a great number of simulations with different parameter combinations did not lead to significant changes in the position and dynamic movement of the fresh-saltwater interface. Nevertheless, the correct shape of the curve (indicating the thickness of the transition zone) could be obtained when simulations were done with different values of the longitudinal dispersivity. A longitudinal dispersivity value of 0.33 m was found to result in the best fit.

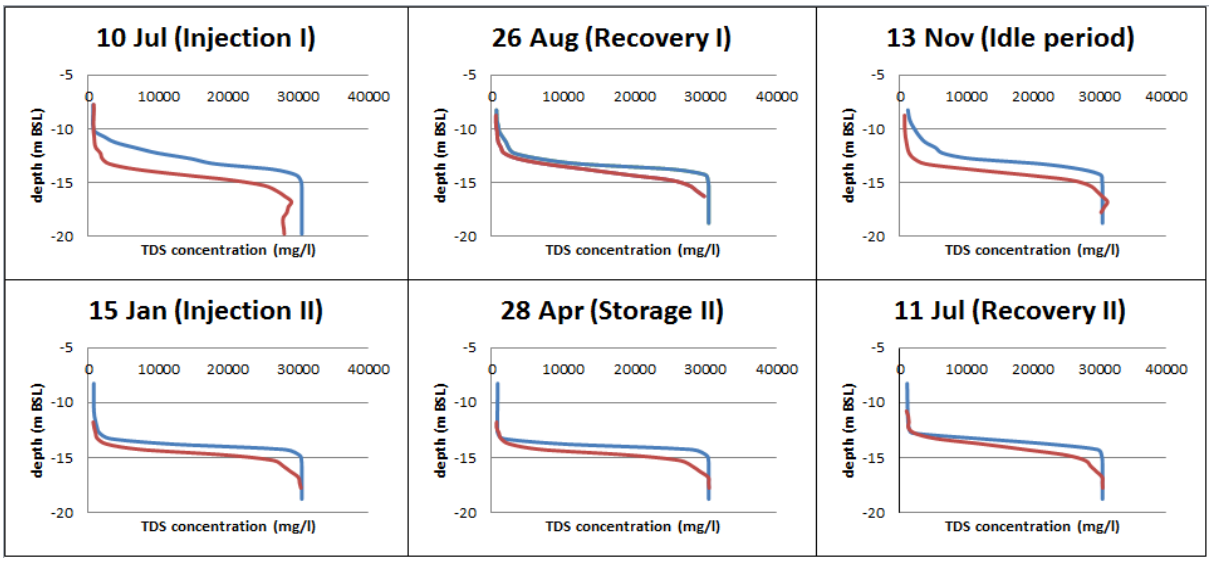

Figure B8 – Initial simulation results of the 2D SEAWAT model for two modelled ASR-cycles. Blue curve = measurement, red curve = model.

B3.2 – A new initial concentration distribution but wrong hydraulic heads

As said before, the model clearly simulated the fresh-saltwater interface not deep enough. The next step to obtain a better fit was therefore to bring the fresh-saltwater interface down by improving the initial TDS concentration distribution. The first initial condition was based on the comparison with the CVES measurement only. This did lead to the correct freshwater lens shape but did not provide a detailed fit of the actual depth of the fresh saltwater interface. Fortunately, a reference geophysical bore hole log was constructed with the EM39 probe. It was possible to obtain a more correct initial TDS concentration distribution after performing various simulations in which the groundwater recharge rates and ditch bottom resistances were modified until a good fit with the CVES measurement and EM39 reference measurement was found. The model fit was significantly improved when simulations were performed with the new initial TDS concentration distribution, a longitudinal dispersivity value of 0.33 m and a VANI of 2 instead of the initial VANI of 4. However, despite the fact that the model correctly simulated the fresh-saltwater interface dynamics, the simulated hydraulic heads variations were not corresponding to the measured hydraulic head variations (see Figure B9). As explained in Appendix C, the hydraulic head measurements cannot be used to calibrate the groundwater flow. Nevertheless, the model should at least be able to capture the dynamics of the head variations as observed in the measurements. However, the model was obviously not yet capable of correctly simulating the hydraulic head dynamics.

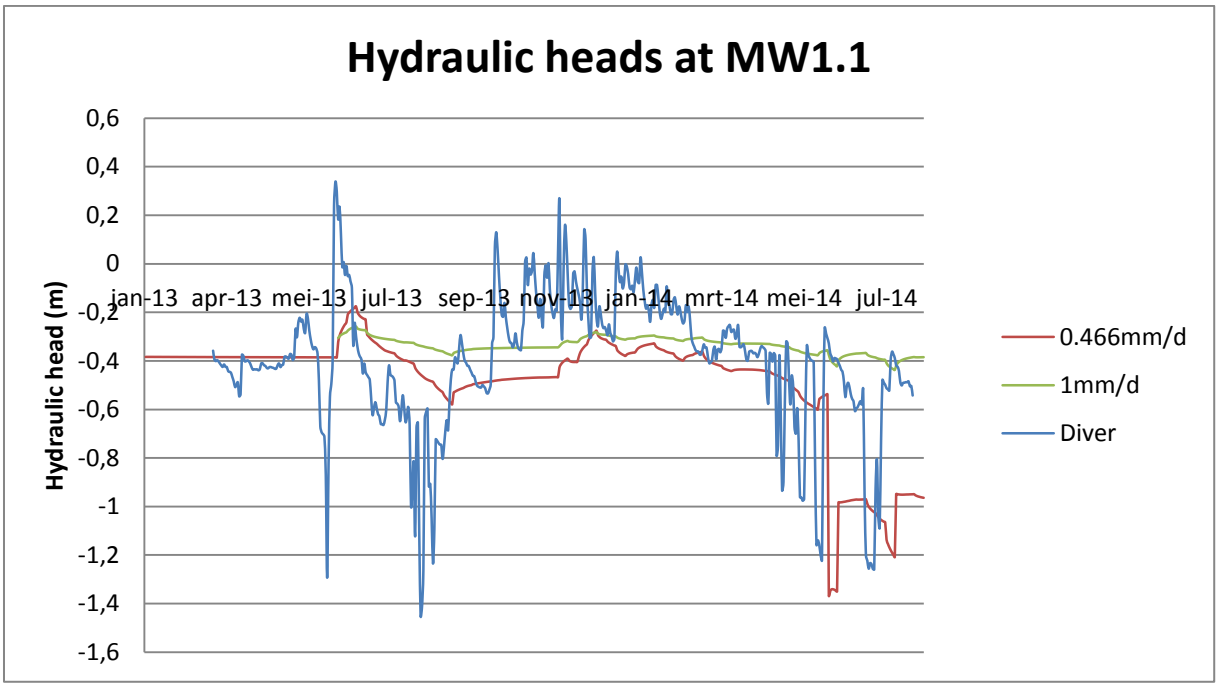

Figure B9 – Simulated (red and green curves) versus measured (blue curve) hydraulic heads at MW1 for two different scenarios which both lead to a good TDS concentration fit. 1st scenario (red curve): average recharge rate of 0.46 mm/d, 2nd scenario (green curve) constant recharge rate of 1 mm/d.

B3.3 - Possible explanation: hydraulic conductivity too large

One possible explanation of the fact that the hydraulic heads were not correctly simulated is that the hydraulic conductivities used in the model were too large. The reason that the hydraulic conductivity was chosen too large may be an artefact from the way how the initial freshwater lens geometry was obtained: by changing recharge and ditch bottom resistances only. However, the shape of the steady state freshwater lens depends both on the recharge rate and the hydraulic conductivity. The correct initial TDS concentration distribution can therefore be obtained by either changing the value of the groundwater recharge or the hydraulic conductivity, or both. It was therefore hypothesized that the applied recharge rate was too high, resulting in hydraulic conductivities that were also too high. Water budget calculations showed that the vertical leakage rate through a ditch close to the Freshmaker was 0.23 m/d, which is unreasonably high indicating the simulated recharge rates are indeed too high.

B3.4 –Good model fit after applying a realistic groundwater recharge rate and lower hydraulic conductivity

Real time meteorological data from the KNMI were analysed to obtain a more realistic groundwater recharge rate. A detailed description of how the groundwater recharge was derived from real time data is given in Appendix D. An annual average recharge rate of 0.46 mm/d was derived from this analysis. In reality the groundwater recharge rate is not constant but follows a cosine function with a positive groundwater recharge in winter and a negative recharge in summer. Since the largest discrepancies between model outcomes and measurements were in the summer period (Recovery phases I and II), simulations were done with daily actual recharge rates derived from the meteorological data analysis. After changing the hydraulic conductivity to 0.45 m/d in the semi-confining layer, 2.5 m/d in the aquifer and 0.001 m/d in the clay aquitard, the model resulted in a good fit with TDS concentration measurements (Figure B10 and B11). The simulated hydraulic heads were showing a trend which matched observed hydraulic head dynamics significantly better than the simulations with a recharge rate of 1 mm/d (Figure B9).

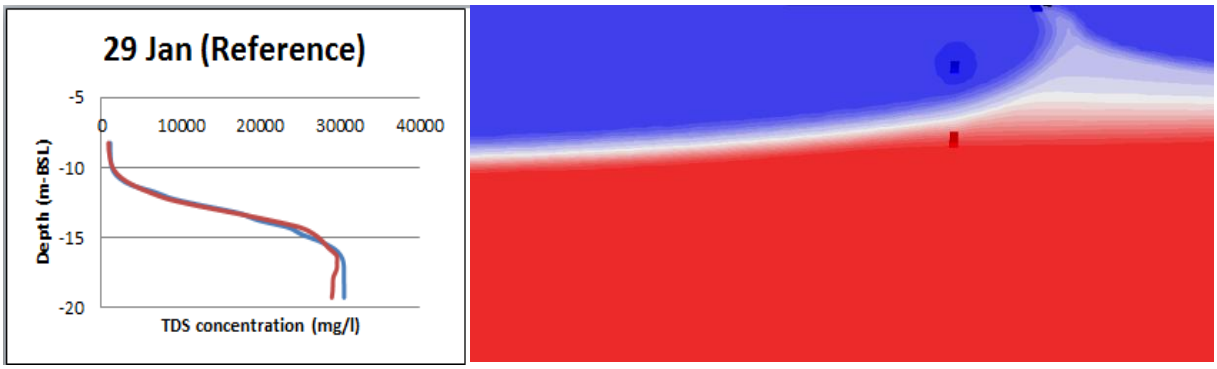

Figure B10 - Initial TDS concentration obtained with a realistic groundwater recharge rate and lower hydraulic conductivities. Left: simulated TDS concentration profile (red curve) versus measured TDS concentration (blue curve) at MW1. Right: Resulting shape of the freshwater lens.

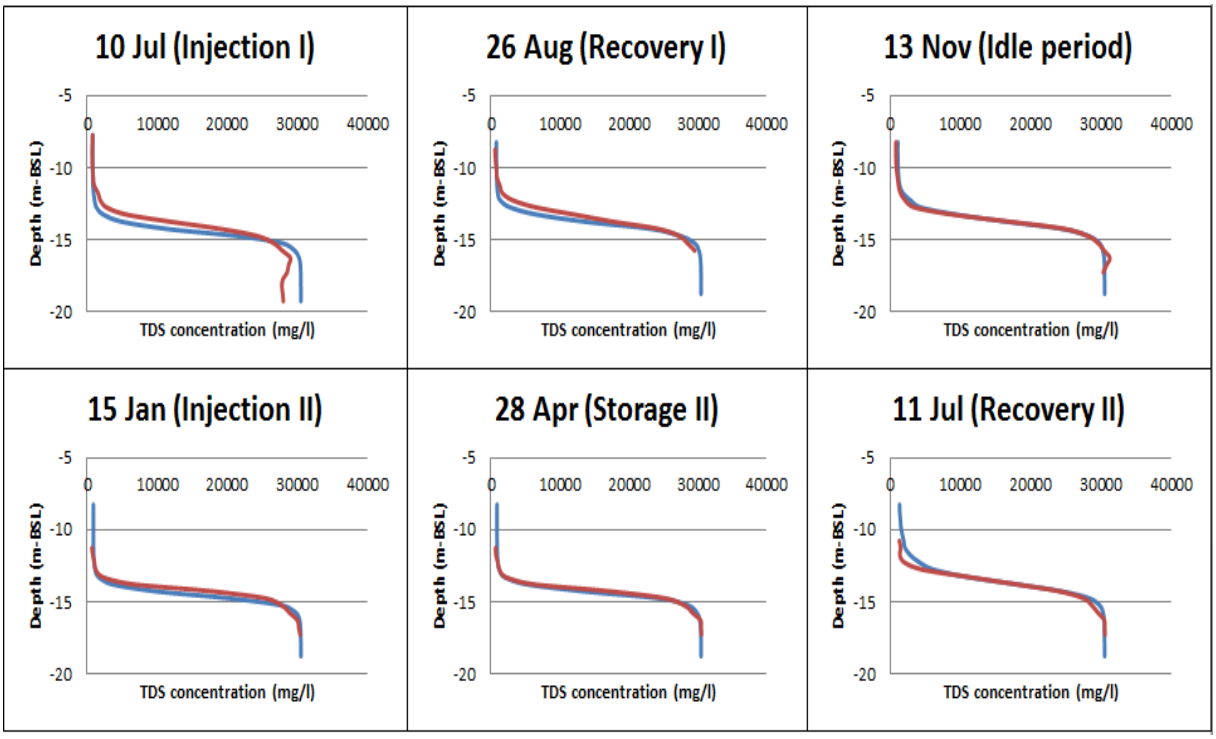

Figure B11- Model results of the calibrated 2D SEAWAT model for two modelled ASR-cycles. Blue curve = measurement, red curve = model.

B4. FAT model: Freshmaker Applied in Theory

B4.1 - Model dimension and boundaries

The FAT is a cross sectional model with a thickness of 10 m. The model dimensions are shown in Figure B12 and the hydrogeological parameters in Table B4. Model top and bottom boundaries have a Neumann boundary condition. The left and right model boundaries have Dirichlet boundary conditions for head and concentration.

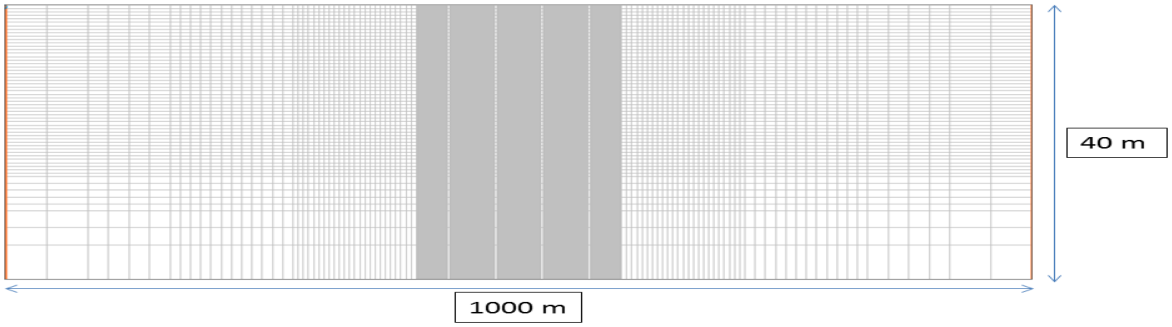

Figure B12 - FAT-model dimensions. The model is refined in the center, where cells are 0.5 high and 1 m wide. Not to scale.

Table B4- Properties of the FAT-model.

Model property	Value
Top elevation (m)	0
Bottom elevation (m)	-40
Cross Section thickness (m)	10
Horizontal extend (m)	1000
Hydraulic conductivity (m/d)	10
Effective Porosity (-)	0.33
Specific Yield (-)	0.25
Storativity (m^{-1})	0.0001
Vertical anisotropy (-)	1

B4.2 - Initial chloride distribution

Initially, freshwater (50 mg Cl/l) was on top of saline water (16800 mg Cl/l) (Figure B13). Between the two water types, from 10 m depth onwards, a transition zone with a thickness of 4 m was present. Figure B14 shows the depth profile of the chloride concentration. The transition zone was obtained with the following formula:

$$[Cl]_z = [Cl]_{fresh} + 2e^{z_1 - z_n}$$

Where:
$[Cl]_z$ = chloride concentration at depth z (mg/l);
$[Cl]_{fresh}$ = chloride concentration in the freshwater (50 mg/l);
z_1 = 10 m;
z_n = depth at node n (10 m < z < 14 m).

Figure B13 - Initial chloride distribution of the FAT-model. Concentrations vary from 50 mg/l (blue) to 16800 mg/l (red).

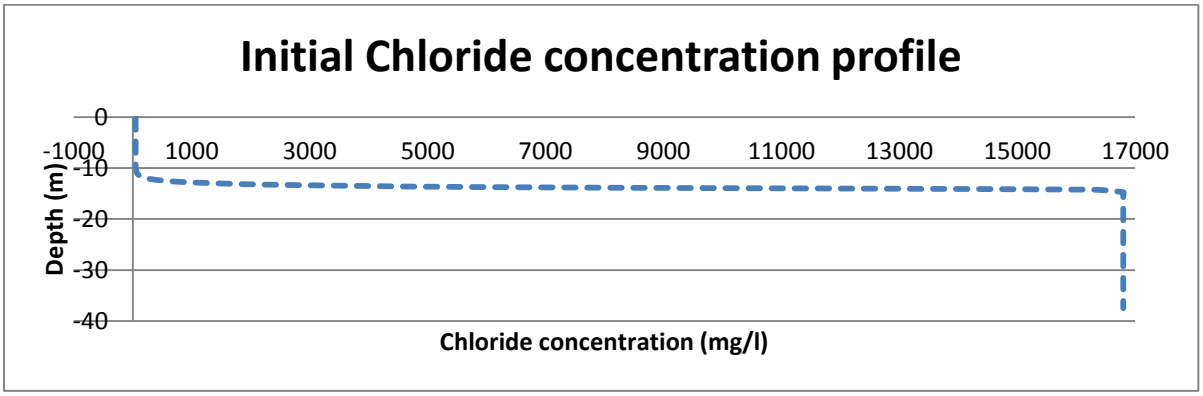

Figure B14 - Initial chloride concentration profile with depth.

B4.3 - Initial head distribution

The initial heads were hydrostatic all over the model. Hydrostatic means that there is no vertical flow. Since heads in SEAWAT are dependent on density, the hydrostatic head distribution had to be computed (Figure B15). This was done by the following steps:

1. Calculate water density using the equation of state for chloride:

$$\rho_z = \rho_f + \frac{\partial \rho}{\partial C} C_z$$

Where:
ρ_z = water density at depth z (kg/m^3);
ρ_f = freshwater density (999.48 kg/m^3);
$\frac{\partial \rho}{\partial C}$ = density slope (1.3989);
C = chloride concentration at depth z (kg/m^3).

2. Calculate the hydrostatic pressure using the water density from the previous step:

$$P_n = P_{n-1} + \rho_z g (z_n - z_{n-1})$$

Where:
P_n = hydrostatic pressure at node n (Pa)
ρ_z = water density of the column water above depth z (kg/m^3)
g = gravitational constant 9.81 (N/kg)
z_n = depth of node n (m)

3. Calculate head by:

$$h_z = \frac{P_n}{\rho_z g} + z$$

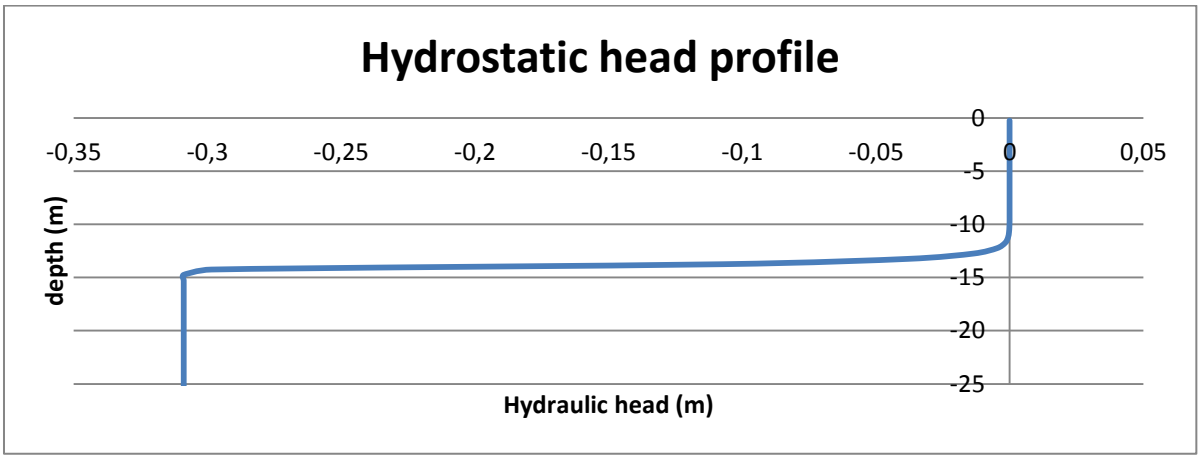

Figure B15 - Hydrostatic head profile used as initial head distribution in the FAT-model.

Appendix C - Data analysis

During the calibration process, the FAP-model was simulated with actual Freshmaker pumping rates. Section C1 describes how these rates were obtained from pumping data. The FAP-model was calibrated using data from geophysical measurements. However, geophysical measurements provide information on the electrical conductivity of the groundwater while the model results are solute concentrations. For this reason the geophysical measurements needed to be converted into solute concentrations. This is explained in detail in Section C2. Section C3 describes the hydraulic head measurements.

C1 - Pumping data

The flow rates were derived from recordings of flow meters at the Freshmaker control unit. The cumulative pumped volumes of the Freshmaker since the beginning of the pilot are shown in Figure C1. For each flow meter measurement, the pumped volume (m^3) was divided by the time difference between the previous measurement (d) in order to obtain the average flow rate (m^3/d). The resulting flow rates were documented separately for HDDW1 (injection and recovery of freshwater) and HDDW2 (interception of saltwater). As the recordings were taken irregularly the flow rates were translated into average daily flow rates per week. The resulting flow rates which were used in the model calibration are shown in Figure C2.

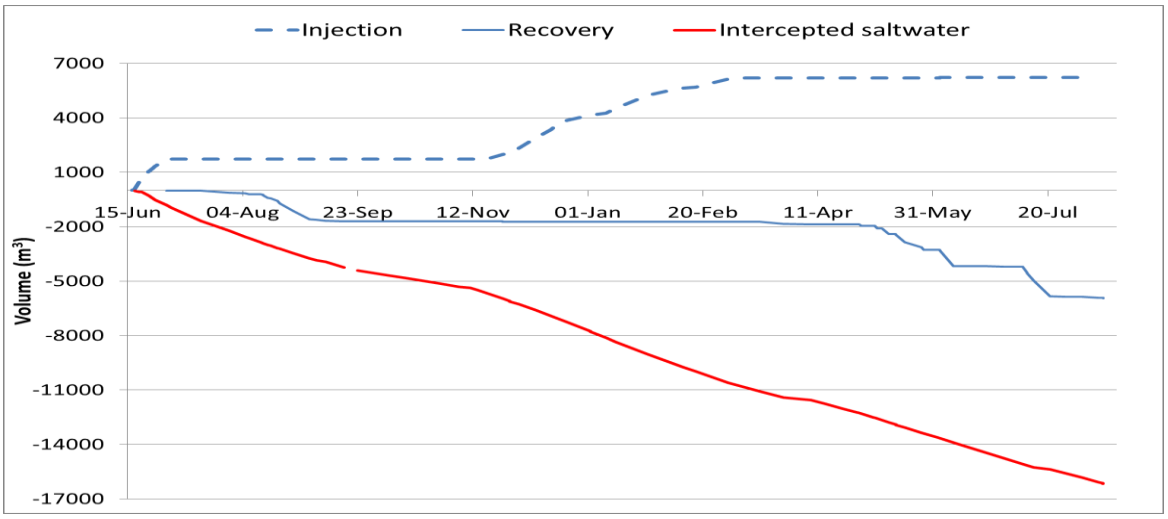

Figure C1 – Pumping history of the Freshmaker since the start of operation.

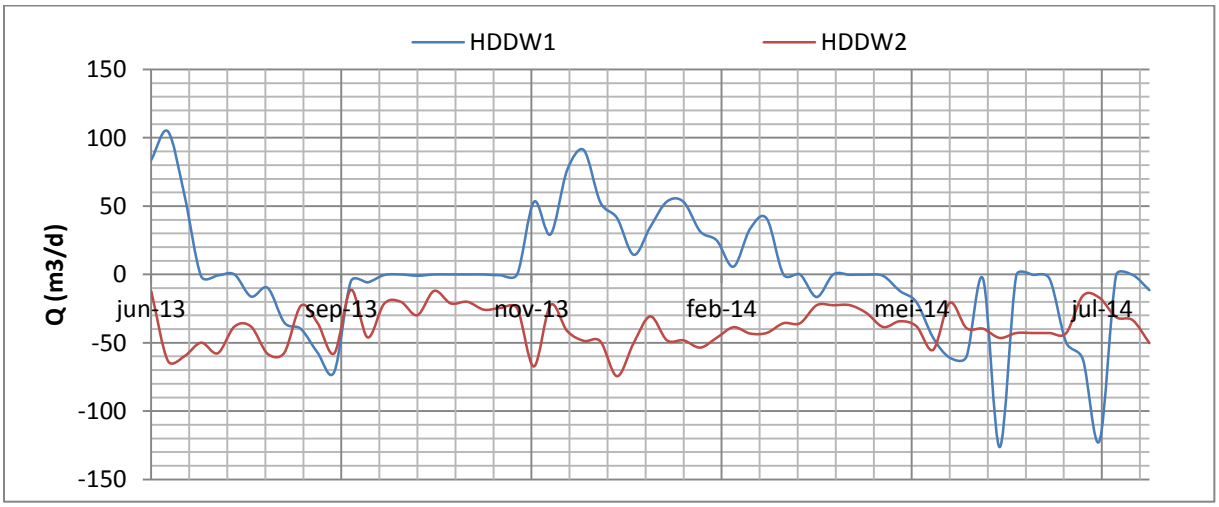

Figure C2 – Freshmaker flow rates simulated during the model calibration.

C2 - Geophysical measurements

C2.1 – Measuring electrical conductivity

Geophysical borehole logs using an EM39 probe (source) were constructed to monitor the position of the fresh-saltwater interface and follow its response on the activity of the Freshmaker. The borehole logs were constructed on a monthly basis at three monitoring wells but only the results from MW1 were used since this monitoring well is located in the middle of the HDDWs. Measurements were taken from -5 to -25 m-BSL with a step size of 20 cm. The EM39 provides measurement of the electrical conductivity (EC) of the soil and rock surrounding the monitoring well, using the inductive electromagnetic technique. This technique involves the interaction of magnetic and electric fields. The EM39 probe has an intercoil spacing of 50 cm to provide a substantial radius of exploration into the formation. An alternating current is applied to the transmitter coil present in the probe which creates an alternating magnetic field in the soil surrounding the probe. This magnetic field generates alternating currents loops in the soil which in turn generates a magnetic field in the soil. The magnetic field in the soil is out of phase compared to the magnetic field of the transmitter coil and as a consequence this generates an in-phase voltage in the receiver coil. This generated voltage is a proxy for the EC of the formation since the voltage depends on the magnetic field generated in the soil which is thus characteristic for the properties of the soil. Summarizing all of the above: the direct result of the EM39 measurements is the EC of the formation.

However, the EC of the formation is a combination of the EC of the soil matix and the EC of the pore water. Nevertheless, as the EC of the soil matrix remains constant over time, temporal changes in the EC of the formation indicate a change in the EC of the pore water and thus a movement of the fresh-saltwater interface. As can be seen in Figure C3, the EM39 results show an up- and downward movement of the fresh-saltwater interface, clearly following the ASR phases of the Freshmaker. The EM39 measurements could therefore directly give qualitative insight in the effect of the Freshmaker on the fresh-saltwater interface.

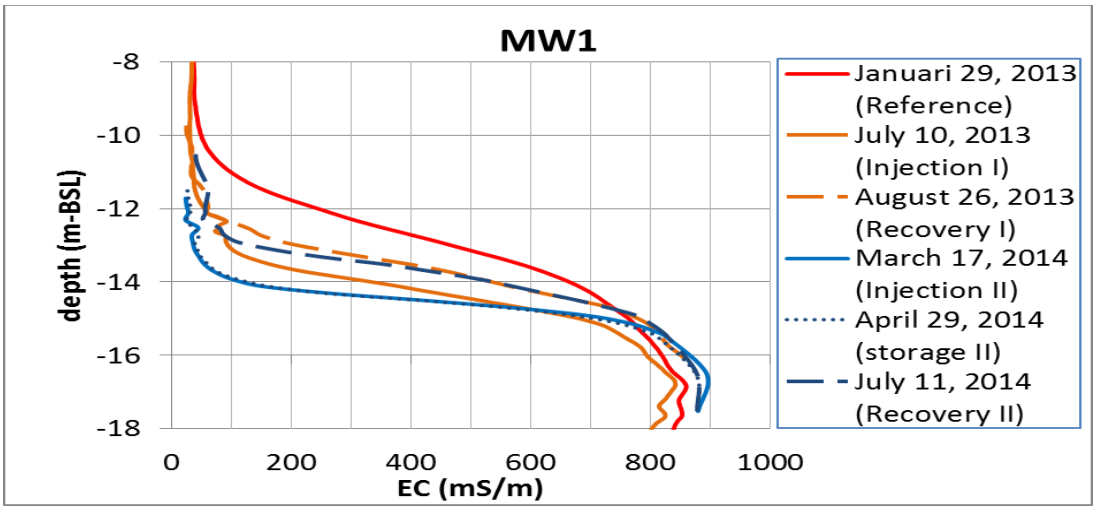

Figure C3 - EM39 measurements at MW1.

C2.2 – Converting EC measurements to TDS concentration measurements

If the FAP-model was calibrated well, it should produce the same movement of the interface as observed in the geophysical measurements. However, the EM39 results cannot directly be used to calibrate the FAP-model since the model does not simulate EC but solute concentrations. So, before the EM39 measurements could be used for model calibration, the EM39 measurements needed to be converted into solute concentrations. This conversion was performed using the following procedure:

1. Temperature correction for σ_f
2. Estimate groundwater electrical conductivity (σ_w) with Archie's Law.
3. Estimate TDS concentration from σ_w.

The following subsections describe each subsequent step in detail.

C2.2.1 - Temperature correction of EC measurements

Electrical conductivity varies with temperature. The conductance of different samples and measurements cannot be compared because of this dependency of temperature, unless the measurements are taken at the same temperature or adjusted to a reference temperature (Smith, 1962). Since the EC measurements were not taken at the same temperature, they were corrected to a reference temperature of 20˚C. This correction can be performed with the following relationship (Acacia, 2014):

$$\rho_{f,20} = \rho_f * \frac{1.8T+39}{75} \qquad (1)$$

Where:
$\rho_{f,20}$ = formation electrical resistance at 20˚C [Ωm].
ρ_f = measured formation electrical resistance [Ωm].
T = temperature [˚C].

Since the EM39 and CTD diver measurements did not give electrical resistance but electrical conductivity (which is the reciprocal of electrical resistance) Equation 1 was modified into:

$$\sigma_{f,20} = \sigma_f * \frac{75}{1.8T+39} \qquad (2)$$

Where:
$\sigma_{f,20}$ = formation electrical conductivity at 20˚C [mS/m].
σ_f = measured formation electrical conductivity [mS/m].

For the EM39 measurements no groundwater temperature measurements were directly available so a temperature of 12 ˚C was assumed for all bore hole loggings. This is reasonable according temperature measurements from groundwater samples at the pilot location.

C2.2.2 – Derivation of EC_w with Archie's Law

The EC of the subsurface is determined by the water saturation, salt concentration of the groundwater, temperature, and lithology. The EC that the EM39 probe measures is therefore the combination of all the determining factors. Since there has already been a correction for temperature in the previous step and the measurements were performed in the saturated zone (i.e. water saturation = 100%) the only remaining unknowns are lithology and salt concentration of the groundwater.

Archie (1942) found from laboratory studies that under water saturated conditions, the relation between the measured formation and water resistances is constant:

$$F = \frac{\rho_f}{\rho_w} \qquad (3)$$

Where:
F = formation factor [-].
ρ_f = measured formation electrical resistance [Ωm].
ρ_w = measured groundwater electrical resistance [Ωm].

The formation factor is a proxy for the lithology and the groundwater electrical resistance is a proxy for the salt concentration of the groundwater. Some formation factors for typical Dutch unconsolidated sediments are shown in Table C1. Since the EM39 measurements does not provide electrical resistance but electrical conductivity Archie's Law is reworked into:

$$\sigma_w = \sigma_f * F \qquad (4)$$

Where:
F = formation factor [-].
σ_f = measured formation electrical conductivity [mS/m].
σ_w = groundwater electrical conductivity [mS/m].

It is now possible to derive σ_w for each EM39 measurement by using a suitable formation factor from Table C1. However, given the fact that the grain size distribution at the pilot locations shows a fining upward trend at the depth of the fresh-saltwater interface, the formation factor is most likely not constant there. In order to

avoid possible errors due to this fining upward lithostratigraphy the formation factor was determined manually for the Freshmaker pilot site.

The formation factor was derived using Archie's Law by dividing the σ_w measured in groundwater samples taken at different depths by the σ_f measured by the EM39 probe at that same depth. In between these points the formation factors were linearly interpolated. The formation factor profile that was ultimately obtained is shown in Figure C3. With the formation factor now known at every depth, Equation 2 was used to determine σ_w profiles for each EM39 well log.

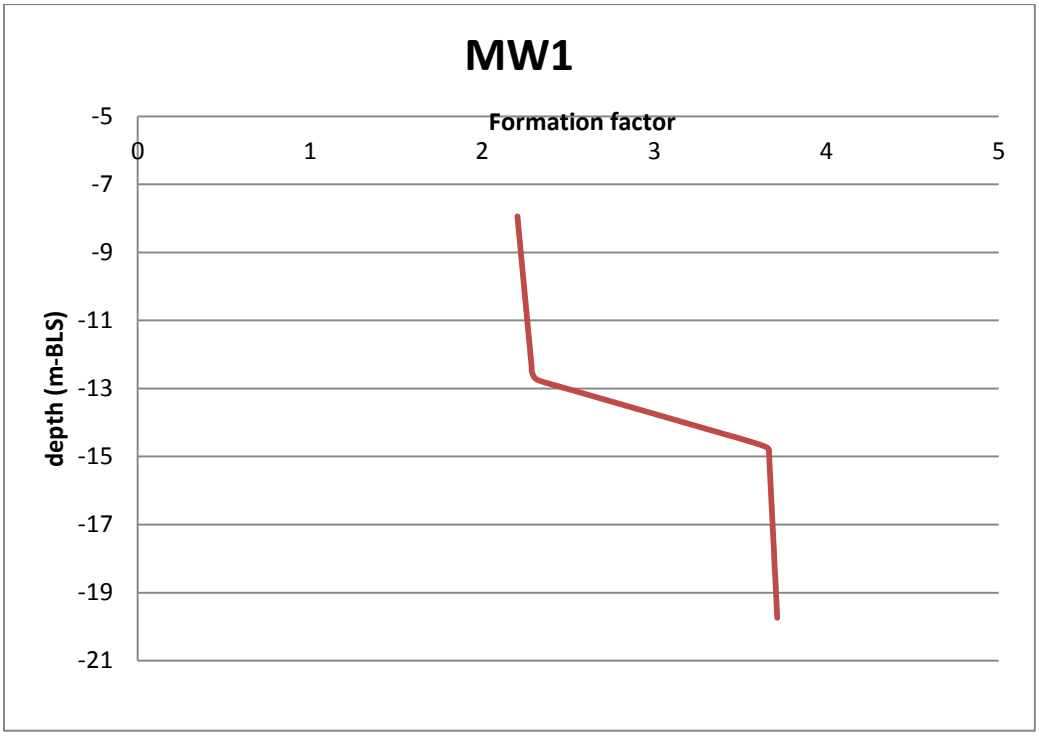

Figure C3 – Depth profile of the formation factor at MW1.

Table C1- Typical formation factors for unconsolidated sediments in the Netherlands. Source: Goes et al. (2009).

Lithology	Formation factor
Gravel with sand	7
Coarse sand with gravel	6
Coarse sand	5
Medium coarse sand	4
Sand with some silt	3
Silty sand	2.5
Strong silty sand	2
Clay	1-2
Peat	~1*

* apparent formation factor

C2.2.3 – Calculation of the TDS concentration from EC_w using an empirical relation

With the derivation of σ_w, it becomes possible to convert the EM39 measurements to solute concentration measurements by making use of a relation between EC and solute concentration. Mulder and Spoelstra (1995) proposed the following empirical relations between chloride and EC:

$$Cl = 3.9831 - 256.4 * \sigma_{w,20} \qquad (5)$$

However when this relation was used to convert EC into chloride it did not provide a good fit in the upper part of the EM39 curves, i.e. the regions where chloride concentrations are low. This was most likely caused by the fact that the relative influence of other cations/anions such as bicarbonate and phosphate becomes more prominent when chloride concentrations are low. An investigation of the water quality measurements show that bicarbonate concentrations are indeed relatively high in the upper part of the aquifer, furthermore, they are significantly variable. As can be seen in Figure C4, the bicarbonate concentration decreases by a factor 2 when injection takes place. This can be explained by the fact that the injected freshwater is surface water which has a significantly lower bicarbonate concentration then groundwater.

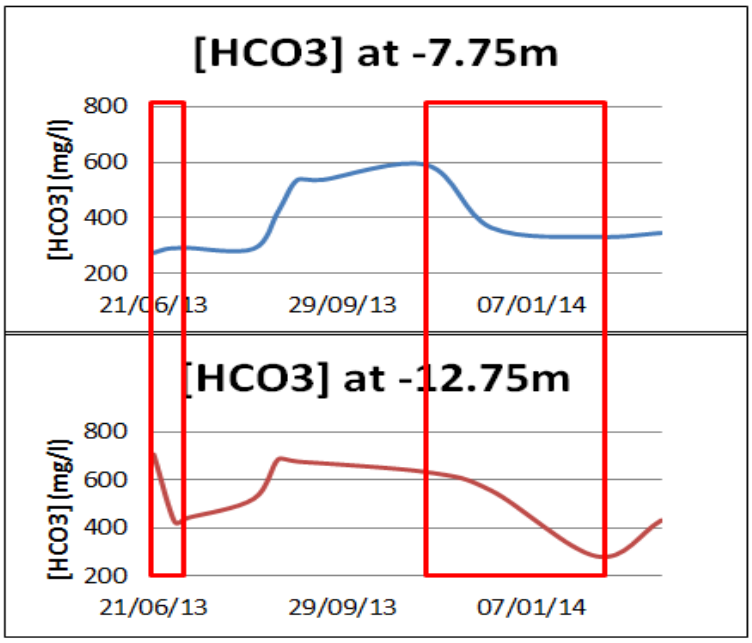

Figure C4 - Bicarbonate concentration at MW1. The red boxes indicate the injection phases.

The influence of bicarbonate on EC was believed to be significant but there were no sufficient bicarbonate measurements present at all depths where EM39 measurements were performed. Since the conversion formulas stated in the literature were not giving accurate results for chloride, instead of converting EC measurements to chloride, they were converted to TDS. All relevant constituents are included in TDS (i.e. also bicarbonate), so it was believed that if it was possible to construct an empirical formula between EC and TDS this formula would also be valid in the freshwater domain.

At the pilot location, water samples were taken from monitoring wells, from the injection water reservoir, and from the ditches near the Freshmaker. The samples were analysed in the lab for the main composition and trace elements. From this information the total dissolved solids (TDS) concentration was calculated. An empirical relation between EC and TDS concentration could be obtained as the EC was also measured in the lab. This relation is assumed to be valid for geophysical measurements at the pilot location since a large number of groundwater quality measurements from the pilot location were used. The following linear relation between EC and TDS was found (see Figure C5):

$$TDS = 0.7585\ \sigma_w + 76.57 \qquad (8)$$

Where:
TDS = concentration total dissolved solids (mg/l)
σ_w = groundwater electrical conductivity ($\mu S/cm$)

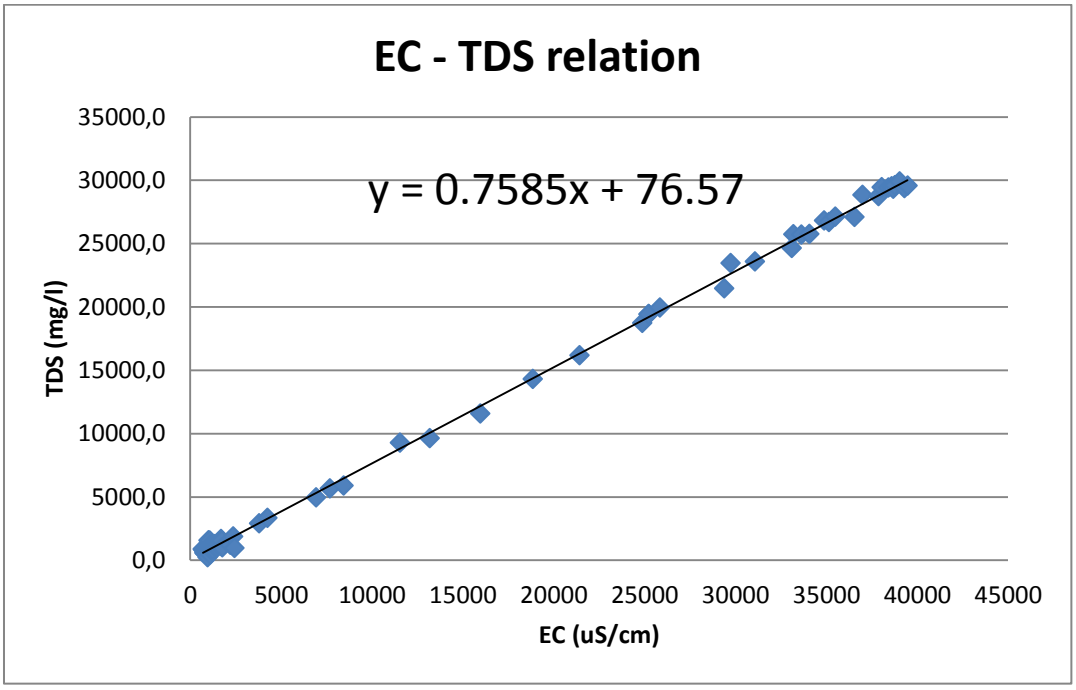

Figure C5 - Relation between EC and TDS as obtained from groundwater samples at the Freshmaker pilot site.

EM39 measurements were successfully converted into TDS measurements by making use of Equation 8. Resulting TDS concentration profiles are shown in Figure C6. These are the TDS concentration profiles which were used in the SEAWAT model calibration process.

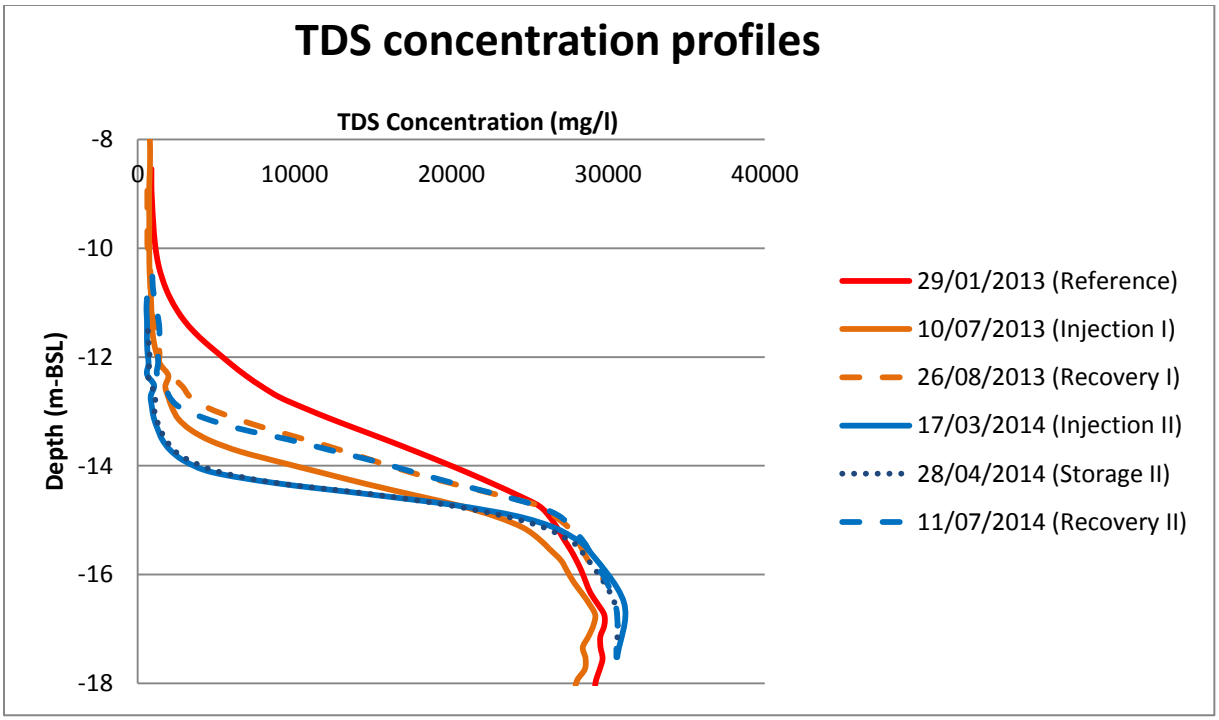

Figure C6 - TDS concentration profiles at MW1 as derived from EM39 measurements.

7.1 Hydraulic head measurements

Hydraulic heads were measured both by hand at monitoring wells on a monthly basis and by CTD divers at MW1 on a continuous basis. The salinity of the water influences the resulting hydraulic head. Therefore, only measurements in fresh to slightly brackish groundwater were used to calibrate the model. Figure C7 shows the time series of hydraulic head as derived from the CTD diver at MW1.1. The hydraulic heads which were measured manually at the monitoring wells near the Freshmaker were found to be highly sensitive to whether the Freshmaker was active at the time of measurement or not. This was caused by the large pressure fluctuations in the aquifer following the on/off switching of the wells. As measurements were taken on a monthly basis the real hydraulic head time series was difficult to reproduce by these type of measurement. For this reason, the manually measured hydraulic heads were not used for model calibration, only CTD diver measurements. However, what could be learned from the manual measurements was that during the injection phase, the hydraulic head was higher in the middle of HDDW1 than on the outer ends while during the recovery phase the head was lower in the middle of HDDW1 (see Figure C8). This means that there is a 3D effect that is not captured when the Freshmaker is simulated in the cross sectional model. For this reason it was also believed to be necessary to model the Freshmaker in 3D.

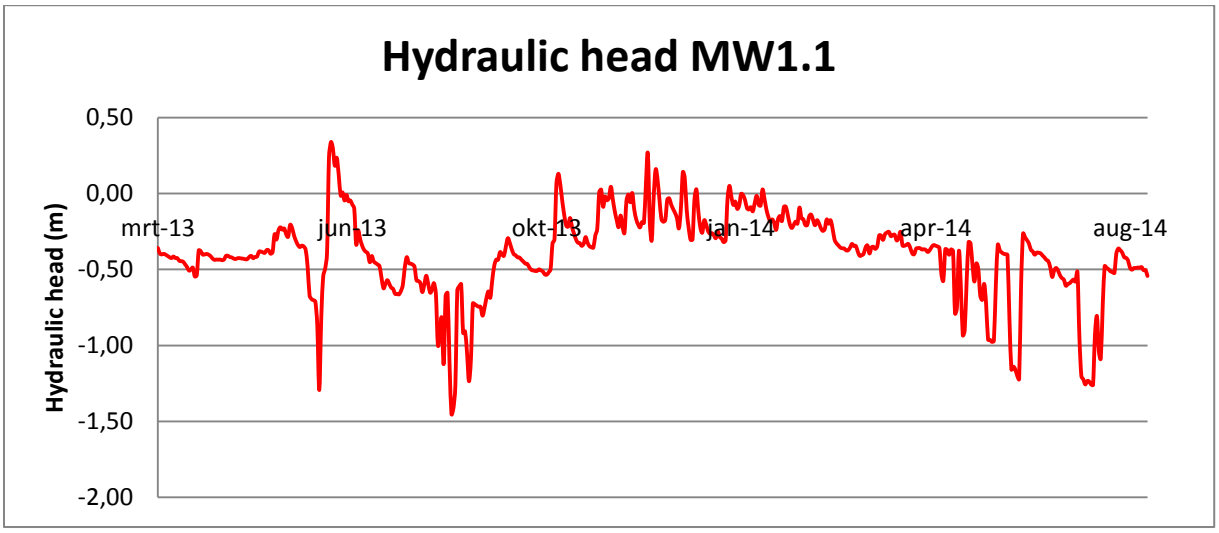

Figure C7 - Hydraulic heads measured at MW1.1 by a CTD-diver.

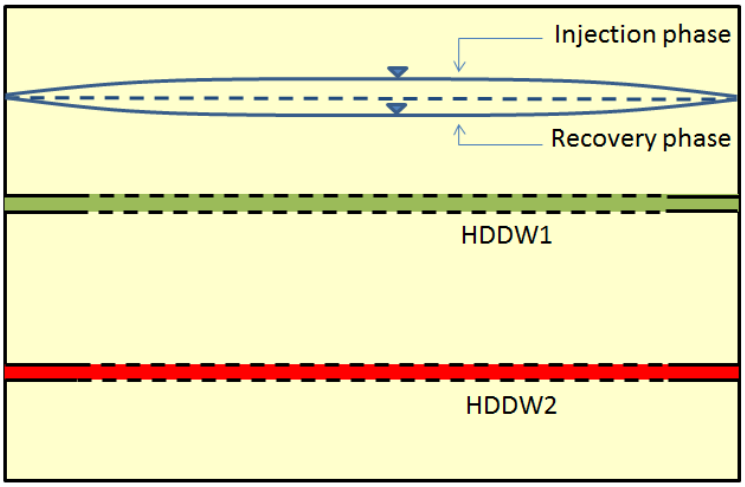

Figure C8 – Conceptual hydraulic heads at the Freshmaker pilot site during the injection and recovery phases.

Appendix D Meteorological data analysis

D1 - Realistic daily varying recharge rate

The freshwater lens in the initial FAP-model was generated by letting freshwater infiltrate with an average recharge rate of 1 mm/d. For the development of the initial shape and dynamics of the freshwater lens this was suitable, however, the resulting hydraulic heads during the simulated activity of the Freshmaker were not correct. For this reason, it was needed to derive a groundwater recharge rate that is realistic for the pilot location.

Furthermore, for the purpose of simulating the Freshmaker on a weekly basis the assumption of a constant recharge rate might not be desirable. In reality, the groundwater recharge varies on a temporal basis due to changing precipitation and evapotranspiration patterns during the different seasons of the year. Given the fact that the shape of the freshwater lens is slightly dynamic it was believed to be important to take this into account during the calibration process. Since the fresh-saltwater interface will move up (in dry periods) and down (in wet periods) the resulting mixing zone will be different from a mixing zone in a non-dynamic freshwater lens. Implementing a temporal varying groundwater recharge will therefore lead to a more realistic rainwater lens and mixing zone.

For the determination of the groundwater recharge values it was assumed that all precipitation surpluses infiltrate into the soil and recharges the groundwater. In terms of the water balance this means that:

$$Q_{recharge} = P - ET \qquad (1)$$

Where:
$Q_{recharge}$ = groundwater recharge [L/T]
P = precipitation [L/T]
ET = evapotranspiration [L/T]

In order to derive the time series of $Q_{recharge}$, time series of P and ET were needed. The resulting time series of $Q_{recharge}$ and the monthly average recharge rates are shown in Figures D1 and D2 respectively. The long term average groundwater recharge was found to be 0.466 mm/d. The following subsection describes how the time series of $Q_{recharge}$ was obtained by showing how time series of P and ET were derived.

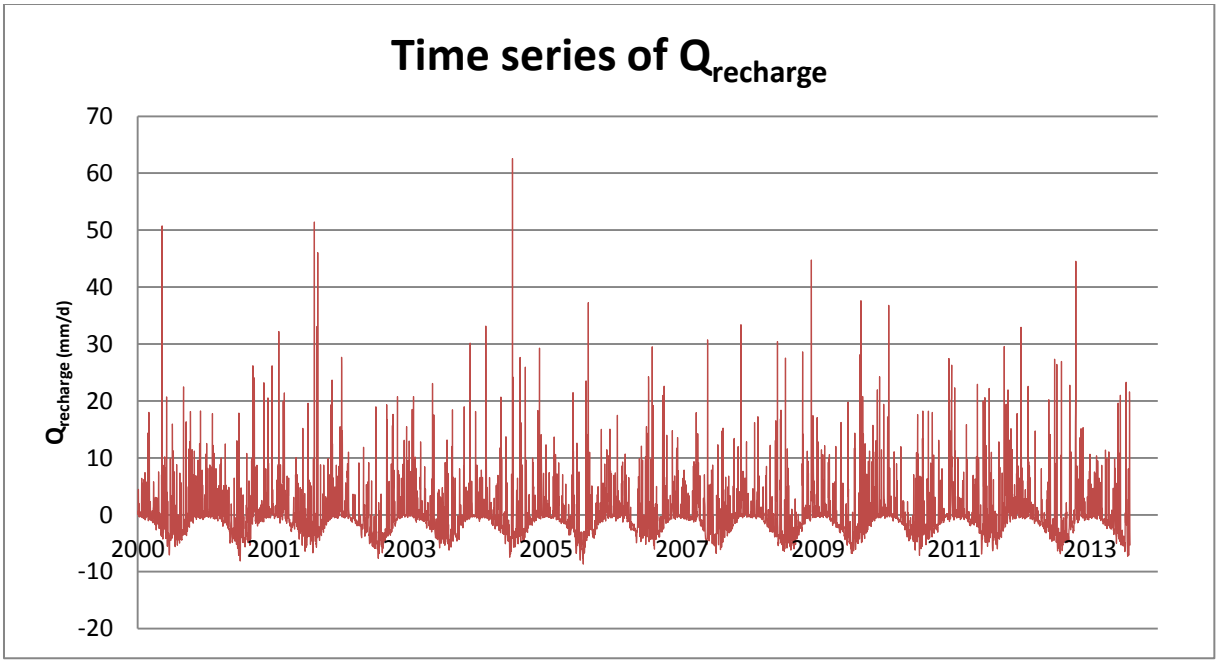

Figure D1 - Time series of $Q_{recharge}$ derived from meteorological data at KNMI station Vlissingen.

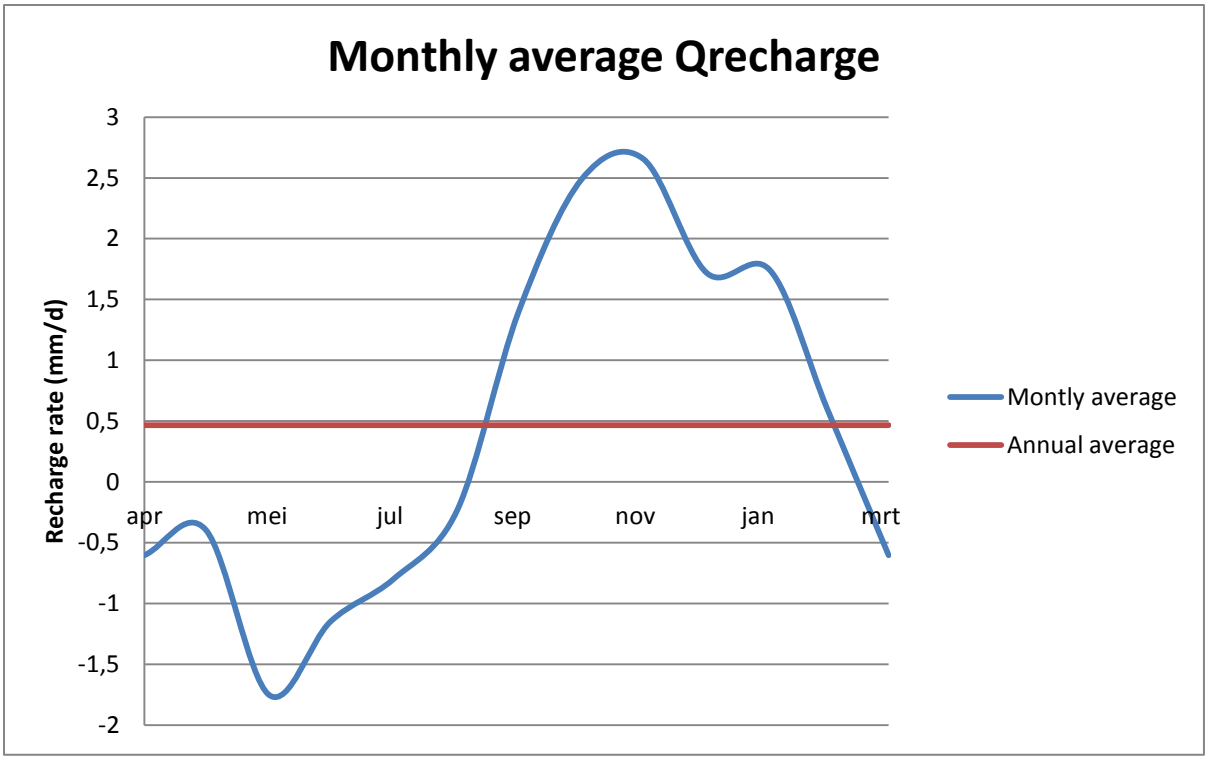

Figure D2 – Monthly average groundwater recharge rate. As can be seen recharge rates are negative from April till August (dry season) and positive from August till April (wet season). Shown in red is the annual average recharge rate: $Q_{recharge,\ average}$ = 0.466 mm/d.

D2 - Derivation of $Q_{recharge}$

D2.1 - Precipitation

The Royal Dutch Meteorological institute (KNMI) measures daily precipitation (P) at 325 stations in the Netherlands. Fortunately, one of these stations is located in Ovezande. The daily precipitation measured at Ovezande since 2000 is shown in Figure D3.

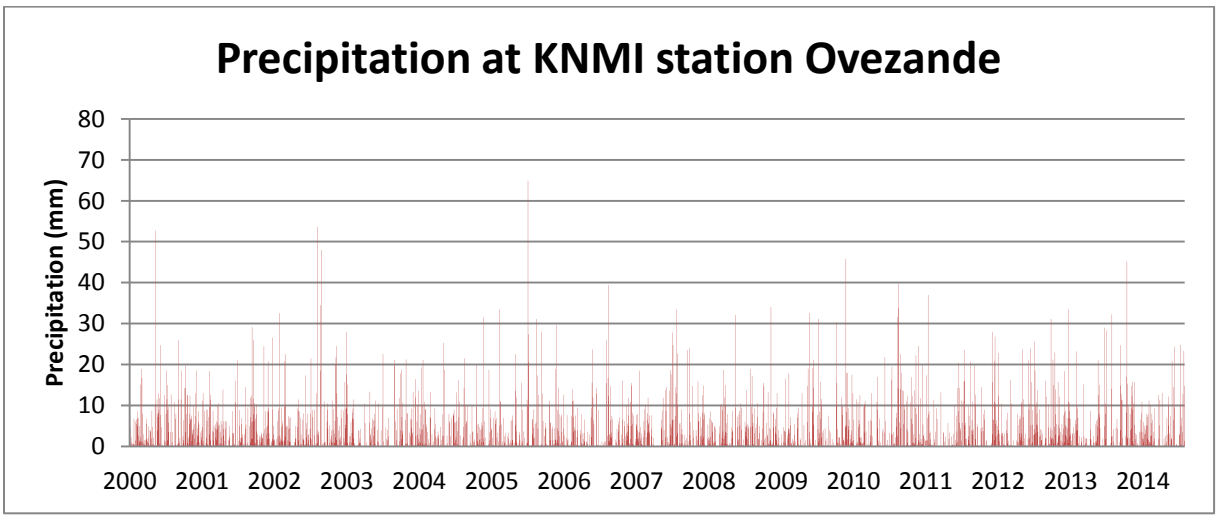

Figure D3 – Daily measured precipitation at Ovezande. Measurements from 01/01/2000 onwards are shown.

D2.2 - Evapotranspiration

In the Netherlands, about 70% of the annual precipitation evaporates. This makes evaporation after precipitation the most important term in the water balance. However, opposed to precipitation, evaporation cannot be directly measured. Furthermore, it is import to distinguish between actual- and potential evapotranspiration. The potential evapotranspiration is the maximum evapotranspiration that can take place under the prevalent meteorological conditions. How much water actually evapotranspirates is dependent on land use type and the prevailing hydrological conditions (e.g. soil moisture, available nutrients).

The major part of the pilot location consists of fruit trees that are well watered so it is assumed that the actual evapotranspiration rate (ET_{act}) of the soil around the Freshmaker is equal to potential evapotranspiration (ET_{pot}). ET_{pot} can be estimated using so-called "reference crop methods". In these methods, the potential evapotranspiration of a reference crop (usually clipped grass) is calculated. The evapotranspiration rate derived by such methods only hold for the reference crop and is therefore called the reference evapotranspiration (ET_{ref}). Other land use types than grass will evaporate and transpire at a different rate due to differences in ground cover, canopy properties and aerodynamic resistance. The effects of characteristics that distinguish field crops from grass are integrated into the crop coefficient (K_c), which is therefore crop specific. The crop specific ET_{pot} is then calculated by multiplying ET_{ref} by K_c.

The following equation summarizes all of the above:

$$ET_{act} \approx ETpot = K_c * ET_{ref} \qquad (2)$$

Where:
ET_{act} = actual evapotranspiration [mm/d],
ET_{pot} = potential evapotranspiration if the crop is experiencing no stress [mm/d],
ET_{ref} = reference crop evapotranspiration as calculated with the FPM equation [mm/d],
K_c = crop factor [-]

The resulting time series of ET_{pot} is shown in Figure D4. Subsection D2.2.1 describes how ET_{ref} was derived and subsection D2.2.2 how the K_c was derived.

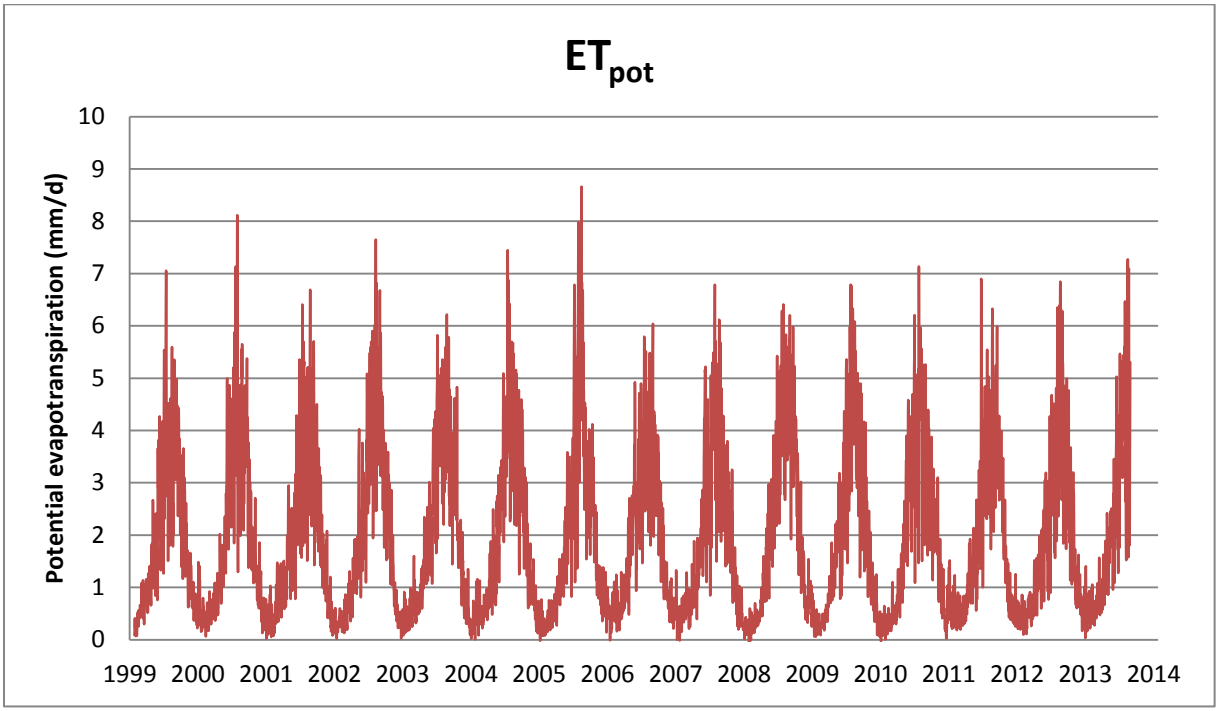

Figure D4 – Time series of the derived potential evapotranspiration at Ovezande for a period of 15 years. Note the difference between evaporation rates in summer and winter.

D2.2.1 - Derivation of the reference crop evapotranspiration

D2.2.1.1 – Makkink versus Penman reference evaporation

The KNMI provides estimates of the reference evapotranspiration using the Makkink method, which is the national standard since 1987. However, the Makkink equation assumes evaporation is only driven by temperature and incoming shortwave solar radiation. This assumption is valid for most days in the summer season. From April till September radiation is indeed the major driver behind evapotranspiration. In the other months this is not the case and a physical basis for the Makkink equation is not present. Internationally, the FAO-Penman-Monteith (FPM) equation is the standard to estimate reference crop evapotranspiration. Schuurmans and Droogers (2009) propose it is better to use the FPM-equation instead of the Makkink equation since the FPM-equation also takes the aerodynamic driver of evaporation explicitly into account. Since the Freshmaker pilot is located in the province of Zeeland, a coastal province which is relatively windy compared to the rest of the Netherlands, neglecting the aerodynamic term may lead to an underestimation of the actual evapotranspiration rate. As observed in the calibration process (Appendix B), simulations with recharge rates that are too high result in wrongly simulated hydraulic heads. The FPM-equation was therefore used for the determination of the reference crop evapotranspiration at the Freshmaker pilot location. Meteorological data required in this process were obtained from the KNMI meteorological station in Vlissingen, which is in near proximity of the Freshmaker pilot location (< 20 km).

The ET_{ref} derived with the FPM-equation and directly obtained from KNMI measurements (Makkink) is shown in Figure D5. As can be seen, the Makkink equation indeed underestimates the potential evapotranpiration at the Freshmaker pilot site.

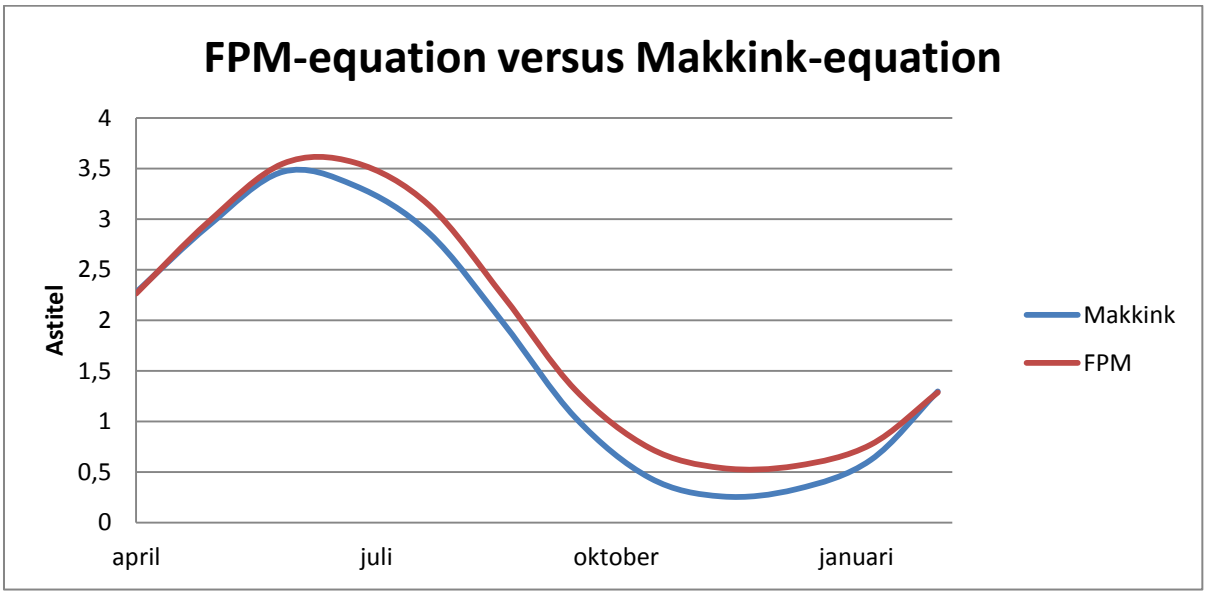

Figure D5 – Monthly average reference crop evapotranspiration obtainded with the FPM-equation and the Makkink-equation. The Makkink equation structurally underestimates the evapotranspiration rate.

D2.2.1.1 - Derivation of ET_{ref} using the FAO-Penman Monteith equation

The Food and Agricultural Organisation (FAO) concluded a modified Penman-Monteith equation is suited best for the estimation of the potential evapotranspiration for a wide range of crops on a global scale. However, the Penman-Monteith equation is limited in its use by the lack of available parameter data. Especially the parameters of the surface resistance and the aerodynamic resistance are hard to come by since they are crop specific and growth stage dependent. For that reason it was needed to come up with a function that calculates a "reference crop" evaporation. From this reference crop evaporation it would then be possible to calculate the potential evaporation of a certain land use type by correcting for a crop coefficient factor.

In the FPM equation, the reference crop is defined as clipped grass with a height of 0.12 m, an albedo of 0.23 and a fixed surface resistance of 70 s/m. Furthermore, a standardized height for wind speed, temperature, and humidity measurements at 2 m above the ground are used. By using these reference values, knowledge of the two parameters which are the hardest to get (aerodynamic resistance and surface resistance) is no longer needed. The FPM-equation is formulated as (Allen, 1998):

$$ET_{ref} = \frac{0.408\,\Delta\,(R_n - G) + \gamma \frac{900}{T+273} u_2 (e_s - e_a)}{\Delta + \gamma(1 + 0.34 u_2)} \qquad (3)$$

Where:
ET_0 = reference crop evapotranspiration (m/d)
R_n = net radiation (MJ/m^2/d)
G = soil heat flux (MJ/m^2/d)
$(e_s - e_a)$ = vapour pressure deficit of the air (kPa)
Δ = slope of the saturation vapour pressure temperature relationship (kPa/˚C)
γ = psychrometric constant (at sealevel ~0,066 kPa/˚C)
u_2 = wind speed at 2 m height (m/s)

The parameters needed to calculate ET_{ref} with the FPM-equation cannot directly be obtained from KNMI data. Additional derivations were needed to before the KNMI data could be used to calculate the ET_{ref}. The data manipulations which were done are explained in the following subsections.

Derivation of Δ

The slope of the saturation vapour pressure temperature relationship was obtained from the daily average temperature. The following relation was used (Allen et al., 1998; Equation 13):

$$\Delta = 4098 \left[\frac{0.6108 * \exp\left(\frac{17.27\,T_{average}}{T_{average}+237.3}\right)}{(T_{average}+237.3)^2} \right] \qquad (4)$$

Where:
Δ = slope of the saturation vapour pressure temperature relationship [kPa/˚C]
T_{averag} = average daily temperature [˚C]

Derivation of γ

The following relation was used to calculate the psychrometric constant (Allen et al., 1998; Equation 8):

$$\gamma = \frac{c_p P}{\varepsilon L} = 0.665 * 10^{-3}\, P \qquad (5)$$

Where:
γ = psychrometric constant [kPa/˚C]
c_p = specific heat at constant pressure, $1.013*10^{-3}$ [MJ/kg/˚C]
P = atmospheric pressure [kPa]
ε = ratio molecular weight of water vapour/dry air = 0.622
L = latent heat of vaporization, 2.45 [MJ/kg].

As can be seen the psychrometric constant is dependent on the air pressure and depends therefore on the altitude. However, the relation with altitude is weak (Schuurmans and Droogers, 2009) and therefore a

constant atmospheric pressure of 1 atm or 100 kPa was assumed at the Freshmaker pilot site. This resulted in a value for γ of 0,066 kPa/˚C.

Derivation of G

The soil heat flux (G), is the energy needed to heat the soil. This flux is positive when the soil heats and negative when the soil cools. The soil has a relatively large heat capacity. The daily trend of the soil heat flux is correlated to the daily temperature trend in the soil. As this trend is sinusoidal during the day, the net soil heat flux is small. Compared to the net incoming radiation (R_n) the soil heat flux is in significant and was therefore neglected.

Derivation of u_2

Wind speeds above a surface above the surface vary as a function of height above that surface. Shear friction at the surface result in lower wind speeds near the surface. For this reason, wind speeds are measured at a standard height, which is for most KNMI stations 10 m above the land surface but at Vlissingen the sensor is at 27 m height. However, the FPM-equation uses wind speeds at a standard height of 2 m above the surface. As the wind speeds in the zone between 2 m and 50 m height increase logarithmically with height, the KNMI wind measurements were translated into measurements at 2 m height. The following relationship was used (Allen et al., 1998; Equation 47):

$$u_2 = u_z * \left(\frac{4.87}{\ln(67.8\, z - 5.42)}\right) = u_z * \frac{4.87}{\ln(67.8*27 - 5.42)} = u_z * 0.65 \qquad (6)$$

Where:
u_2 = wind speed at 2 m above the surface (m/d)
u_z = measured wind speed at z m above the surface (m/d)
z = height of measurement above ground surface, 27 m (m)

Derivation of (e_s - e_a)

The vapour pressure deficit (e_s - e_a) is defined as the difference between the saturated vapour pressure (e_s) and the actual vapour pressure (e_a). This indicates how much water can still be taken up by the air under a given temperature and is therefore a measure for the atmospheric heat demand. Plants respond to the vapour pressure deficit by opening their stomata further when the deficit is large. This means that more water will evaporate when the vapour pressure deficit is large.

The saturation vapour pressure only depends on temperature and was derived by the following relationships (Allan et a., 1998; Equation 11 and 12):

$$e_0 = 0.608 * \exp\left(\frac{17.27\, T}{T + 273.3}\right) \qquad (7)$$

$$e_s = \frac{e^0(T_{min}) + e^0(T_{max})}{2} \qquad (8)$$

Where:
e_0 = saturation vapour pressure at temperature T [kPa]
e_s = average saturation vapour pressure [kPa]
T_{min} = minimum temperature [˚C]
T_{max} = maximum temperature [˚C]

The actual vapour pressure can impossibly be measured directly. Instead, the actual vapour pressure is usually derived from the relative humidity:

$$RH = \frac{e_a}{e_s} \rightarrow e_a = RH * e_s \qquad (9)$$

Where:
RH = relative humidity [-]

Derivation of R_n

Net radiation (R_n) is defined as the difference between the net incoming shortwave radiation (solar radiation) and the net outgoing longwave radiation (terrestrial radiation). R_n is not measured by the KNMI. Therefore it had to be calculated manually. The following equation holds:

$$R_n = \left(S^{\downarrow} - S^{\uparrow}\right) - \left(L^{\downarrow} - L^{\uparrow}\right) \quad (10)$$

Where:
$S^{\downarrow}$ = Incoming short wave radiation [W/m^2/d]
$S^{\uparrow}$ = Outgoing short wave radiation [W/m^2/d]
$L^{\downarrow}$ = Incoming long wave radiation [W/m^2/d]
$L^{\uparrow}$ = Outgoing long wave radiation [W/m^2/d]

$S^{\downarrow}$ is measured by the KNMI and the outgoing short wave radiation can be calculated from the albedo as this is the portion of the short wave radiation that is reflected by the earth surface. The net short wave radiation is therefore given by:

$$S^{\downarrow} - S^{\uparrow} = (1 - \alpha)\, S^{\downarrow} \quad (11)$$

Where:
$S^{\downarrow} - S^{\uparrow}$ = net incoming shortwave radiation [W/m^2/d]
α = albedo [-] which is 0.23 for the reference crop used in the FPM-equation.

The long wave radiation emitted by the earth's surface is expressed quantitatively by the Stefan-Boltzmann Law. However, the net long wave radiation leaving the earth's surface is less than given by the Stefan-Boltzmann Law as the atmosphere adsorbs a portion of the energy and radiate it back to the surface of the earth. Water vapour, clouds, carbon dioxide and dust are absorbers and emitters of longwave radiation present in the atmosphere and additional correction terms are needed to account for them. A corrected form of Stefan-Boltzmann law for the net outgoing long wave radiation with empirically derived correction terms are given by Allen et al., 1998; Equation 39:

$$L^{\downarrow} - L^{\uparrow} = \sigma \left(\frac{T_{min}^4 + T_{max}^4}{2}\right) (0.34 - 0.14\sqrt{e_a}) \left(1.35 \frac{S^{\downarrow}}{S_0^{\downarrow}} - 0.35\right) \quad (12)$$

Where:
$L^{\downarrow} - L^{\uparrow}$ = net outgoing longwave radiation [W/m^2/d]
σ = Stefan-Boltzmann constant [5.67E-8 W/m^2/T^4]
T_{min} = maximum air temperature during the day [K]
T_{max} = minimum air temperature during the day [K]
e_a = actual vapour pressure [kPa]
$S^{\downarrow}$ = Incoming short wave radiation [W/m^2/d]
$S_0^{\downarrow}$ = Incoming clear sky short wave radiation [W/m^2/d]

$S_0^{\downarrow}$ was not known and was calculated from the extra-terrestrial radiation using the following relation (Allen et al., 1998; Equation 37):

$$S_0^{\downarrow} = (0.75 + 2 \cdot 10^{-5} z) \cdot S^{ext} \quad (13)$$

Where:
$S_0^{\downarrow}$ = Incoming clear sky short wave radiation [W/m^2/d]
Z = elevation above sea level
S^{ext} = extraterrestrial radiation [W/m^2/d]

The extra-terrestrial radiation for each day of the year and for different latitudes can be estimated from the solar constant, the solar declination and the time of the year by (Allan et al., 1998; Equation 21):

$$S^{ext} = \frac{G_{solar}\, d_r}{\pi} [\omega_s \sin(\varphi) \sin(\delta) + \cos(\varphi) \cos(\delta) \sin(\omega_s)] \quad (14)$$

Where:
S^{ext} = extraterrestrial radiation [MJ m-2 day-1]
G_{solar} = solar constant [1366 W/m^2/d]
d_r = inverse relative distance Earth-Sun (Equation 15)
ω_s = sunset hour angle [rad], (Equation 18)
φ = latitude [rad] (Equation 17)
δ = solar decimation [rad] (Equation 16)

The inverse relative distance Earth-Sun, d_r and the solar decimation, δ, were calculated from:

$$d_r = 1 + 0.033 \cos\left(\frac{2\pi}{365} J\right) \quad (15)$$

$$\delta = 0.409 \sin\left(\frac{2\pi}{365} J - 1.39\right) \quad (16)$$

Where J is the number of the day in the year between 1 (January 1st) and 365 or 366 (December 31st).

The latitude, φ, of the Freshmaker pilot site is 51°26.546'N. However, the latitude is needed in radians. The conversion of decimal degrees to radians was done as follows:

$$[Radians] = \frac{\pi}{180}[decimal\ degrees] \rightarrow \varphi_{Freshmaker} = \frac{\pi}{180}\left(51 + \frac{26.546}{60}\right) = 0.898\ rad \quad (17)$$

The sunset hour angle, ω_s, is given by:

$$\omega_s = \arccos[-\tan(\varphi)\tan(\delta)] \quad (18)$$

Summarizing, it was possible to calculate the net radiation, $R_{n,}$ from temperature, relative humidity, and incoming short wave radiation measurements. As R_n was calculated in W/m²/d while the FPM equation uses R_n in MJ/m²/d a conversion factor of 0.0864 was needed. A time series of the calculated net radiation in Ovezande is shown in Figure D6.

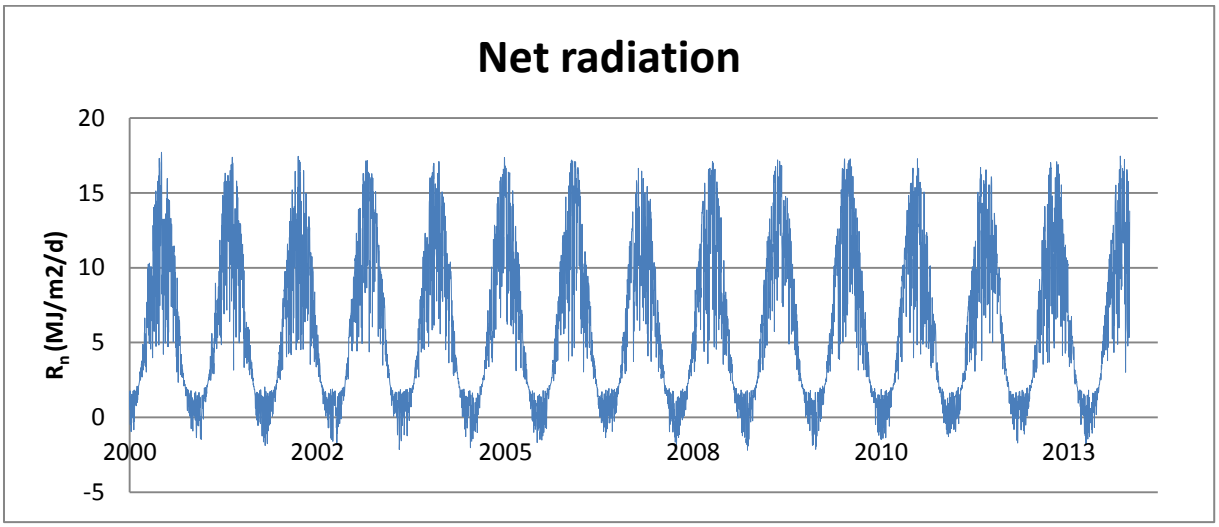

Figure D6 - Time series of net radiation at Ovezande.

D2.2.2 – Calculation of the crop coefficient at the Ovezande pilot

The crop coefficient is unique for each crop type and will vary during the growth stages of the crop. As the crop develops, the ground cover, crop height and the leaf area change. Due to differences in evapotranspiration during the various growth stages, the Kc for a given crop will vary over the growing period. The growing period can be divided into 5 distinct growth stages:

I. Initial stage
II. Crop development stage
III. Mid-season stage
IV. Late season stage
V. Winter stage

The land use at the Freshmaker pilot location consists mainly of apple and pear orchards. The crop coefficients for the different growth stages of an orchard containing apple and pear trees which lose leafs during the winter is shown in Table D1. From these values it was possible to estimate the year-round daily crop factor (Figure D6). During the winter period, where the trees lose their leaves, the crop factor is assumed to be equal to the crop factor in the initial stage. The daily results of the FAO-Penman-Monteith equation (ET_{ref}) were multiplied by the daily crop factor to obtain the daily potential evapotranspiration rates (ET_{pot}).

Table D1 - Crop factors and stage lengths of the different growth stages of an apple orchard Source: Allen et al, 1998.

Growth stage	Stage duration (d)	Crop factor
Initial	20	0.8
Development	70	0.8-1.2
Mid-season	90	1.2
Late-season	30	0.85
Winter	155	0.8

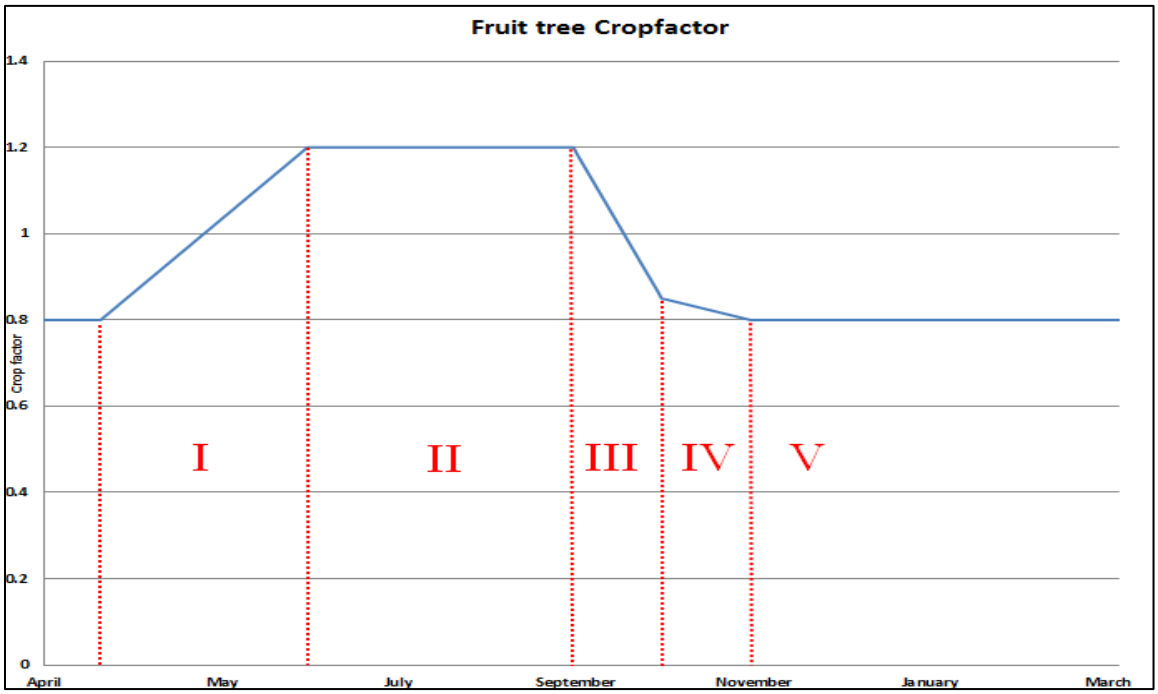

Figure D6 - Crop factor of the dominant land use type at the pilot location: Apple Orchard. The 5 different growth stages are separated by the dashed lines.